Non-contact flow rate measurements in turbulent liquid metal duct flow using time-of-flight Lorentz force velocimetry

Dissertation

zur Erlangung des akademischen Grades

Doktoringenieur

(Dr. – Ing.)

vorgelegt der
Fakultät für Maschinenbau der
Technischen Universität Ilmenau

von Frau

Magister für Ingenieurmechanik Nataliia Dubovikova
(geb. Ponomaryova)
geboren am 09.01.1983 in Kemerovo, Russland

CONTENTS

ACKNOWLEDGMENT

I would like to take this opportunity of thanking my supervisors, Prof. Christian Karcher, Dr. Christian Resagk and Prof. Yuri Kolesnikov, for their support, advices and rational criticism.

I would like to express appreciation to DFG for funding of Research Training Group Lorentz force velocimetry and Lorentz force eddy current testing and this research particularly (GRK 1567). Special thanks are extended to Anna Kholodova and Jonas Ketterer for their support in measurements.

My knowledge of this subject and the result of the current project has benefited from many others with whom I have worked and talked over these years – my colleagues. It would be difficult to name all, but I am grateful for everything they made to move me forward. Every day these people give me new ideas, inspiration and support.

And the warmest thanks to those who gave me the motivation and reasons to keep moving – to my family.

ZUSAMMENFASSUNG

Die Durchflussmenge von Flüssigmetallströmungen zu bestimmen ist in industriellen Anwendungen wie der Gießereitechnik von größter Bedeutung, um Prozesseffizienz und Produktqualität zu gewährleisten. Invasive Messmethoden versagen hierbei, da die Elektroden dem heißen und chemisch aggressiven Medium nicht dauerhaft standhalten können. Durch die Opazität des flüssigen Metalls entfallen optische Methoden ebenfalls. Kontaktlose Messverfahren bieten deshalb eine vielversprechende Lösung für derartige Durchflussmessungen. Ein derartiges Verfahren, welches derzeit Gegenstand der Forschung ist, ist die Lorentzkraftanemometrie (Lorentz Force Velocimetry, LFV). Eine mögliche Abhilfe für dieses Defizit bietet eine Kombination der klassischen Lorentzkraftanemometrie mit einem Laufzeitmessverfahren (time-of-flight), die sogenannte time-of-flight LFV. Hierbei wird durch einen Wirbelgenerator ein Wirbel im Fluss erzeugt, welcher zwei in bekanntem Abstand stromabwärts positionierte Magnetsysteme durchläuft. An jedem der Magnetsysteme ist ein eigener Kraftmesssensor angebracht, der den das Magnetfeld durchlaufenden Wirbel in Form einer signifikanten Störung des Kraftsignals wahrnimmt. Anhand der Zeitdifferenz der Störung der beiden Kraftsignale kann auf die Durchflussrate geschlossen werden.

Die vorliegende Dissertation untersucht experimentell die time-of-flight LFV unter Verwendung eines Flüssigmetallstromes in einem geschlossenen, rechteckigen Kanal welcher von einer elektromagnetischen Pumpe angetrieben wird. Als Arbeitsfluid dient dabei eine bei Raumtemperatur flüssige Legierung aus Gallium (Ga), Indium (In) und Zinn (Sn) (GaInSn). Im Gegensatz zu vorangegangenen Arbeiten werden dabei erstmals dreiachsige Kraftsensoren zur Messung der Lorentzkraft verwendet, um die Effekte der eingebrachten Störungen auf die time-of-flight LFV Durchflussmessung in verschiedenen Richtungen zu untersuchen. Dazu wurde der Prototyp eines time-of-flight LFV Durchflussmessgertes entwickelt und unter Laborbedingungen durch verschiedene Experimente charakterisiert. Ein neues Pumpsystem, welches eine elektromagnetische Pumpe nutzt, wurde getestet und auf die Verwendbarkeit als Flussanregung für zukünftige Anwendungen des Kanals getestet. Ferner wurden unterschiedliche Methoden zur Erzeugung der Wirbel und ihre relative Effektivität systematisch untersucht.

ABSTRACT

Measuring flow rates of liquid metal flows is of utmost importance in industrial applications such as metal casting, in order to ensure process efficiency and product quality. Contact based methods fail as the measurement probes cannot withstand the hot and chemically aggressive environment in the flow. Optical methods too are unsuitable due to the opacity of liquid metals. Hence non-contact techniques have been the most promising for such flow measurements. One of such techniques of recent interest is known as Lorentz force velocimetry (LFV), the principle of which is to determine flow rates through measurement of Lorentz force that act on magnet systems that are placed close to the flow. However, this method also depends on the electrical conductivity of the fluid and the applied magnetic flux density, which are not known a priori in a typical scenario. This shortcoming is overcome by combining the classical LFV with the time-of-flight principle, which is known as time-of-flight LFV. In this method, a vortex generator is used to generate an eddy in the flow, with two magnet system separated by a known distance placed downstream of the vortex generator. Each of the magnet systems has a force sensor attached to them which detects the passing of the eddy through its magnetic field as a significant perturbation in the force signal. The flow rate is estimated from the time span between the perturbations in the two force signals.

In this thesis, time-of-flight LFV technique is demonstrated experimentally for the case of liquid metal flow in a closed rectangular duct loop that is driven by an electromagnetic pump. A liquid metal alloy of gallium (Ga), indium (In) and tin (Sn) – GaInSn – is used as the working fluid. In contrast to prior works, for the first time, three-dimensional strain gauge force sensors were used for measuring Lorentz force to investigate the effect of flow disturbances in different direction for flow measurements by time-of-flight LFV method. A prototype time-of-flight LFV flowmeter is developed, the operation of which in laboratory conditions is characterized by different experiments. Furthermore, different methods of vortex generation and their relative effectiveness have been systematically studied.

ABBREVIATIONS

DAQ data acquisition
LDV laser Doppler velocimetry
LFV Lorentz force velocimetry
LTV Lorentz torque velocimetry
MHD magneto-hydro dynamics
MTV molecular tagging velocimetry
NTC negative temperature coefficient
PC personal computer
PIV particle image velocimetry
SNR signal-to-noise ratio
UDV ultrasonic Doppler velocimetry

NOMENCLATURES:

A the cross-section area of the duct [m^2]
a wave path [m]
$\mathbf{B}$, B vector and absolute value of the magnetic field correspondingly [T]
$\mathbf{b}$ the induced magnetic field [T]
C_d drag coefficient
c sound speed [m/s]
D distance between the measurement zones [m]
D_H hydraulic diameter of the duct [m]
d conductor (duct or aluminum plate) height [m]
$\mathbf{E}$ electric field vector [H]
e conductor (duct or aluminum plate) length [m]
$\mathbf{f}$, F vector density [N/m^3] and absolute value of Lorentz force [N]
G statistical average or expectation
H distance between the pump discs [m]
h width of the permanent magnet of the electromagnetic pump [m]
Ha Hartman number
$\mathbf{j}$ eddy current density [A/m^2]
k calibration coefficient
L characteristic length of bluff-body [m]
l Lorentz torque lever [m]
m conductor (the duct or the aluminum plate) width [m]
N interaction parameter
p pressure [Pa]
Q volumetric flow rate [m^3/s]
R distance from rotation center of the pump to the conductor [m]
Re Reynolds number
Re_m magnetic Reynolds number
St Strouhal number
s velocity slip
SD standard deviation value
T Lorentz torque value [N/m^2]
t time [s]
$\mathbf{u}$, u the vector and absolute value of velocity [m/s]
V voltage [V]
W heat losses [W]
w frequency [Hz]
α temperature coefficient

β blockage ratio
δ correlation coefficient
ϵ probability distribution function
η efficiency
Δl distance between Vives-probe electrodes [m]
Θ angle between UDV-transducer and main flow direction [grad]
μ magnetic permeability [H/m]
ν kinematic viscosity [m^2/s]
ρ density [kg/m^3]
σ electrical conductivity [S/m]
τ time-delay

Subscripts:

0 value at room temperature K
A amplifier
bb bluff-body
cr critical
d duct
E effective value
e basic emitting
L liquid metal
loc local
m mean value
mag magnetic
max maximal value
N nominal value
prf pulse repetition frequency
p related to pump
ref reference value
S related to sensor
sc scaled value
v vortex shedding
x main flow direction
y magnetic field lines direction
z gravity direction

1. INTRODUCTION AND PROBLEM DESCRIPTION

Flow rate measurements play an important role in different aspects of human life. Various flow measurement approaches are applying within engineering investigations and scientific researches, as well as in everyday use. Nowadays, various techniques [1] are used for flow rate measurements, and all of them can be divided into two big groups: direct and indirect methods. The direct methods presume collecting of a flowing liquid to a vessel, followed by an estimation of liquid's weight or volume. The implementation of direct methods is rather simple; the obtained results are of high accuracy, and therefore such techniques are usually used for flowmeters calibration [2], [3]. However, direct flow rate measurement methods have a significant limitation – they cannot be applied to a continuous processes, hence such measurements are not in extensive use.

In contrast, the indirect flow rate measurements gain widespread acceptance and are used among others for such research trends as power generation [4] or blood tests in medicine [5]. The indirect methods rely on a registration of effects of a different nature, produced by a flowing stream; the methods are adjustable for various liquids and conditions. The indirect flow measurement techniques include a large variety of optical, mechanical and electromagnetic methods.

The optical flow measurement methods [1] are non-invasive. Some of the techniques, for example particle image velocimetry (PIV) [6] or laser Doppler velocimetry (LDV) [7], require the addition of tracer particles to a liquid. Others, like molecular tagging velocimetry (MTV) [8], relies on molecules premixed or naturally present in a liquid. The particles movement is detected usually in a form of periodic images to obtain the velocity pattern of the flow. Another typical representative of the optical methods is the ultrasound Doppler velocimetry (UDV). The ultrasonic Doppler method utilizes the Doppler shift frequency of the echo, caused by signals reflected from moving tracing particles, to obtain instantaneous velocity profiles in a flow field [9]. In spite of possessing certain features of good measurement capabilities and non-invasive nature, optical flow measurement techniques have some disadvantages like complex signal processing, high cost and a requirement of liquid transparency. These methods rely on the presence of tracing particles in the flow that not only follow all flow velocity fluctuations, but also are sufficient in number to provide the desired spatial or temporal resolution of the measured flow field.

A big branch of the indirect flow measurement methods is based on probes offset or pressure change under the flow influence (Coriolis and drag effects, displacement techniques) [10]. Their advantages are the high accuracy and reproducibility, simple design and operation principles, as well as the independence to temperature fluctuation. Such flowmeters require direct contact with an investigated liquid, which puts restrictions on the liquid quality and the material of a sensitive element of the flowmeter due to presumable mechanical damage and corrosion.

One of the pressure-based flow measurement methods, which we would like to consider in more details, is a vortex-shedding technique [11]. The method is based on detection of vortical structures moving with a flow. The passing vortices are created artificially and are, in fact, flow perturbations that can be registered by pressure change on the pipe/duct wall or into a liquid directly. Within the classical vortex shedding techniques one typically utilize a piezoelectric pressure sensor to detect vortex shedding frequency. The application of such sensors is thresholded by the upper temperature limit of about 400°C [12]. However this limit can be extended [13], but then the flow measurements results become less accurate.

Nowadays a large variety of different flow measurement techniques are available, but progress always sets new challenges. As, for instance, in industry field, where flow measurement holds great importance. Here, velocity defines the properties of a final product, its further functional use; in industry of continuous liquid metal casting the flow measurement is still an unsolved problem [14] due to troublesome investigated medium (severe temperature and chemical conditions, flow distortions due to geometry, thermo-wells, misalignments, etc.). Most of the methods described above will fail in such severe and challenging conditions as the high temperature liquid metal flow. At temperatures over 500°C any measurement device submerged in the flow will be either molten or dissolved. Contactless optical techniques do not present an alternative, since liquid metals are opaque.

Another branch of the methods is electro-magnetic flow measurement techniques [15]. They can be applied for flow measurements of any type of conductive liquids, and provide flow and velocity estimations by measuring of potential difference or electromagnetic force. These methods can be either invasive or non-invasive. Vives-probe [16] method is a local velocimetry technique, it requires direct contact with liquid and is easy to operate and maintain. Lorentz force velocimetry (LFV) [17] can be applied when the investigated conductive liquid is hot, opaque or aggressive, hence standard methods (most of which are invasive) are not applicable. Until recently, the only requirement for the investigated liquid in the LFV was sufficient electrically conductivity. But this limitation has been already overcome and the method can be applied even for water [18]. The application of the LFV has been extended to industrial liquid metals flow such as molten aluminum [19] and steel [20].

The goal of the described research is to develop a design of the functional setup and the operating scheme for a particular technique – time-of-flight Lorentz force velocimetry [21]. The time-of-flight principle is in great request of different flow measurement techniques. It is used to detect a flow velocity by the time delay between spins exited by magnetic resonance tomography [22], [23], by heat pulses transported with the gas [24] or liquid flow [25], and consequent resistance change due to moving particles [26] or bubbles [27]. The time-of-flight LFV belongs to the group of indirect flow measurement techniques and its working principle combines both electromagnetic and vortex shedding operational concepts. The method allows to extend the vortex-shedding principle to opaque and aggressive liquids by the application of the LFV flowmeters to detect passing vortices. In the context of the method, vortices, created artificially or due to natural reasons, are moving with a flow. Their motion is detecting by two non-contact sensing elements (LFV flowmeters) distanced from each other by a certain interval. Every passing vortex creates flow disturbances that are detected by the both flowmeters with some time delay, which is equal to the time, the vortex needs to pass a known distance between the sensing elements. The flow rate of a liquid is proportional to the ratio between the distance between the elements to the time-of-flight

value. The classical LFV operational principle is based on the interaction of magnetic field and conductive fluid. The LFV method itself does not require a direct contact between the magnets and liquid under investigation, but depend on temperature, electrical conductivity of a liquid and magnetic flux density. The time-of-flight LFV combines advantages of vortex-shedding and LFV techniques and does not require information about physical properties of a liquid or temperature conditions.

The technique under study – the time-of-flight LFV – was previously investigated both experimentally and by numerical simulations. This simple principle does not require additional information about the liquid's properties, temperature or magnetic flux density. The researcher [28] was concentrated at the next points:

- Experiments on the time-of-flight LFV. Two types of the tests were performed within the investigation: in the first case the volume of a flow was used as an examined area, in the second the surface of a liquid was under analysis. The volume tests were provided within the duct flow of the liquid metal alloy of gallium Ga, indium In and tin Sn (GaInSn) for the next flow velocity range: from 0.18 m/s to 0.32 m/s; the measurement part of LFV was represented by a pair of permanent magnets and an one-dimensional strain gauge sensor. The applied magnetic system connected to the sensor had relatively high weight and strong inertness that limited response time of the system. The second experimental technique was applied to the surface of three types of liquid metals: GaInSn at room temperature, SnPbBi at 210°C and a liquid steel at 1700°C. Here a piece of foam or surface structure (waves) were used as the flow fluctuations to be detected.

- Numerical simulations were done to enlighten next several problems:

  – The investigation of the bluff-body as a generator of artificial vortices within the duct flow. The represented bluff-body had a cylindrical shape and was positioned vertically through the whole duct height.

  – The investigation of a magnetic field influence of two consequent permanent magnets on the flow pattern.

The research [28] highlighted the time-of-flight LFV as a flow measurement method, but both the experimental investigation and the design of applied measurement devices raised more challenges for further research than gave answers. To improve the time-of-flight LFV conception, to extend boundary of the method to different flow regime and to improve sensitivity of a measurement system, an advanced measurement system was developed and tested in liquid metal flow environment.

This thesis is devoted to the performance targets of the time-of-flight LFV technique for its prospective application in high temperature liquid metal flow. This work focuses on different features related to the design and operating capabilities of a time-of-flight Lorentz force flowmeter, and includes detailed description of the measurement setup and its practical operation. Optimal measurement system shapes and sensing technologies, operational schemes and signal processing aspects are summarized in the main part of the thesis. Experimental investigations confirm feasibility of the method to detect flowing vortical structures within a liquid metal, estimate the time delay between signal perturbations and to evaluate a flow rate

value. Although the method can be applied to a wide range of flow measurement situations, the thesis concentrated on liquid metal flow in rectangular closed duct. The strain gauge force sensors were applied for Lorentz force measurement. In the contrast to the existing works, three-dimensional force sensors were used to investigate the effect of flow disturbances in different directions on the time-of-flight LFV measurements. Numerous experiments were performed to analyze the operation of the prototype of time-of-flight Lorentz force velocimeter in laboratory conditions as well as different methods of producing vortices within flow are discussed within the current work.

The electromagnetic pump was investigated in detail as the device that has two main functions in the experiment operation:

- driving of the liquid metal flow (this leads to huge influence on the flow pattern from the pump side);
- measurement of the flow rate.

The theory on which time-of-flight LFV based is presented in the second chapter; the third chapter contains the description of experimental and calibration setups; in the fourth chapter the time-of-flight LFV technique described as well as measurement results are shown and the methods of the measurement data analysis are explained in details. Chapter 5 summarizes all the results and findings of the research.

2. THEORETICAL BACKGROUND

Here a short summary of the theoretical background of the project will be given; it forms the basis of the present measurement principle. Lorentz force velocimetry action is based on magnetohydrodynamics (MHD) principles [29]. Magnetohydrodynamics is the study of the interaction between magnetic fields and moving conducting fluids. The theory of electromagnetic flowmeters is a branch of applied magnetohydrodynamics that combines two classical disciplines: fluid mechanics and electrodynamics.

The qualitative understanding of the magnetohydrodynamic phenomena is highly important for the systematic analysis of LFV. As in the case of many electrical devices, the underlying principle of the electromagnetic flowmeters is the Faradays law of electromagnetic induction [15]. The law states that, when a conductor moves through a magnetic field of a given strength, a voltage is generated in the conductor that is dependent on the relative velocities between the conductor and the field. Faraday foresaw the practical application of this principle to the flow measurements of different liquids, since many of them are electrical conductors to some extent. A conventional LFV flowmeter consists of a permanent magnets pair or system, and a force sensor connected to the magnets pair. The magnetic field interacts with the moving charge carriers in the liquid by means of the Lorentz force, causing an electrical field $\mathbf{E}$ within the flow. The Lorentz force is generated in a conductor (here conductive liquid) as a result of the interaction of magnetic field $\mathbf{B}$ with eddy currents generated in the fluid under the magnetic field influence (Fig. 2.1) .

The operating principle of LFV can be understood better if one derives the basic scaling law for this device by invoking Ohm's law for a moving electrically conducting material in the following form [29]:

$$\mathbf{J} \quad = \quad \sigma(\mathbf{E} + \mathbf{u} \times \mathbf{B}). \tag{2.1}$$

In a conductive fluid the same law applies, only now the electric field is measured in a frame, which is moving with the local velocity of the conductor. In this case Lorentz force exerted on the free charges, which are ultimately transmitted to the conductor; in the frame of the project we are interested in a bulk Lorentz force acting on the flow. The Lorentz force acting on a single charge q is:

$$\mathbf{f} \quad = \quad q(\mathbf{E} + \mathbf{u} \times \mathbf{B}). \tag{2.2}$$

Here q is electric charge.

According to the statements in [29] we may evaluate the Lorentz force per unit volume:

$$\mathbf{F} \quad = \quad \mathbf{J} \times \mathbf{B}. \tag{2.3}$$

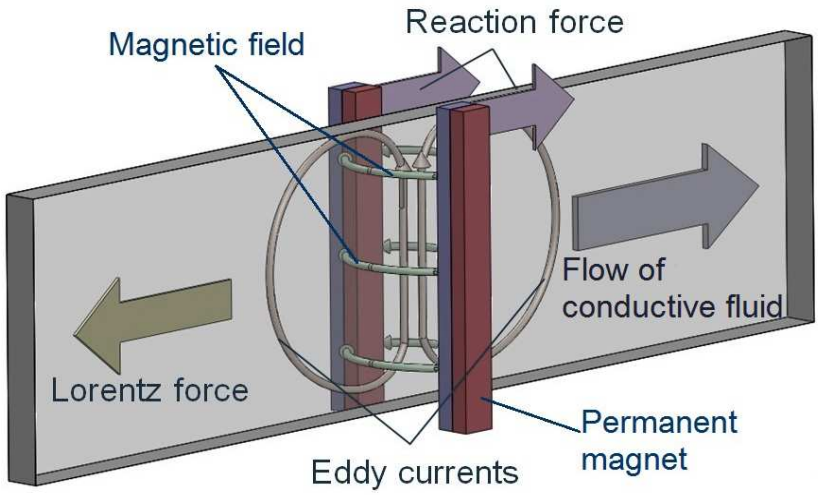

Fig. 2.1: Operating principle of LFV. The interaction of a conductive fluid and an applied magnetic field induces eddy currents within a conductive liquid. Lorentz force, which tends to brake the flow, is generated due to the interaction of the magnetic field and eddy currents. A reaction force equal in value to Lorentz force acts on permanent magnets and is proportional to the flow velocity.

An order-of-magnitude estimation, based on this law, readily shows that the component of Lorentz force along the direction of mean flow can be evaluated as follows [17]:

$$F \quad \sim \quad \sigma u_m B^2 L^3. \tag{2.4}$$

The reaction force is equal to the Lorentz force and opposite in direction and can be estimated by using (2.4); the equation shows that the force is proportional to the square of the amplitude of the magnetic flux density, which indicates that the construction of lightweight high-field magnet systems is of crucial importance for designing LFV with high sensitivity.

We consider the case when the magnetic field $\mathbf{B}$ influences the velocity $\mathbf{u}$ (via the Lorentz force $\mathbf{F}$), but the velocity $\mathbf{u}$ does not significantly perturb the field $\mathbf{B}$. To ensure that the field $\mathbf{B}$ remains unaffected by the conductor velocity $\mathbf{u}$, we can estimate the range of magnetic Reynolds numbers Re_m within the application of the LFV technique:

$$Re_\mathrm{m} \quad = \quad \mu\sigma u_m L. \tag{2.5}$$

In the most laboratory experiments and industrial processes, Re_m value for molten metal flows is in the range from 0.001 to 0.1. This occurs due to the velocity (in the range of 1 m/s) and characteristic size L (approximately 0.1 m) limitations. The essence of the low-Re_m approximation is that magnetic field, induced by the eddy currents $\mathbf{J}$, is negligible in comparison with the applied magnetic field. The presence of the current $\mathbf{J}$ has strong effect on the liquid metal flow, but the flow cannot significantly influence the magnetic field magnitude.

The duct used within the experiments has non-conductive walls hence all the current induced in the liquid metal closes through boundary layers in the fluid itself [30]. The

Lorentz force appears due to the interaction of the eddy current with the applied magnetic field. The force acts on the conductive liquid and change its velocity profile. Moreover, two boundary layers develop in the vicinity of the walls [31]. The thickness of the layer depends on a dimensionless parameter Ha – Hartmann number:

$$Ha = BL\sqrt{\frac{\sigma}{\rho\nu}}. \tag{2.6}$$

Hartmann number Ha is a measure for the strength of the electromagnetic forces in relation to the viscous forces.

Another important dimensionless parameter is the interaction parameter or Stuart number N; it provides the ratio of electromagnetic forces to inertia forces within a conductive liquid:

$$N = \frac{\sigma LB^2}{\rho u}. \tag{2.7}$$

The hydraulic diameter D_{H} [32] is a commonly used characteristic size in the case of flow in non-circular ducts. For the rectangular duct d×m, I used the D_{H} value as the characteristic size:

$$D_{\mathrm{H}} = \frac{2dm}{(d+m)}. \tag{2.8}$$

The volumetric flow rate Q can be calculated when the mean velocity u_{m} of a liquid and the cross-section area A of an used duct are known:

$$Q = Au_{\mathrm{m}}. \tag{2.9}$$

The section gave just a brief introduction to the theoretical background of the applied time-of-flight LFV technique; all additional information, including theoretical description of the applied methods, is provided directly at the next two sections.

3. EXPERIMENTAL FACILITIES

In this section the equipment for the current investigation of time-of-flight LFV measurement process is described. The description includes applied time-of-flight LFV facility and additional calibration setups. The functional components of each device are introduced in order to consider the structure and interaction between the facility components.

The main goal of the performed research is a development and experimental optimization of an operational measurement system for the time-of-flight LFV, as well as an application of the method for flow rate evaluation of liquid metal flow. The operational principle of the technique is based on a contactless detection of flow disturbances created by vortices, passing with flow. The vortices are detected by two identical sensing elements, positioned one after another along the liquid metal flow. The sensing elements have an electromagnetic nature of operation (Lorentz force measurement principle), and each of the systems is composed of a pair of permanent magnets and a strain gauge force sensor. As the result of the permanent magnets/liquid metal flow interaction, Lorentz force is generated. The moving vortices caused perturbations of the force, which are measured by commercial strain gauge force sensors K3D40. The sensors measure force in three directions; this fact allows to invesitage and compare the influence of vortical perturbations on flow in different directions. The main demand to the choice of applied force sensors was their sufficient resolution to detect a minor force variations due to the transit vortices. Another important component of the time-of-flight LFV measurements is a vortex generation method, several options of which are investigated in the separate section.

The experimental facility (Fig 3.1) consists of the closed rectangular duct with rectangular cross-section, filled with liquid metal alloy GaInSn. The flow within the duct is created by the contactless electromagnetic pump. The test section of the duct contains three flow rate and velocity measurement devices: time-of-flight LFV system, Ultrasound Doppler Velocimetry system and electro-potential probe. A water heat exchanger is mounted to control temperature conditions wihtin the duct. All measurement systems stay stationary while the liquid metal is moving. UDV and Vives-probe are connected directly to the duct and have proximate contact to the liquid metal. The time-of-flight setup is mounted separately on the 10 kg brick to avoid a mechanical contact to the duct. The brick is immersed into a sand box to suppress mechanical vibration transfered to the measurement system.

The description starts with the conditions and medium of experiments: the duct geometry and liquid metal characteristics. Both are disclosed in the first subsection. The medium description follows by flow excitation element – the electromagnetic pump which combines both pumping and flow measurement functions. The next subsection is devoted to a force measurement component of time-of-flight LFV – force measurement system. The two reference devices – electro-potential probe and UDV – are discussed at the end of the section. Each description consists of functional properties as well as short principal background of

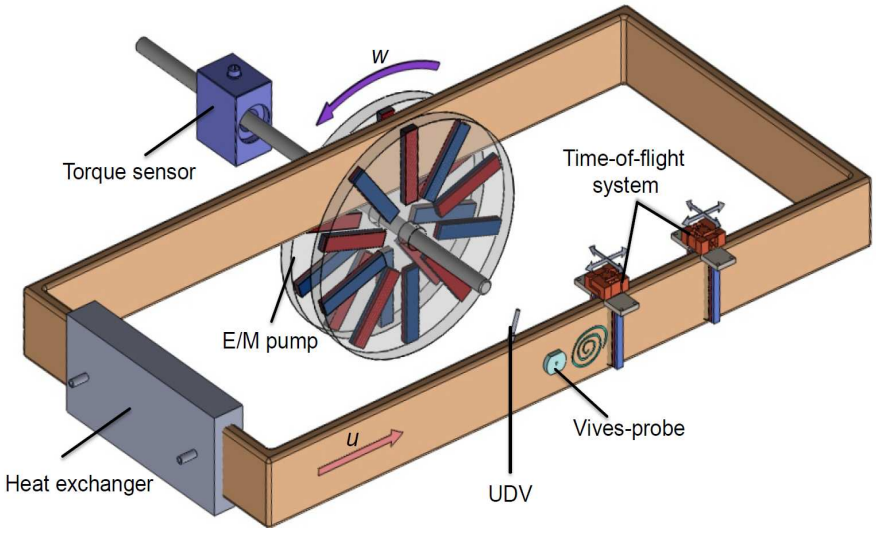

Fig. 3.1: Schematic of the experimental facility. The closed rectangular duct is filled with GaInSn alloy which is pumped by an electromagnetic pump. The test section allows to install several measurement devices including ultrasound Doppler velocimetry (UDV) setup, Vives-probe and the time-of-flight LFV facilitiy. The heat exchanger provides controlled temperature condition within the duct.

the setups.

3.1 Duct geometry and liquid metal characteristics

The experiment was performed within a liquid metal duct (Fig 3.2) with non-conductive walls and rectangular cross-section with dimensions 80×10 mm^2. The duct has rectangular geometry with two 800 mm long sections and two 400 mm short sections. The sections are connected at sharp corner 90° edges. The duct walls are made from a non-conductive material plexiglass and have 10 mm width. Outer surface of the walls is covered by epoxide polymer to prevent cracking of the plexiglass under fast change of flow pressure. The test section and zone near the electromagnetic pump are left uncovered for visualization of flow effects. An expansion tank, made from glass, is mounted at the duct end face to prevent its damage by temperature expansion of GaInSn.

In fact, the duct has several drawbacks: its geometry contains the described sharp edges which affect the flow by additional flow disturbances. The non-conductive walls create insulating conditions and eddy currents generated by the pump are circulating around the whole duct length. As a result, the eddy current and liquid metal flow themselves generate an additional mesurement noise.

Temperature control of the liquid metal is provided by combination of the temperature sensor and the heat exchanger. A commercial NTC thermistor P300 is applied for the temperature measurements; the sensor has measurement range from -40°C to 120°C with 0.1 K resolution and ±0.5 K accuracy. The heat exchanger presented as a copper plate, one side of which keeps in direct contact with liquid metal and another side is undergoing water

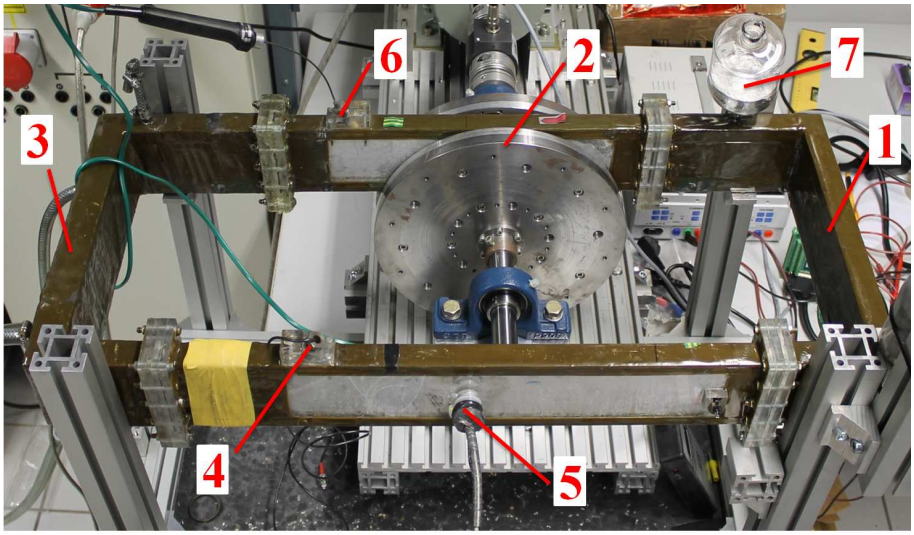

Fig. 3.2: The experimental closed duct (without the time-of-flight LFV part). 1 – rectangular duct. 2 – electromagnetic pump, 3 – heat exchanger, 4 – UDV-transducer, 5 – Vives-probe, 6 – temperature sensor, 7 – expansion tank.

washing. The flow rate of the water and hence cooling rate can be controlled by the gate valve (not shown at the picture).

The duct is completely filled with the eutectic alloy of gallium, indium and tin GaInSn, which is liquid at the room temperature. This fact makes GaInSn a very convenient medium for liquid metal experiments in laboratory conditions, whereas an experimental study on an industrial scale with hot metallic melts require significant efforts and expenses. The low melting point of the alloy enables the realization of the cost-saving model experiments, and permits detailed investigations of the flow structure and related problems with high grade of flexibility. GaInSn physical parameters at the room temperature and under temperature change are given in appendix A.

The alloy has significant advantage: it is not poisonous unlike mercury Hg, which produces high concentration of vapor even at the room temperature. The concentration of GaInSn vapor is negligible at the room temperature, hence it does not affect living organisms as well as there are no evidence of negative influence of the alloy on the skin. Nevertheless rubber gloves are recommended during work with GaInSn to prevent metal contamination. Furthermore, the gloves have important insulating function: because GaInSn is an electrical conductor, spills may provide a conductive path to a voltage-carrying equipment or any electrical grounds.

When GaInSn is exposed to outer atmosphere, it oxidizes and forms Ga_2O_3 that contaminates the alloy. The oxide has different physical properties than the original alloy, including lower alloy density and electrical conductivity. This can affect measurement results, hence the GaInSn alloy has to be cleaned periodically to remove oxide inclusions. Ethanol and hydrochloric acid solution can be mixed with the aspect ratio of two parts of acid and one part of ethanol [34] for GaInSn cleaning purpose. The solution should be mixed with a contaminated GaInSn (in reliance to final volume with 20% of the solution, 80% of Galinstan).

The acid reacts with Ga_2O_3 and deoxidization of Ga takes place. The ethanol, as a GaInSn-mixable liquid, plays role of an acid-solvent and allows the acid (non-mixable with GaInSn) disseminate upon the alloy, which intensify the deoxidaition. An appropriate ventilation and precautions are necessary during the cleaning procedure to exhaust the acid, ethanol vapors and hydrogen created as the reaction products.

Argon can be used as a cover gas to prevent oxidation during GaInSn storage and experiment. Unfortunately, argon atmosphere was technically impractical to apply within the provided investigation. Instead, the expansion tank mentioned above was used to collect oxides: according to relatively lower density, Ga_2O_3 tends to deposit into the expansion tank from the main duct due to buoyancy force.

The eutectic alloy GaInSn is chemically compatible with a wide variety of metals (except aluminum and its alloys), plastics, rubbers, and glasses at low temperatures [35]. The reaction between aluminum and GaInSn is strong, especially in the presence of water; aluminum details can be fully destroyed as a result of a direct contact with the alloy, which has to be taken into account under duct and measurement system designing processes.

GaInSn is an appropriate liquid metal for the model experiment. The alloy can be successfully used for tests in laboratory conditions and does not require a special temperature regime, which allows to decrease the application and energy costs. The tests should be carried out with proper precautions: using of rubber gloves for hands is necessary, and any direct contact between GaInSn and aluminum details should be avoided.

3.2 The electromagnetic pump

This section contains detailed description of the electromagnetic pump components. The working principle of the pumping function is represented in the first subsection and its additional application as a flow rate measurement setup is explained in the second. In the current project a new pump was utilized, and its alignment took significant part of the work (preliminary tests, calibration of measurement system). The investigation results are described in this section.

The pump discs are moving by an electro-motor; the pumping element has a shape of two discs with ten pairs of permanent magnets embedded in them. The discs are connected to the motor by a steel shaft where a torque sensor is mounted. The permanent magnets during the discs rotation generate pumping force acted on the liquid metal in the duct. The electromagnetic force pumps liquid metal into direction of the disc rotation. The torque sensor measures the torque that acting on the shaft by the pumping force.

3.2.1 Operation principle of the pump

The main function of the pump in the described experiment is its pumping function. The electromagnetic pump [36] is a non-contact flow-controlling device that pumps a conductive fluid (here liquid metal) in the duct by the generation of Lorentz force (Fig. 3.3) due to an interaction of the moving magnetic field and the conductor. The pump consists of two ferrous base discs with 350 mm diameter and 30 mm width each. Every disc contains ten embedded NdFeB permanent magnets with sizes 90 mm×20 mm×10 mm. The magnets are positioned in a such way, that the north pole of every magnet at one disc is directed to the south pole

of the magnet on the other disc. The liquid metal duct is enclosed in the gap between the two discs. No direct contact exists between the duct and the discs: the gap width is 37 mm, which is sufficient for 30 mm outer width of the duct.

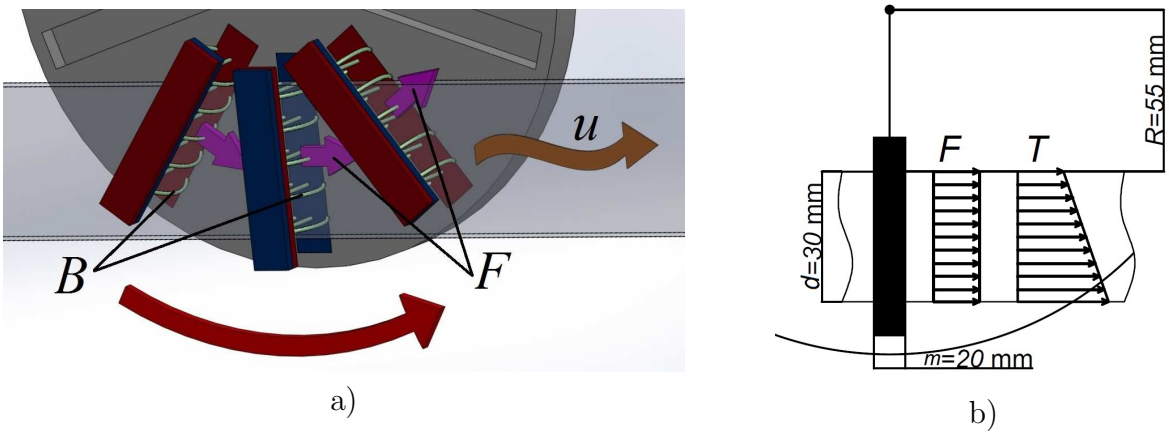

a) b)

Fig. 3.3: The schematic design of the electromagnetic pump (a); the force and torque created by one magnet (b). Lorentz force induced by the relative motion of the magnetic field and conductive fluid. The force pumps liquid metal in the duct positioned between the discs of the pump in the direction $\vec{u}$ (the second disc at the picture is transparent, only permanent magnets are shown). B – magnetic field lines; F – Lorentz force; T – torque; u – flow velocity.

The pump discs are arranged on a shaft connected to the electrical motor that puts them into a controlled rotation. An asynchronous AC motor with maximal rotation frequency 15.75 Hz and power 2.2 kW was used for the experiment. A frequency converter was applied to control the motor rotation frequency. Frequency converters are used to change frequency and magnitude of the grid voltage to a variable load voltage. Converters are especially useful in variable frequency AC motor drives.

The maximal magnetic field value in the middle cross-section of the duct is reached 0.305 T, as was obtained experimentally. The duct should be positioned precisely in the middle of the gap between the pump discs. The rotation of the discs and hence the embedded permanent magnets generates a time-dependent magnetic field within the gap between the discs, moving with the velocity:

$$u_{\mathrm{f}} \quad = \quad e_{\mathrm{p}} w_{\mathrm{p}}. \tag{3.1}$$

The rotation of the discs induces Lorentz force within the liquid metal as a result of relative motion of conductor and magnetic field (2.3). In other words, the generated Lorentz force creates a pumping effect on GaInSn. The imposed magnetic flux density B orthogonally oriented to the liquid metal flow. The field B rotates uniformly and varying sinusoidally with time at each point of the duct due to the discs rotation (Fig. 3.4). The eddy currents within the liquid metal alloy induce liquid metal flow with the mean velocity u_{f}, which, due to the friction in the fluid, is slower than the speed of the field u_{f} motion. The rotation rate directly influences the velocity. Electromagnetic pumping effect creates liquid metal flow of turbulent and transient regimes (from Re 4000). Laminar regime of the flow is not reachable due to the lower limit of the motor rotation frequency.

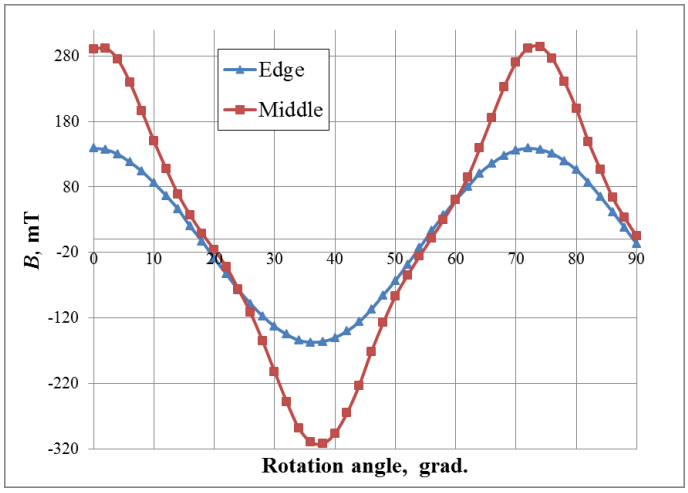

Fig. 3.4: The magnetic field distribution in the pump gap. The magnetic field distribution in the pump gap. The magnetic field distribution in the middle cross-section between the pump discs along the circle with the radius at the middle line of the magnets.

3.2.2 Flow rate estimation

The applied pump can be additionally used for the flow rate measurements of pumped liquid. For this purpose, the torque sensor was applied to measure torque created by the integral pumping (Lorentz) force. This method called Lorentz Torque Velocimetry (LTV). The rotary magnetic field generates flow-driving force that pumps the liquid and acts on the pump shaft as a back reaction. The commercial strain gauge torque sensor is mounted on the shaft to measure the torque that is exerted into the liquid or solid conductor. The liquid metal flow rate is expected to be proportional to the measured torque and estimated as:

$$Q = \frac{k_{\mathrm{p}} T}{\sigma B^2 l}. \tag{3.2}$$

The calibration factor k_{p} depends on the following LTV characteristics: magnetic field distribution, transversal end effects, pump and duct geometry, etc. But even precise estimation of the coefficient and measurement of the torque will not give automatically the precise flow rate value without considering another important parameter – the temperatures of the liquid metal Θ_{L} and magnets Θ_{mag}. After taking into account temperature factor, the equation (3.2) can be changed to:

$$Q = \frac{k_{\mathrm{p}} T}{\sigma(\Theta_{\mathrm{L}}) B^2(\Theta_{\mathrm{mag}}) l}. \tag{3.3}$$

In the applied LTV we use NdFeB permanent magnets. Their magnetization depends on the temperature, as was experimentally proved by Kolesnikov et al. [19]. Magnetic induction of the block magnet was measured at the different temperature values in the range from 293 K till 363 K. As the result of the tests, the linear dependence of the magnetic field from the temperature in the given range and coefficient α were estimated:

$$B(\Theta_{\mathrm{mag}}) = B_{293}[1 - \alpha(\Theta_{\mathrm{mag}} - \Theta_0)]. \tag{3.4}$$

The temperature coefficient is determined to be α=1.116×10^{-3}K^{-1}. Therefore, temperature must be permanently measured or controlled during the flow rate measurement. The graphical dependence of the electrical conductivity of GaInSn $\sigma(\Theta_{\mathrm{L}})$ is given in Appendix A.

The next two types of experiments were performed within the pump research: solid, where aluminum plates of several sizes were positioned in the discs gap; and liquid metal experiment, where the duct with GaInSn was used. The measurement technique includes application of the electromagnetic pump both as the flow-controlling and the flow-measuring device.

The experimental setup comprises of the flow driving unit, represented by the electromagnetic pump, and a measurement unit, represented by the digital torque sensor (Fig. 3.5).

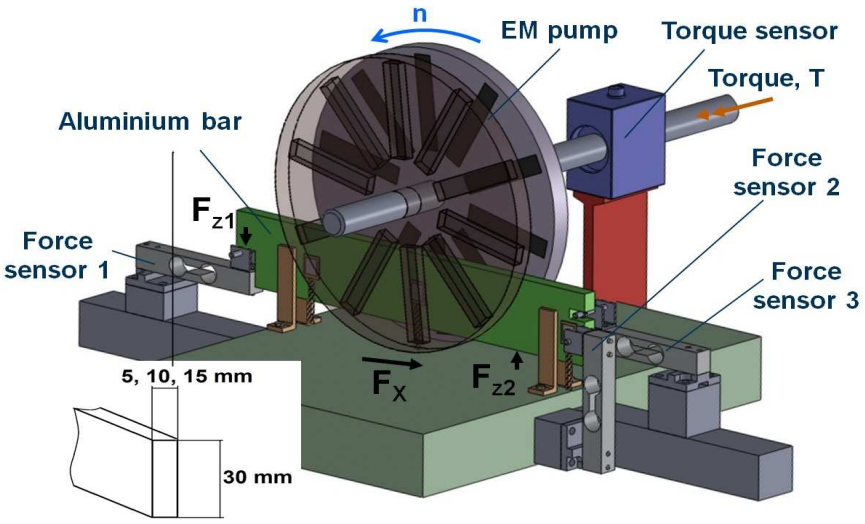

Fig. 3.5: The principal scheme of LTV solid test. Electromagnetic pump rotation frequency is controlled by the electromotor; created momentum is measured by the torque sensor on the pump shaft. For this test aluminum plates are used instead of the liquid metal and Lorentz force is measured simultaneously by three force sensors.

The proposed method of flow rate measurement is a prospective technique that can be applied in cases of the high temperature liquid metal examinations. The LTV can be used to measure flow rates of a time-variable flow. At the moment the experiments with the LTV prototype are underway and the device has shown stable and reproducible results described below.

3.2.3 Solid tests

Preliminary calibration is necessary before mounting of the Lorentz torque device to the experimental duct. First of all we need to estimate a torque lever l or the distance from the center of the pump shaft to the point where integrated Lorentz force is acting within the duct. The value is essential for the Lorentz force calculation and flow rate estimation by equation 2.4. To obtain l value one needs to perform the next calibration procedure: to

measure Lorentz force F and torque T simultaneously. The relation of the measured values gives us the lever magnitude:

$$l = \frac{T}{F}. \tag{3.5}$$

Direct measurement of the force that acts within a liquid metal is a complicated task. Therefore so called solid calibration was performed, where a solid metal used as a conductor instead of the liquid metal duct. For this purpose conductive and non-magnetic aluminum plate was used. It is well known, that the conductivity of aluminum ($\sim 3.5 \cdot 10^7$ S/m [37]) is one order of magnitude higher than conductivity of GaInSn ($\sim 3.5 \cdot 10^6$ S/m). So the results obtained by the calibration are well correlated with the parameters of the liquid metal duct with corresponding scaling.

The solid calibration procedure was carried out as it is shown on Fig. 3.5. For the Lorentz torque device calibration, the aluminum plates were inserted in the discs gap and the generated Lorentz force was measured by three separate force sensors. The sensors 1 and 3 measure component of the force in z direction (F_{z1}, F_{z2}) from the both sides of the pump (the enter and exit zones). In this case the two sensors are used to prevent an influence of the gravity force on a result. The sensor 2 measures the x-component (F_x) of the generated Lorentz force. The resulting force was estimated as a vector product of F_x and the mean value of F_{z1} and F_{z2}. A strain gauge torque sensor was chosen for the torque measurements because of their long-term stability with static loads and high precision characteristics.

The total force was calculated from the two force components (x and z) by a superposition principle and the resulting Lorentz force with the measured torque used to determine the value of the lever for an every dimension of the aluminum plates.

The plates of different dimensions (from 30×5 mm^2 to 30×15 mm^2) were used for calibration. They were positioned in the middle of the gap between the pump discs, hence an applied magnetic field was distributed along the duct section and there was expected no significant y-component of the Lorentz force.

The figures 3.6a and 3.6b show the measurement results of a resulting force and a torque estimation. Graphs present a scaled representation of the measured value. The mean experimental levers value means that the Lorentz force is applied at this specific distance from the shaft center. The obtained value is less than the distance from the shaft middle to the magnets center due to the shift to axis of the maximal B value. It acquires because in the case of a round pump we have several magnets, which influence the plate at the same time and only part of them are acting perpendicularly to its long side. All other inserted magnets have different levels of inclination, i.e. their affected zone is higher than the middle line of the plate. The motivation for the measured Lorentz force and torque re-scaling is explained hereafter. The Lorentz force and the torque produced by the force increase with enlarging of the cross-section area of the conductive material. This fact can be explained as follows: the change of the aluminum plate width causes an alteration of three parameters: the first one is the volume of the conductive material that is under an influence of the magnetic field, the second parameter is the plate full electric resistance to an induced eddy current and the last one is the air gap between the discs of the electromagnetic pump. Besides, magnetic field distribution between the discs is not homogeneous: it decreases from the discs surface to the middle of gap. Hence the magnetic field that passes through a thicker plate has higher

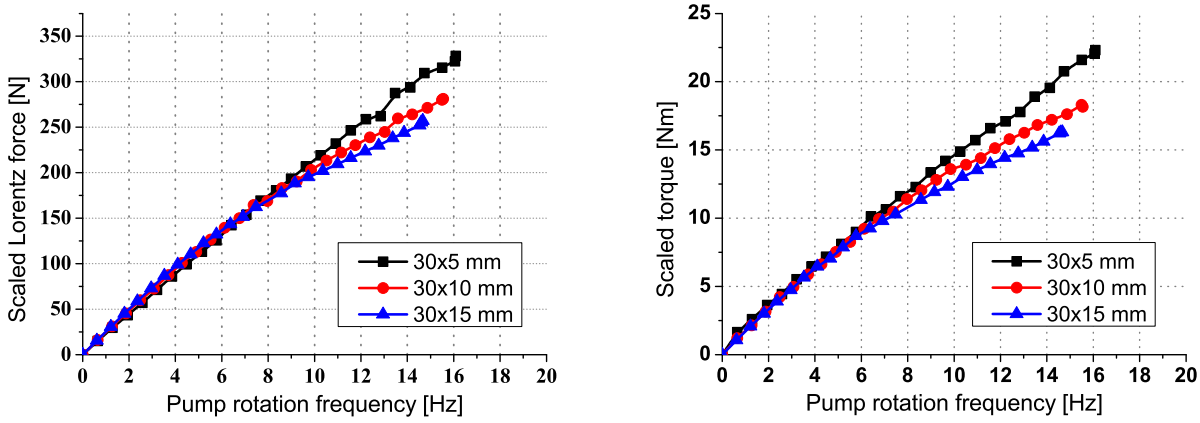

a) b)

Fig. 3.6: Results of solid LTV tests. (a) The measured Lorentz forces scaled for different aluminum plates dimensions in relation to rotation frequencies of the pump. (b) The measured torque scaled for different aluminum plates dimensions under variable rotation frequencies of the pump

integrated magnitude than in the case of a thin one.

The scaled values of the Lorentz force and torque F_{sc} and T_{sc} can be obtained by multiplication of their measured value to the ratio of the width of the gap between the pump discs H and the width of the aluminum plate a measured at each moment of time:

$$F_{\mathrm{sc}} = \frac{FH}{m}. \tag{3.6}$$

and

$$T_{\mathrm{sc}} = \frac{TH}{m}. \tag{3.7}$$

The difference between the demonstrated scaled values of the measured torque and Lorentz force under a relatively high rotation frequency of the electromagnetic pump is caused mainly by the change of magnetic Reynolds number Re_{m} for aluminum plates (up to 1.5). Increase of the aluminum plate width results in the increase of the parameter Re_{m} estimated by (2.5). This described magnification is in evidence due to the increase of the characteristic length scale L, which indicates the dimensional ratio of an electromagnetic interaction. As it is known from magnetohydrodynamics [29], the larger values of magnetic Reynolds number Re_{m} indicate the stronger induced magnetic fields b that act against the applied primary field B. This gives rise to decrease of the overall magnetic field that contributes to the Lorentz force. Therefore the measured values of the torque T and Lorentz force F are lower in the cases of thicker plates (here 15 mm) under high rotation frequencies (here above 10 Hz).

According to the presented geometry of the plates and size of the pump, at each moment of time three full magnets are influencing the aluminum plate (Fig. 3.3). The height of the permanent magnets is higher than the duct height, so one can assume that permanent

magnets intersect the whole duct height. Such observation allows to evaluate the Lorentz force and the momentum as the integration in the interval of the plate height:

$$F = \int_R^{R+d} \sigma B^2 w_\mathrm{p} dm\mathrm{d}r, \tag{3.8}$$

$$T = \int_R^{R+d} \sigma B^2 w_\mathrm{p} dmr\mathrm{d}r. \tag{3.9}$$

The width of the permanent magnet m and the height of the aluminum plate d were taken as the characteristic length values. The r represents the distance from the pump discs center to the point of integrated Lorentz force application (lever as a variable). According to the evaluation, the received lever value is equal to $(R+d/2)$ or 70 mm, which is 3 mm higher than the experimentally obtained one. This difference occurs due to the fact that during the real pumping cycle not just three, but four permanent magnets can simultaneously influence the aluminum plate (at specific positions of the pump). In this case at least one of the magnets acts only by part of its length, hence an application point of the integrated Lorentz force is displaced to the pump center.

The final lever values were calculated by (3.5) from the experimental torque and Lorentz force values for different sizes of the aluminum plates. All plates were positioned in a such way that their symmetry line did coincide with the middle of the vertically positioned permanent magnet of the pump. Obtained results show sufficient repeatability and have mean value $l = 67$ mm. The identical tests were provided for the aluminum plates of different sizes, including the plate with the size similar to the duct (80×10 mm^2). The results of the lever estimation are presented in the table 3.1.

Tab. 3.1: Lever values for the aluminum plates of different sizes under the solid tests of the electromagnetic pump.

Plate size [mm^2]	Mean lever value l [mm]	Plate size [mm^2]	Mean lever value l [mm]
–	–	80×5	66.7
50×10	66.4	80×10	66.8
50×15	66.5	80×15	66.3

Another interesting effect that was observed during the experiments is a pump rotation frequency limitations occurring under the examinations of the aluminum plates with 15 mm width. After the reaching of some certain limit value of frequency w_p there was no possibility to increase the w_p even by a higher power application to the motor. This effect can be caused by overshoot of magnetic Reynolds number Re_m over one or by a relatively fast increase of temperature.

A rotating magnetic field creates eddy currents inside the aluminum plates. The eddy currents dissipate part of their energy by Joule heating and this leads to an increase of temperature of the aluminum plates. The change of temperature was detected experimentally by three thermocouples type K connected to the plates directly within the magnetic field influence zone. A high temperature change per relatively short time within one test can cause significant increase of a measurement error, because such temperature change influences an electrical conductivity of any conductor [19] (here the aluminum plates). This fact prompted us to short the measurement duration to less than one minute for a test to decrease measurement error. But even though the observed temperature variations reached 100 K for the thin plates (here 5 mm) tests.

The temperature increase depends on rotation frequency of the pump discs. With the change of a pump rotation frequency we can observe rise of a temperature value. According to [29], an imposed high-frequency magnetic field generates heat at a rate of $(B^2/4\mu)w_\mathrm{p}\delta$ per a unit surface area, where δ is the skin depth and w_p is the rotation frequency of the pump. The skin depth δ can be estimated by the following equation:

$$\delta \quad = \quad (\frac{2}{w_\mathrm{p}\sigma\mu})^{1/2}. \tag{3.10}$$

The skin depth δ change of the aluminum plates as well as a rise of Re_m under influence of the rotating magnetic field are shown on Fig. 3.7a and Fig. 3.7b. The magnetic field diffuses inwards a conductive medium by a distance of under $(2t/\sigma\mu)^{1/2}$ in a time t, which caused the skin effect: the ability of a conducting medium to exclude high-frequency fields; i.e. the field will penetrate only a finite distance into the conductive medium. The skin depth defines the penetration layer. In all our investigated cases the skin depth exceeds the half of plate width and does not influence significantly the pumping force.

3.2.4 Liquid metal tests of electromagnetic pump

For evaluation of the second calibration parameter – the experimental coefficient k_p – one should perform fluid experiments with the liquid metal of interest. This calibration factor depends on a number of specific experimental parameters: the aspect ratio of the flow duct, the actual geometric arrangement of the permanent magnets, electromagnetic and turbulent friction in liquid, heat losses due to Joule heating, etc. The influence of the parameters and their physical background is precisely analyzed by empirical model, suggested in [39].

For successful calibration procedure one needs to measure the same value at least by two methods - one is the method under calibration and the second one is a reference. The velocity measurement device that was applied as the reference, is electro-potential probe [4]. The facility allows us to measure local two-component velocity u_max in the middle of our duct. To transform the obtained velocity value to volumetric flow rate one can apply (2.9). To improve the accuracy of calculations we used mean velocity approximation – $0.85u_\mathrm{max}$ – instead of local velocity value. Here 0.85 is an empirical coefficient calculated by analysis of turbulent velocity profile in our specific duct, which well corresponds to standard hydraulic ratio 0.82 for developed turbulent duct flow [40].

The result of volumetric flow rate estimation is presented on Fig. 3.8a. As one can clearly see, the flow rate change has non-linear character. This effect may be caused by different

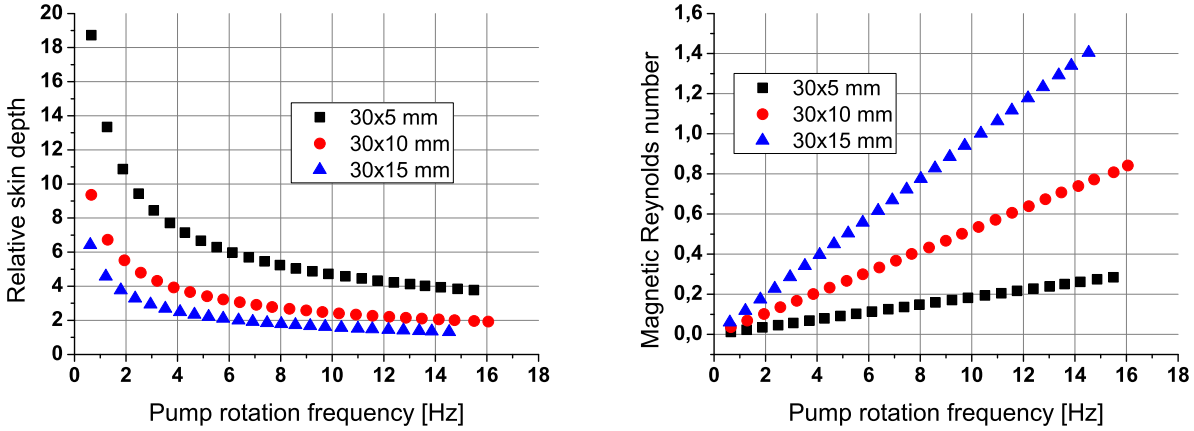

a) b)

Fig. 3.7: Skin depth (a) and magnetic Reynolds number (b) for three aluminum plates with width 5 mm*, 10* mm*, 15* mm*. Calculated values of the skin depth and magnetic Reynolds magnetic number for the different plates dimensions in the relation to the rotation frequency of the pump.*

reasons such as moderate Re_m influence, skin effect, power and friction losses due to pump operation, etc. Impact of first two factors was evaluated by (2.5) and (3.10) correspondingly, the liquid metal flow parameters are shown at Fig. 3.8a, 3.8b. Moreover, skin depth is shown as relation to the half-width of the duct $m/2$ - 5 mm. According to obtained data, the influence of both parameters on flow rate non-linearity can be neglected since $Re_\mathrm{m} \ll 1$ and $\delta \gg m/2$. It means that the advection of magnetic field is small relative to its diffusion and eddy currents penetrate whole width of the duct without let or hindrance.

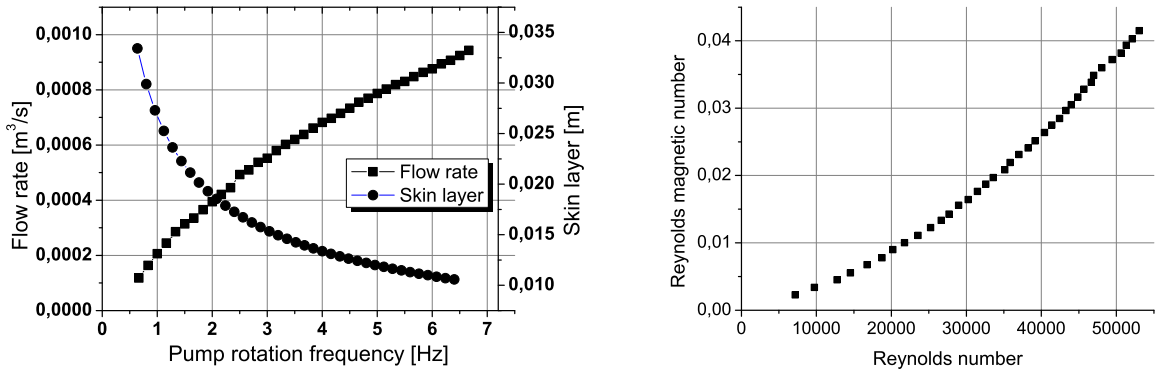

a) b)

Fig. 3.8: Flow rate of liquid metal under different rotation frequency of the electromagnetic pump and relative skin depth (relation of skin depth value to duct half-width) (a). Experimentally obtained magnetic Reynolds number (b)

To investigate the influence of the other parameters to flow rate we use interaction param-

eter N (2.7). Due to relatively high value of magnetic field, N of LTV reaches an intermediate magnitude (Fig. 3.9a) and creates a strong anisotropy in the flow. Which, in turn, leads to the increase of turbulent friction losses. By taking into account the hydraulic losses due to duct geometry and heat energy losses, the electromagnetic pump efficiency was derived (Fig. 3.9b).

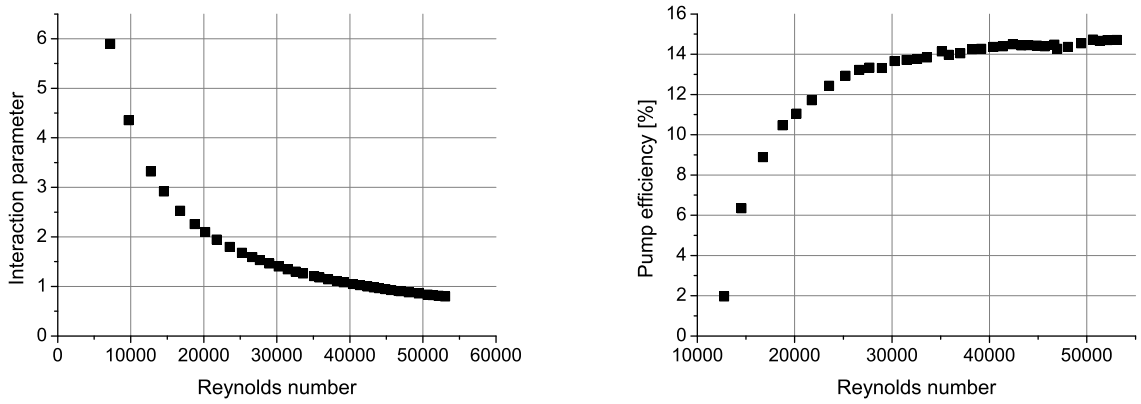

a) b)

Fig. 3.9: Interaction parameter under different Reynolds number of the flow (a). Pump efficiency considering hydraulic, turbulent friction and heat losses of the pumping process (b)

Figure 3.10a shows the dependence of measured torque on the liquid metal flow rate. The relation between torque and flow rate for presented geometry shows parabolic behavior, hence liquid metal flow rate depends linearly on the square root of torque value:

$$Q = 0.001(0.6T - 0.103)^{1/2}. \tag{3.11}$$

The relation has non-linear character due to the increase of hydraulic losses when rotation frequency is increased. The losses occur because of the pump geometry: the permanent magnets under movement at the duct influence zone generate vortices in the liquid metal, in particular within the duct at the pump entrance and exit regions. Such vortex requires a part of hydraulic flow energy and was visualize by adding of 4% acid solution to the duct as it is shown at Fig. 3.10b. This drawback of decreasing the flow energy can be avoided by "omega" duct configuration [41] which, in fact, requires significant reconstruction of the duct or loop.

The difference between linear flow rate dependence on torque expected in (3.2) and obtained by experiment relation (3.11) takes place on the ground of described vortices generation within duct; effect should be taken into account by careful calibration factor evaluation, that will include hydraulic losses influence. The described system of electromagnetic pump and torque sensor can also be applied without pump driving. In this case the device shall work as rotary permanent magnet flowmeter [42].

As was expected [42], the electromagnetic pump efficiency is less than the usual efficiency of mechanical pumps and reaches 15%. On the initial curve section with relatively low Reynolds number one can observe rapid efficiency increase until pump reaches its optimal operation regime. The optimal working parameters of every type of pump are well determined

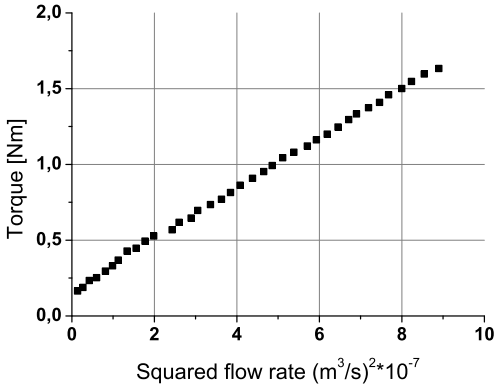

a)

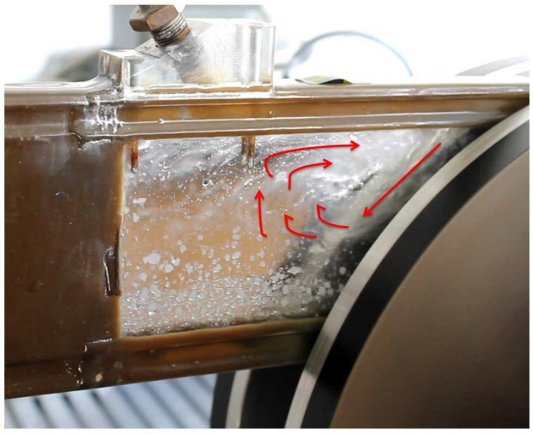

b)

Fig. 3.10: Dependence of experimental torque on liquid metal flow rate values. Each point represent a combination of the torque measured by the commercial sensor and value of the flow rate evaluated by Vives-probe tests during the same experiment.

by the intersection of its pressure-flow rate (pQ) characteristics and system characteristic curve (Fig. 3.11a). The system characteristic graphically display the relation between developed pressure and generated flow rate and characterizes flow resistance within a duct. The intersection of pQ curves and system characteristic gives us information about so-called pump operation points. They are presenting optimized modes in case of most suitable balance between pump efficiency and the characteristic of duct-pump system.

All investigated parameters have their influence on the LTV work, hence they should be included in resulted calibration factor. Raw experimental coefficient k_p is calculated by:

$$k_\mathrm{p} = \frac{Q\sigma B^2 l d}{T}. \tag{3.12}$$

The total pump efficiency consists of hydraulic energy of liquid metal flow in the closed loop pQ and Joule losses that are defined as:

$$W = \frac{\sigma(B^2 u_\mathrm{f} s)^2 e_\mathrm{d} d m k_\mathrm{p}}{2}. \tag{3.13}$$

Considering the losses, the electromagnetic pump efficiency is:

$$\eta = \frac{pQ}{(pQ + W)}. \tag{3.14}$$

The observed law of k_p distribution is not well-ordered (Fig. 3.11b), thereby can be presumed that k_p depends on pump working parameters at each operating mode and cannot be assumed as an universal experimental coefficient for the every regime of pumping. To take the pump characteristics into account we chose the pump efficiency as a congregate value. The resulting experimental coefficient was estimated as $k_\mathrm{p}\eta$. The combined experimental coefficient shows relatively stable linear behavior after the reaching of optimal operation

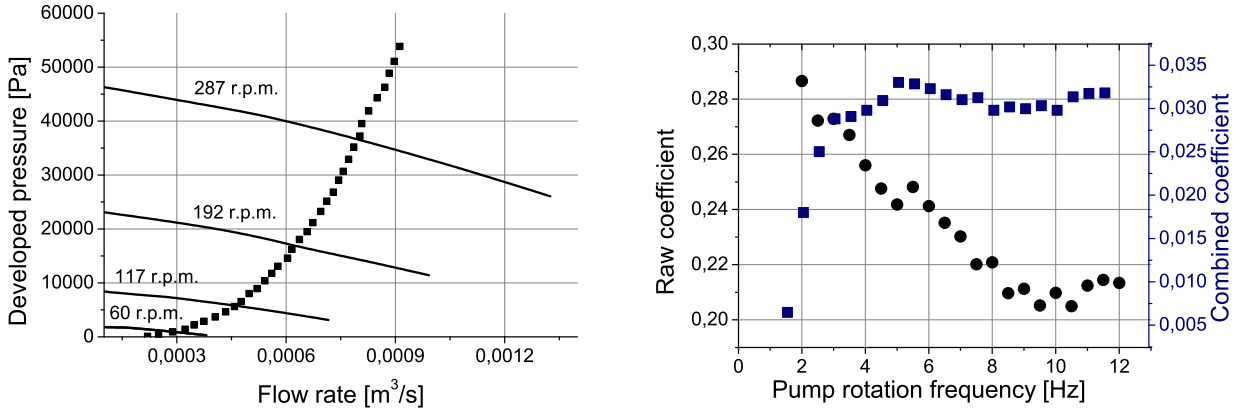

a) b)

Fig. 3.11: Qualitative characteristics of the pump. (a) pQ characteristics of the pump at different rotation frequency (lines) and characteristic of the system pump-duct (dots). Their intersections give optimal operating parameters. (b) The comparison of raw experimental coefficient k_p (circles) and the combined ηk_p (squares) that includes efficiency of the pump η

mode than the raw coefficient k_p. The mean value of the obtained $k_\mathrm{p}\eta$ can be defined as the general calibration coefficient for our specific combination of the pump, duct geometry and liquid metal.

Understanding of pumping process is crucial for prediction of the liquid metal flow behavior in the closed duct and its application as flow rate measurement setup, which gives additional possibilities for the calibration of time-of-flight LFV.

3.3 System of Lorentz force measurement

As was described before, the Lorentz force occurs in liquid metal as a result of its interaction with an imposed magnetic field. As a secondary consequence of the interaction, a reaction force acts on the source of magnetic field – the permanent magnets. Measurement of the generated reaction force is one of the most challenging parts of the time-of-flight LFV experiment.

3.3.1 Force measurement

The applied measurement system must be accurate enough to detect small force perturbations generated due to vortex movement, hence the force sensor with high resolution characteristics is required. In principle, any sensor, which can detect the periodic fluctuations of velocity or pressure between 1 Hz and 1000 Hz, can be used to detect the passing vortices. An invasive operational principle of the most pressure measurement methods make them inappropriate for the liquid metal application. The dynamic characteristics of the sensor should be sufficient to detect vortices of large frequencies range of appearance. Another requirement to the force sensors is ability to measure forces of all three dimensions at the same time. The turbulence in liquid metal flow, as well as vortices, have three-dimensional structure within the duct.

This consideration allows to affirm that the flow perturbations can have different direction and created Lorentz force will have non-homogenious spatial distribution within the duct. According to this, the reaction force disturbances can have any direction as well as vortices, and the force sensor should be able to measure all components of them. The further core requirement to the force sensors for laboratory tests by time-of-flight LFV are: high sensitivity and accuracy in a low forces measurement range. The level of Lorentz force in the current laboratory conditions does not exceed 10^{-2} N. In the case of time-of-flight LFV, applied force sensors have to be even more sensitive, because the flow disturbances as a result of vortex movement are lower than 10^{-3} N. In order to satisfy the requirements, the commercial three-dimensional strain gauge sensors K3D40 (Fig. 3.12a) were chosen. The sensors have the next characteristics: declared sensitivity value 40 N, rated output k_S=0.5 mV/V and measurement range F_N=2 N (ME-Messysteme, Germany). Three-component force sensors allow to not only detect different directions of the flow perturbation, but also make it possible to investigate the ratio of different velocity constituents in a turbulent flow. The operation principle of

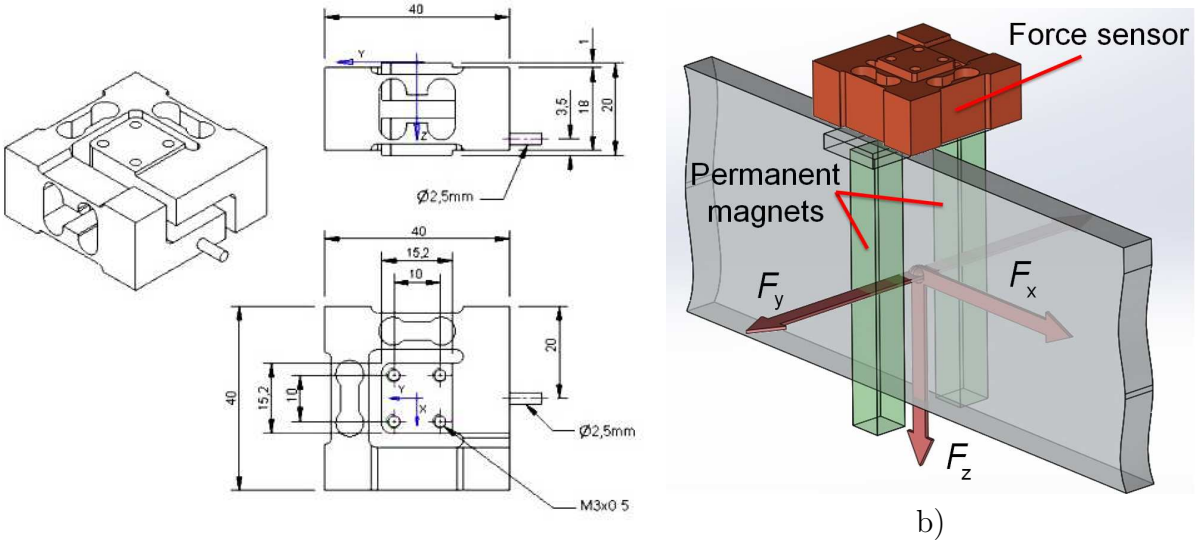

Fig. 3.12: The force sensor geometry (a) and measurement schema of time-of-flight LFV system (b) that included the force sensor coupled with the pair of permanent magnets. All dimensions are given in mm*, F_X, F_Y and F_Z are integrated force components measured by the force sensor*

strain gauge force sensors is measurement of a voltage alteration due to resistance changes under the application of force or strain [43]. Strain gauges in general are devices which utilize piezoresistive properties (i.e., change in resistance due to strain) of an elastic material: metal, alloy, semiconductor or cermet. This change in resistance takes place both due to the change in the resistive element dimensions as well as due to the change in the material resistivity. The resistance change can be measured by inserting the strain-sensitive resistor in one of the arms of a Wheatstones bridge. Standard strain gauges can sense the displacements as small as 5 μm, what makes them capable to detect small changes of an applied force. As sensors material, aluminum was selected because of its non-magnetic nature and smooth stress-strain

behavior in the measurement force range.

An additional calibration procedure was provided to test the force sensors respond to applied weight: each measurement direction of sensor was gradual loaded with standard balance weights from 1 g to 50 g mass. Each mass was loaded separately and the induced reactions of all three force components were examined. (Fig. 3.13). The value of measured

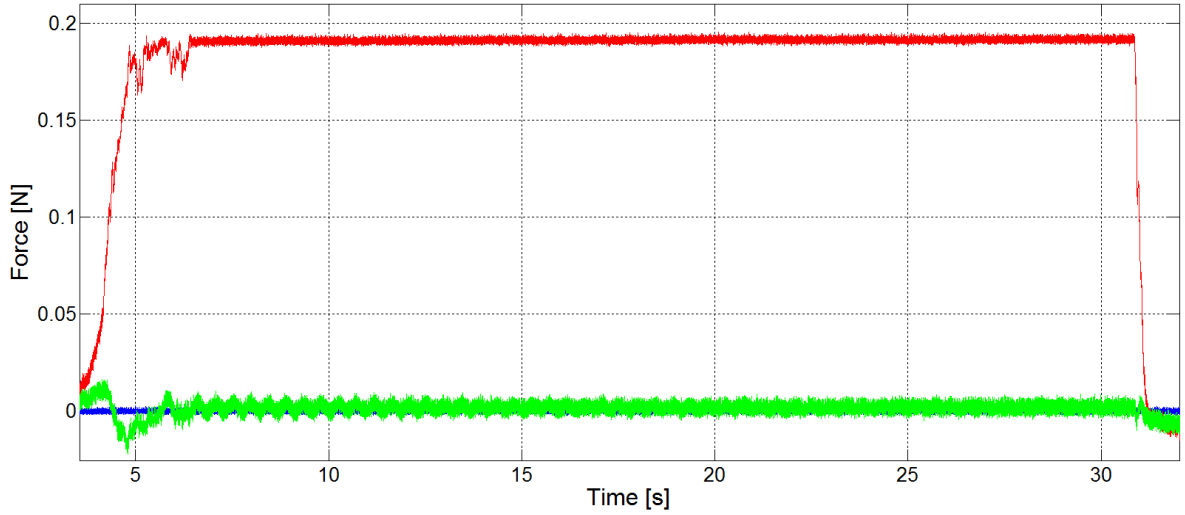

Fig. 3.13: The scheme of the force sensor calibration. Sensor was loaded with 20 g *mass applied from y-direction. Different colors corresponds to next force components: red – y-component, green – x-component and blue – z-component.*

force is slightly displaced (near 4%) from expected rate of 0.2 N due to joint assembly between the sensor and the applied weight. The connection was done by 0.4 mm flexible thread: the mass was hanging on helix screwed down to sensor. The loading of one force direction provokes the response on other component due to coupling between the sensor elements. The observed overlapping value did not exceed 1% declared by the producer.

The Lorentz force, generated within the intersection of the applied magnetic field and the conductive flow, have effect on both magnets at the same time as a consequent reaction force. The main component of the measured force the integrated reaction force F_X acts on the middle point between mass centers of the permanent magnets. The orthogonal component of the reacting force F_Y is caused by multidirectional turbulent fluctuations within the flow and the imperfection of magnets positioning according to flow: disalignment or asymmetry. The value of F_Y could reach significant values, up to 10% of F_X, so accurate mounting of the sensors is necessary to obtain a qualitative force signal. The vertical component F_Z of the reaction force is caused mostly by gravitational force due to the weight of fastening system with permanent magnets.

Each force sensor was rigidly connected to a pair of permanent magnets (Fig. 3.12b) that work as a technologically simple source of the magnetic field. The magnets were positioned from both sides of the duct. To induce high value of Lorentz force the magnetic flux density has to be as high as possible which is reachable with increasing of the magnets size. But enlarging of magnet leads to increase of magnet weight which can overload the force sensor.

The magnet size was optimized according to the created magnetic field and feasibility of force sensors. Each magnet should have less weight than half of measurement range of the force sensor. What is more, the magnets weight should be taken into account jointly with a connection system between the force sensor and the magnetic pair, hence weight of every permanent magnet has to be not more than 40% of measurement range of the force sensor. Otherwise a shielding construction has to be mounted around the sensor to prevent overloading of strain gauge elements.

The aluminum construction was connected to a 10 kg stone which was positioned in a box with sand. The system is applied to prevent an influence of mechanical oscillations on the measurement system and to reduce a noise level. A sand layer is usually used to absorb power or vibrations through inter-particle friction [44]. The sand box was constructed from wood and mounted above two layers of 2 cm reinforced rubber.

The permanent magnet pair must cover all the hight of the duct to detect flow perturbations which can be randomly distributed in the liquid metal. In the goal experiment the magnetic field was generated by two rectangular permanent NdFeB magnets with the cross-section 10×10 mm^2 and 90 mm long. The weight of each magnet was 73 g which is sufficient according to the force sensors feasibility.

Three types of the measurement system combined the force sensors and permanent magnets were tested within the research. One of them had relatively high weight and included a shielding system for the sensors protection, two others were lighter and mounted directly with the force sensor.

The first connection system was designed in a such way, that the force sensor was protected from overload in z-direction (Fig. 3.14). The weight of the whole system without sensor was

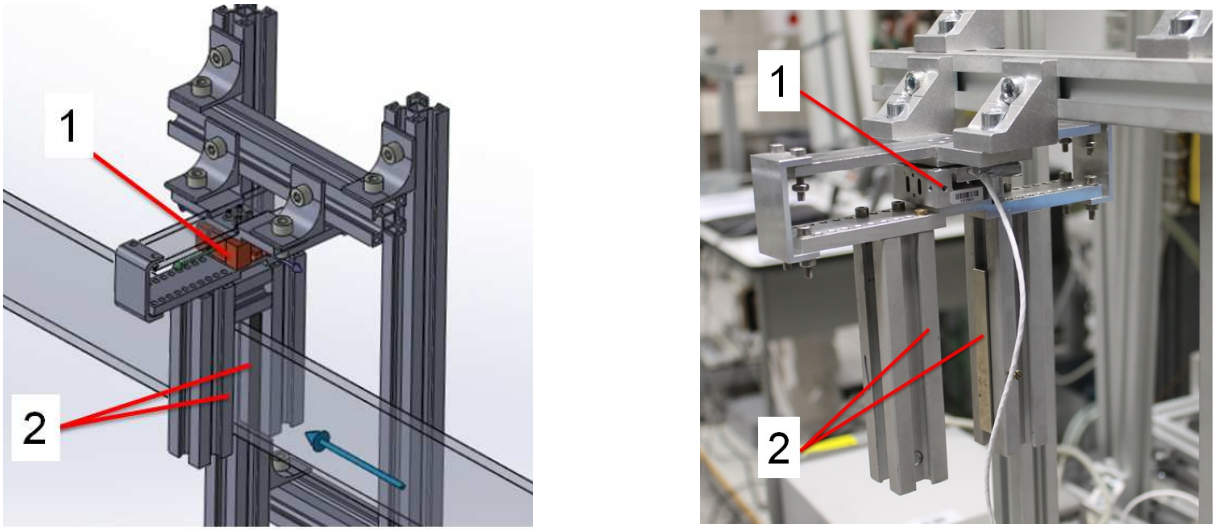

a) b)

Fig. 3.14: The first variant of the time-of-flight LFV measurement system: the scheme (a) and the photo (b). The force sensor 1 is rigidly connected to the permanent magnets 2 by a relatively heavy aluminum construction, therefore a shielding system was applied (the aluminum cage around the force sensor)

574 g which is 287% of sensor measurement range. The permanent magnets were mounted to

standard aluminum profile with a cross-section 30×30 mm^2 from the firm *Henkel and Roth*. The side sections were 140 mm long and the middle one was 40 mm (is not included to the final version of applied system). A shielding system allowed the force sensor displacement within a range 0.1 mm in z-direction and its construction included two specially designed aluminum plates and two clips on the both sides of the plates (exact dimensions are presented in the appendix B). The construction allowed to adjust the distance between the permanent magnets from 35 mm to 80 mm to provide the different magnetic flux density values within the duct.

The shielded measurement system was applied for the liquid metal tests, but the measurement results were no satisfying. Due to a redundant stiffness of the system the force sensor was not able to resolve small fluctuations of the force signal as a reaction to the flow perturbations. This rigidity effects all three direction of the force sensors, hence successful time-of-flight LFV measurements were unachievable without a significant modification or weight reduction of the measurement system.

This assumption leads to the second applied measurement system (Fig. 3.15). Here the

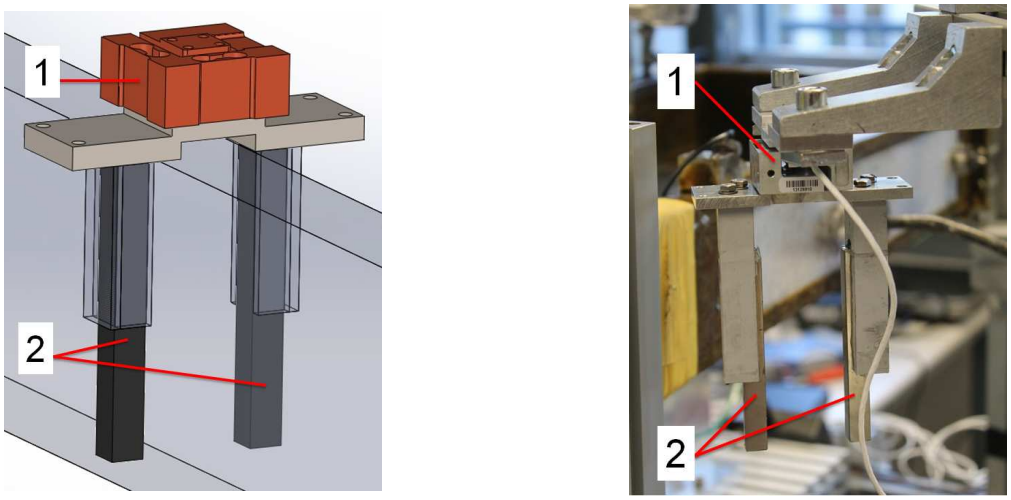

a) b)

Fig. 3.15: The second variant of the time-of-flight LFV measurement system: the scheme (a) and the photo (b). The force sensor 1 is connected to the permanent magnets 2 by a plastic rectangular bar and an aluminum plate.

plastic bars were applied as the permanent magnets holders. The holders had sizes 80×20×15 mm^3 and groove for the permanent magnet at one flat side. The magnets were connected to plastic bars by epoxy glue as it shown at the figure. An aluminum plate (appendix B) was used as an intermediate joint between the permanent magnets and the force sensor. The distance between magnets was fixed and equal to 40 mm. The weight of system was 256 g which was in the range of the force sensors workload. It was sufficient for the goal experiment; the assumptions underlying the fact that in a workload range the force sensor can work correctly, only with lower precision than in the application within its measurement range.

The second measurement system had a significant drawback that made it complicated to detect the flow perturbations: a low reaction time. The drawback was caused by an

elastic nature of the connection between elements. To avoid the limitation the third system was designed (Fig. 3.16). Standard square aluminum profile was applied for the system

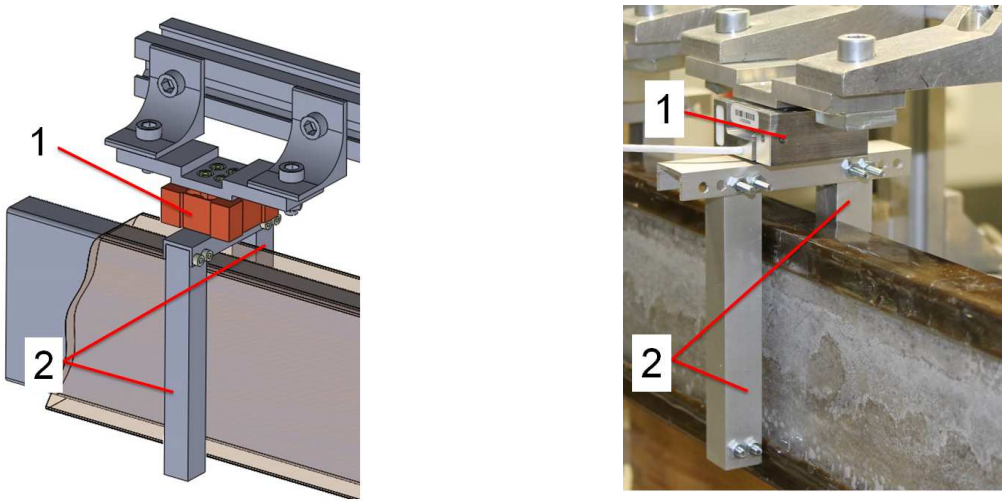

a) b)

Fig. 3.16: The third variant of the time-of-flight LFV measurement system: the scheme (a) and the photo (b). The force sensor 1 is connected to the permanent magnets 2 by standard aluminum profiles of square and channel beam shapes.

construction which allowed to lower the weight of the holding system considerably – to 190 g. The third system is capable to adjust the distance between magnets from 32 mm to 52 mm so the magnetic field influence on the flow can be differed. The system was applied for the further time-of-flight LFV experiments.

The magnetic field, generated by the permanent magnets pair within the third connection system, was varying from 0.08 T to 0.1 T in the middle of the duct. The obtained value is substantial to detect the passing flow fluctuations. On the other hand the interaction parameter N was in a range of 0.102...1.02, hence the flow pattern does not change significantly. The highest value of N obtained for the lowest velocity, which causes stronger influence of the electromagnetic forces on the flow. This effect could reduce the amount of vortical structure passing both measurement zones, because the first magnetic pair modifies the passing vortices. The interaction parameter was calculated by the equation (2.7) for $B = 0.1$ T, the hydraulic diameter of the duct $D_{\mathrm{H}} = 0.0178$ m and mean flow velocity u_{m} from 0.1 m/s to 1.0 m/s. This fact is important for undisturbed vortex movement from the first measurement zone to the second.

3.3.2 The applied electronics

Nowadays experiments are not possible without qualitative electronics, hence it is a very important task to chose the right electronic instrument for each specific case. The original signals of the strain gauge sensors have in general very small value which makes them hard to be processed without an amplification. Therefore signals of the force sensors of the goal experiment were amplified by two similar analog amplifiers configured specially for the applied

type of the strain gauge sensors and supplied by *ME-Messysteme, Germany*. An amplifier has a task to increase an amplitude of a measured signal before further processing. At the same time the amplifier supply Wheatstones bridge of both force sensors by voltage which is necessary for its operation. Each amplifier has four analog input and output channels, because every force sensor has three differential outputs and all signals have to be measured simultaneously.

After the amplifier the signal processes to the commercial data-acquisition system Agilent U2352A which transfer data to a personal computer (Fig. 3.17).

Fig. 3.17: The scheme of the force signal pre-processing in the goal experiment. Measured value (here voltage) is obtained by the strain gauge sensor, amplified by analog amplifier and undergoing digitalization by the DAQ-system before the reaching PC.

The applied amplifier GSV-1A4 is a four-channel analog device with an effective measurement range V_E equal to 2 mV/V and a maximal analog output signal V_A equal to 10 V. The amplification ratio *Amp* can be calculated as [45]:

$$Amp = \frac{k_S V_A}{F_N V_E} = 1.25. \tag{3.15}$$

The obtained *Amp* value means that the fully loaded force sensor (2 N) after the amplification will produce signal 2.5 V which is 1000× *original force signal*.

A high resolution digital data acquisition system Agilent U2352A was applied for digitalizing of the measurement data. It is an acquisition device with sixteen serial channels and direct USB connection to PC. The applied sampling rate value was 1000 Sa/s per each channel. Full specification of the Agilent U2352A characteristics can be found in the appendix B.

Preliminary state of the measurement system does not have a significant effect on the measurement result: the influence of primary strain, caused by outer conditions, temperature, mutual influence of forces in supplementary directions and so on is neutralized by the preparatory tarring of the both amplifiers. The top side of the both force sensors is rigidly fixed to the loaded aluminum construction to avoid displacement damping due to the bending stresses of coupling elements and mounting system itself. The whole measurement setup is fixed on a stone block and embedded in a box filled with sand in order to suppress the effects of vibrations caused by a mechanical noise. The permanent magnets are emplaced symmetrically in both vertical and horizontal (orthogonal to the flow) directions to the duct flow.

The applied measurement system allowed to obtain reproducible measurement results with the application of time-of-flight LFV and to confirm functional capability of the measurement principle. Significant advantage of the measurement system is its differential measurement scheme: two identical sensors are applied simultaneously; the outer noise influence

both of them at the same time and can be extracted from desired signal by removing equal for each sensor components of the experimental data.

3.3.3 Reaction time

The time delay τ has crucial influence on the flow rate estimation results and its value does not exceed two second. Any τ uncertainties can significantly influence the final flow rate results. Therefore the time parameters of the Lorentz force measurement system are important for precise measurements. The force signal on its way to computer passes several transformations: force to voltage, voltage to digital data. There is no ideal modification system exists in the physical world. The applied system is not ideal as well, hence both transformation systems were examined to estimate the measurements quality.

The first important signal transformation takes place in the force sensor: a strain gauge system is not able to react on excitation immediately and there is a bias between the moment of the force application and the reaction of measurement system on it. To investigate the reaction time an experimental scheme (Fig. 3.18) was designed and exploited to the force sensor. An additional electrical circuit was connected to the sensor and the standard mass in

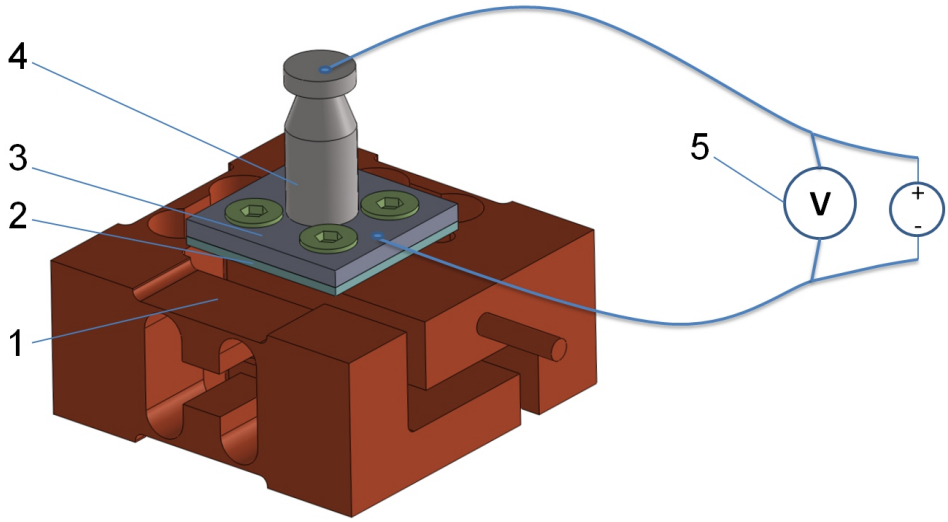

Fig. 3.18: The scheme of reaction time estimation of the force sensor. The contact between an applied standard mass and the aluminum plate was disrupted; the time difference between registered voltage drop and the force sensor reaction was measured. (1 – force sensor, 2 – isolation plate, 3 – aluminum plate, 4 – standard mass, 5 – voltmeter).

a such way, that in loaded state an electrical current can unstintingly flow through the system of aluminum plate 3 and standard mass 4. A power supply generated the voltage with the potential difference 5 V. The voltage change in circuit was measured by voltmeter Agilent and the obtained data were transferred to a computer by the same DAQ-system that was used for force signal measurements, but the sampling rate was increased to 25 kSa/s (as distinct from 1 kSa/s for usual experiments) to get a higher resolution. The test principle was based on the simultaneous measurements of force signal from the sensor and the voltage change

in the additional electric circuit during displacement of the standard mass from aluminum plate. The mass motion breaks the circuit and voltage of it drops to zero.

The test was provided with nine repetitions to take into account an influence of a random noise. The mean reaction time of the force sensor was estimated as 0.2 ±0.012 ms. The value is much less than τ and cannot significantly distort measurement results, particularly in the current research case when both compared force signals have the same reaction time. Nevertheless the result is important to estimate the resolution of the force sensors – flow fluctuations have to be detected in each magnetic field zone which have sizes approximately 0.01 m (magnetic field is not distributed homogeneously, hence we cannot estimate its strict limits). The maximal reached in duct flow velocity is $u_{\max}$=1.5 m/s. If a vortex is moving with this velocity it will need just 0.0067 s to pass the magnetic field zone, hence the resolution limitation of 0.2 ±0.012 ms is already 3% of the passing time of vortex.

The second component of Lorentz force measurement system which causes a bias of measured time delay τ is DAQ-system. The system has eight differential channels, but the working principle of it allows sample data from the channels consequently with some specific value of time delay between iterations. To examine the time bias value eight output signals from the eight adjacent channels were measured. As the input signal a triangle function with 4 V amplitude was generated by a signal generator. The input signal was sent to all eight channels simultaneously and time displacement between output signals was measured. The result was calculated as a mean value of the time delays between each channel pairs and five full periods of generated function. The obtained time is equal to 0.28 ms which is of the same order as the force sensor reaction time. The DAQ-channels time delay does not influence the measurement itself, but was taken into account under the flow rate calculation as the τ correction.

The results obtained within the section showed us an important drawback of the applied measurement system – the time resolution of the force sensors is limited, hence for the improvement of method's accuracy or extending of the method to the wider flow rate range one needs to apply a faster force measurement device.

3.4 Vives-probe

As a reference flow rate Q we used values evaluated by the Vives-probe [16] measurements. Vives-probe is an electromagnetic flowmeter for local velocity measurement in single phase and multiphase flows with non-uniform axial velocity profiles [46]. The method allows to investigate flows from a perspective of the one-point statistics. Permanent magnet is used to produce a near-uniform magnetic field orthogonal to both the flow direction and the plane of electrode pairs (Fig. 3.19). Liquid metal passes through magnetic field of cylindrical magnet which induces eddy currents within metal. The electrodes of the Vives-probe detect the potential differences of the currents which are proportional to local velocity of the liquid metal.

The device (Fig. 3.20) was installed in a middle of experimental duct; that allowed to measure local velocity $u_{\max}$. The method needs direct contact to liquid metal, hence the device was immersed to the duct. The experiments were performed with Vives-probe that includes cylindrical NdFeB magnet with 5 mm diameter and 5 mm height; four copper

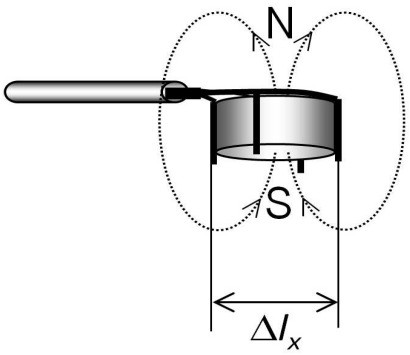

Fig. 3.19: The scheme of Vives-probe. Potential difference between electrode pairs induced by the motion of liquid metal in the magnetic field (eddy-currents voltage). Δl_x is the distance between electrodes

electrodes 0.3 mm are surrounding the magnet. The electrodes were set diametrically opposite to each other. The probe connections were embedded to a plastic tube of 8 mm in diameter. Two pairs of electrodes are used at the same time - according to compass analogy South-North and East-West; one pair of electrodes was parallel to flow, another was transversal. Velocity $u_{\max}$ is estimated as vector product of both measured potential differences which is done to reduce influence of flow fluctuations. In fact, flow was disturbed by Vives-probe itself: fluid eddies were generated around the magnet which served as a solid obstacle. This effect is varying for different velocity value; to take this fact into account calibration procedure was provided.

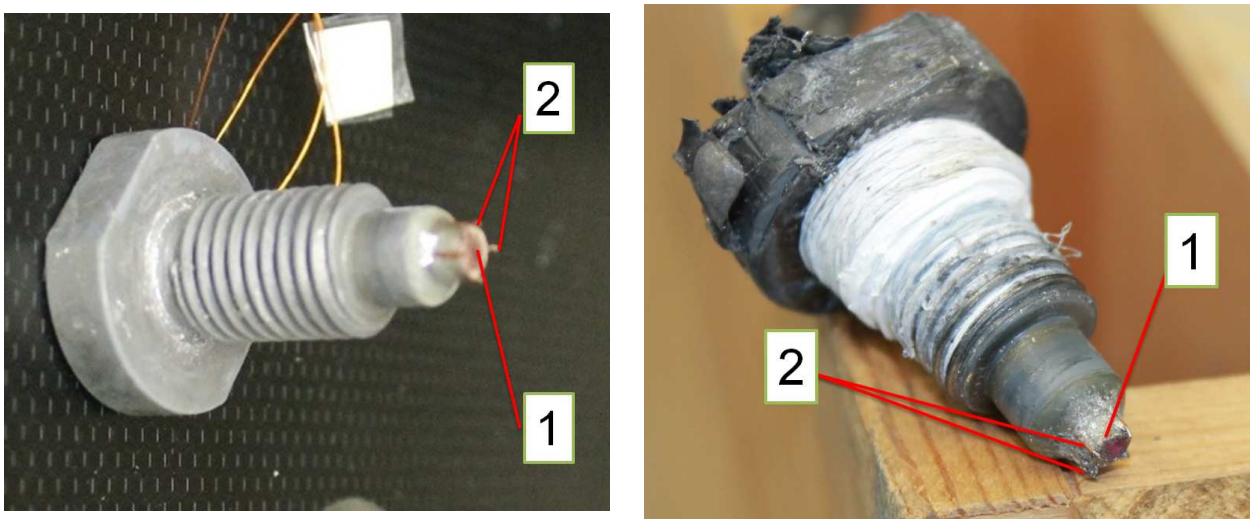

a) b)

Fig. 3.20: Vives-probe (a) Vives-probe before application. (b) Vives-probe after influence of GaInSn. (1 - permanent magnet with ø 5 mm *and 5* mm *length; 2 - copper electrodes ø 0.3* mm*)*

Calibration values for the Vives-probe are obtained by preliminary tests with the predefined velocity values and within similar medium to the experimental one. The tests were

carried out in an annular channel filled with GaInSn at the linear velocity region. The construction of the annular channel, especially the fact that it has an open surface, allows to calibrate the Vives-probe only at the limited velocity range. Because the signal/velocity dependence at the tested region is linear [47], it was assumed that the obtained ratio is valid for all measurement range and the velocity can be estimated by potential differences between the electrodes pairs V_{NS} and V_{EW}:

$$u_{\max} = 4.3 \cdot 10^{-4} \sqrt{V_{\mathrm{NS}}^2 + V_{\mathrm{EW}}^2} + 0.03. \tag{3.16}$$

Vives-probe is a temperature dependent device. In general, the accurate measurements of a local velocity in a liquid metal MHD flows require special conditions due to the physical characteristics of the fluid. The temperature of the liquid metal has to be kept sufficiently uniform to avoid thermo-electrically induced potential perturbations [47]. Work of the pump results in liquid metal heating due to Joule effect, hence a heat exchanger and temperature sensor are designated for temperature regime control; the liquid metal temperature variation during the experiment doesn't exceed $\pm 0.5°\mathrm{C}$. To transform the obtained velocity value $u_{\max}$ to mean velocity u_{m}, mean velocity approximation was used:

$$u_{\mathrm{m}} = 0.85 u_{\max}. \tag{3.17}$$

Here 0.85 is an empirical coefficient calculated by the experimental UDV analysis of the turbulent velocity profile in the working duct, which well corresponds to the standard hydraulic ratio of 0.82 for a turbulent duct flow [40]. The velocity profile in a narrow duct (having width/height ratio1/8) can be assumed two-dimensional, which simplifies the further calculations.

The flow rate through the cross section with an area A can be calculated then by:

$$Q_{\mathrm{ref}} = A u_{\mathrm{m}}. \tag{3.18}$$

The output signal of the Vives-probe has μV range, so a precise multimeter from Keithley Instruments Inc. was applied for the signal detection. The non-uniform liquid metal conductivity as effect of randomly distributed oxides is assumed to be negligible for the Vives-probe measurements. The passing intrusions generate noise which is smoothed over an applied averaging.

Lorentz force provides a braking effect on a conductive fluid. It creates so-called m-profile of velocity [29], that causes deceleration of the flow in the middle of the duct and its acceleration near walls. The impact of the effect can vary and depends on such parameters as magnetic flux density B, electrical conductivity of a fluid σ and the flow velocity u (2.4). The permanent magnets of measurement system can influence the flow by the same way. The Vives-probe was applied to evaluate an influence of the magnetic field of the permanent magnets pair to the middle zone flow velocity. To measure the difference of velocity with and without influence of magnetic field, we placed one permanent magnets pair at two positions in turns: the first position was 20 mm before the Vives-probe and the second one was 20 mm after the Vives-probe in the direction of flow. At the both positions the velocity measurement was performed and the middle zone flow velocity $u_{\max}$ was estimated. The experiments were done at the same day and with a short time difference between (several minutes) to avoid any

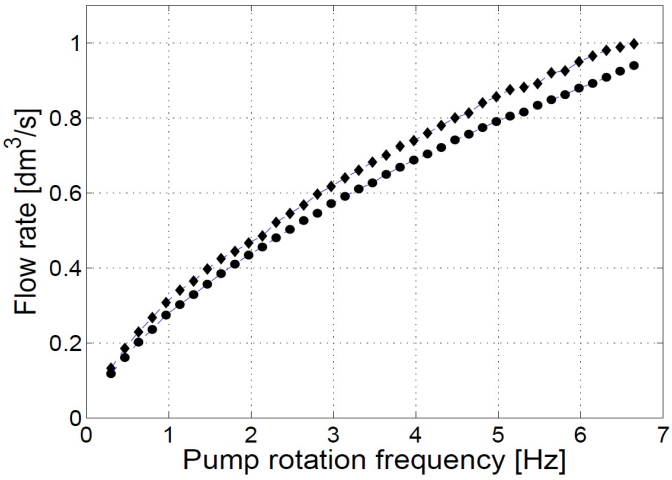

Fig. 3.21: The comparison of the flow rates estimated by the Vives-probe at two position: in unperturbed flow (diamonds) and within the flow influenced by magnetic field (circles).

significant conditions change; the temperature was controlled within $\pm 1°C$. The velocity datum were used for flow rate evaluation for both positions (Fig. 3.21). The difference between flow rate values obtained by the Vives-probe in two positions is purely caused by an influence of magnetic field to the velocity profile. Under magnetic field influence the velocity pattern changes, hence $u_{\max}$ became less with the same u_{m} value. The average difference is estimated as 8%; it was taken into account under further velocity calculation as the additional factor. When the Vives-probe was positioned between the LFV flowmeters the u_{m} velocity value was multiplied by the factor 1.08:

$$Q_{\mathrm{ref}} \quad = \quad 1.08 A u_{\mathrm{m}}. \tag{3.19}$$

The Vives-probe measurements were used as the reference method for the flow rate estimation within the investigated turbulent liquid metal flow. However, the method has substantial drawback: it required a direct contact between the probe and the liquid metal which limits application area to the non-aggressive and low-temperature liquids. Nevertheless, the Vives-probe is an appropriate solution for the performed model experiments within GaInSn under the room temperature.

3.5 Ultrasound Doppler Velocimetry

Ultrasound Doppler velocimetry (UDV) is a velocity profile measurement method widely used for opaque liquids media [47], [48]. The technique is based on periodical propagation of ultrasonic waves through liquid (Fig. 3.22). The UDV method has wide operation conditions: with some extensions (acoustic wave guides and measurements through a wall) it can be applied for liquids under 600°C [49] as well as under magnetic field influence [50]. UDV was used in model experiment to estimate velocity profile shape and to find ratio between local center and mean duct velocities.

The measurement technique is based on the time-of-flight principle [51]. The ultrasonic Doppler method utilizes the shift frequency of the echo caused by reflected signals on moving tracer particles to obtain instantaneous velocity in a flow field. The seeding particles move with a flow and penetrate ultrasonic bursts emitted by UDV. Each particle acts as obstruction for waves and reflects part of wave energy back to transducer. A particle position information is obtained from a time lapse of echo reception after the pulse emission, t; this corresponds to a time-of-flight of the ultrasonic pulse. Note that the path length on which the pulse flies is for both the ongoing and the returning path. By wave path a at two different moments of time, transducer can evaluate the path dx of particle; the transit time t is estimated by predefined pulse repetition frequency of ultrasonic waves. Velocity at each duct hight position is determined as distance dx that is passed by seeding particle per transit time t.

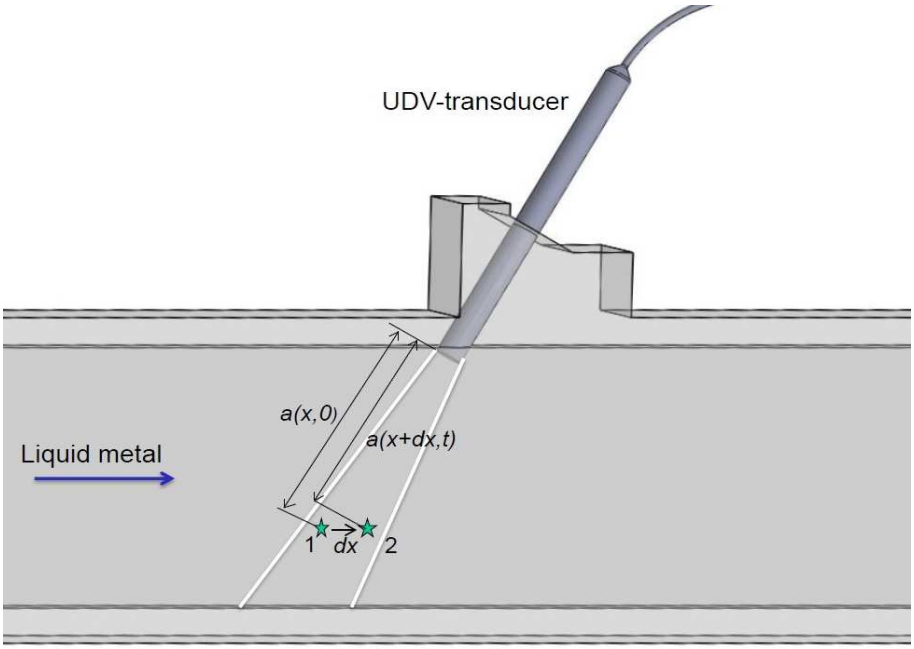

Fig. 3.22: The schematic of UDV measurement. UDV-transducer is the emitter and receiver of ultrasonic waves (pulses). The waves reflect by each passing with flow particle at least two times. The path dx can be estimated by length difference of the two reflections and angle between main flow direction and UDV-transducer position. Transit time is evaluated by the predefined waves pulsation frequency. Velocity at each profile point is calculated as the distance dx per transit time t.

The seeding particles play crucial role at UDV measurements.The size of the particle should be approximately one fourth to one half of the wavelength for appropriate resolution [9]. If the particle is smaller than this, the reflection efficiency becomes lower and the energy of echo is too small to maintain a high signal-to-noise ratio (SNR), leading to a detection error. If the particle is larger, the probability of multiple reflections between particles becomes higher, which would result in a distortion of the profile. The density of the particle is also important. A large difference in densities between fluid and particle might lead to an erroneous result because the particle does not follow the flow faithfully. Further, the

concentration of the particles in the fluid is important; in the ideal case there should be one particle per measuring volume, but this also depends on the velocity level of the flow field to be measured.

Because the ultrasonic echo is generated by particles suspended in fluid, it is absolutely necessary to have particles as a reflector in the fluid in which the velocity profile is to be measured. In the model experiment, the particles sizes and concentrations are not preliminarily controlled. The GaInSn oxides formation naturally exist within the liquid metal flow and can have various dimensions; an extraneous impurity should also be taken into account. Conformably, inhomogeneous tracing particles allow to estimate the shape of velocity profile but not exact velocity value. This fact was used to estimate the ratio between the mean velocity u_{m} and the local velocity u_{loc} for the used duct geometry. Since this time delay is usually very small (< 1 μs), not the time shift itself is taken, but the phase shift of the echo [52]. The correlation technique was applied in used UDV-device DOP2000 to trace particles during several bursts and to visualize the measured velocity profile.

Because an ultrasonic wave is itself invisible, it is very important to monitor the echo signal on the oscilloscope screen, especially for assuring the measurement location of the line where the flow is investigated. It helps to arrange a measurement line with respect to the flow structure to avoid spurious reflected pulses from duct wall. This fact should be taken into consideration in particular for small volumes even more so when duct width has the same range as transducer diameter, hence presence and intensity of echo signal was monitored for each experiment carefully.

The maximum velocity $u_{\max}$ and the maximum measurement depth $a_{\max}$ can be defined by the pulse repetition frequency w_{prf} [51]:

$$u_{\max} = \frac{c w_{\mathrm{rps}}}{4 w_{\mathrm{e}} \cos\Theta}. \tag{3.20}$$

$$a_{\max} = \frac{c}{2 w_{\mathrm{prf}}}. \tag{3.21}$$

A selection of the optimal basic frequency depends on the requirements and purposes of the measurement. For physical research experiments, a high spatial and time resolution are the key issue and require a smaller wavelength, namely, a higher frequency is preferable.

The inclination angle Θ can be determined in a such way that the measured component of the velocity vector shall not exceed the detectable maximum velocity of the device; the angle of positioning should not exceed 90°. If the setting of the transducer is perpendicular to the main flow direction, it makes velocity measurement impossible because a velocity projection component becomes zero. In the model experiment the transducer was mounted under $\Theta = 60°$ in the opposite to flow direction, which is sufficient for the measurement in the liquid metal velocity range 0.1...1.5 m/s.

The UDV technique has several serious drawbacks:

- Temperature change directly affects the measurement accuracy because the measurement positions and velocities are functions of the sound speed in medium, as well as the temperature effects of a solid boundary and a measurement volume have to be taken into consideration.

- In small volumes, a stationary wave caused by interference between reflected waves can cause multiple reflections between the wall and tracer particles. Therefore, the measurement accuracy near the wall must consider the solid boundary effects.
- When the spatial sampling interval is larger than the smallest scale of the turbulence presented in flow, the turbulence at a high wave number is underestimated. The same underestimation occurs when the temporal sampling interval is longer than the fastest scale of turbulence. Thus, turbulence in most cases will be under-read as it increases superficially with a random noise included in the measurement.

As the UDV-transducer (Fig. 3.23) 8 Hz probe with 8 mm outer diameter and 100 mm length was used. The probe is situated from above of the duct through specially manufactured

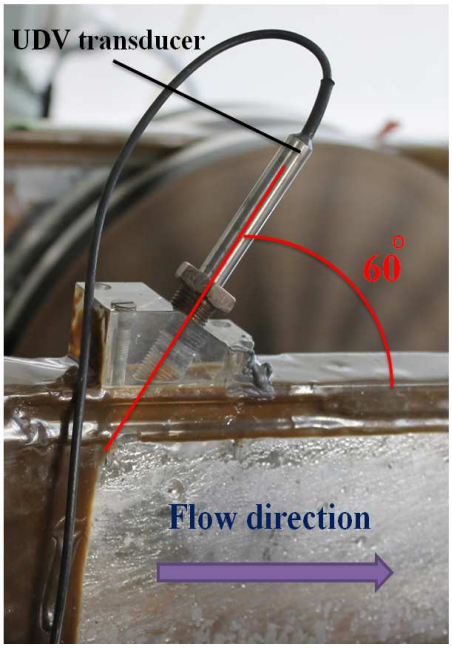

Fig. 3.23: Experimental UDV-transducer. The probe is mounted upflow on the duct at an angle 60° *and has direct contact with the liquid metal.*

8 mm hole and a connector. The connector is long enough to provide a sufficient align and centering of the transducer according to the duct. Within the performed experiment, 400 measured profiles were proceeded to obtain each velocity profile. The digital signal post-processing included averaging of non-zero-values of velocities at each duct depth position to receive the flow velocity profile.

The applied UDV-transducer combines the functions of a waves emitter and a receiver simultaneously; the piezoelectric sensor is applied as a sensitive element. The piezoelectric element is excited by an electric oscillation through the electrodes. A mechanical pressure is generated inside the element and the oscillation of the element generates and emits the ultrasonic wave to the adjacent medium. The transducer was immersed directly in GaInSn, which allows to avoid loosing of the wave power due to the acoustic impedance difference at the boundary between Plexiglas wall and GaInSn. However, the direct contact between a

probe and medium has significant disadvantage: the contact surface of transducer requires regular cleaning from Galistan oxides; this means necessity of lowering the liquid metal level in the duct and increase the risk of further liquid metal oxidation.

The UDV method does not provide accurate velocity data, but allows to estimate the experimental velocity profile within the duct, which played significant role in the reference measurement.

3.6 Vortex generation

The strength, linearity and stability of the vortex are defined by the shape, blockage ratio and other geometrical parameters of the applied vortex generator. The aim of vortex generation is to produce an artificial velocity disturbance in the duct, so the generated fluctuation would be sufficiently strong to be detected by the LFV flowmeters and small enough to move with the mean flow velocity. The mechanism of the vortex generation gives rise to a periodicity in the flow.

Two different types of the vortex generation were applied within presented research: a bluff-body (immersed solid body) and a magnetic obstacle (non-contact). In the first case, hte vortices are shed alternatively from each side of an immersed solid body. The frequency of vortex shedding caused by a solid obstacle is directly proportional to the flow velocity and inversely proportional to the size of the bluff-body. The proportional constant is called Strouhal number:

$$St = \frac{w_{\mathrm{v}} L}{u_{\mathrm{m}}}. \tag{3.22}$$

In the unperturbed and well-formed turbulent flow St value is obtained by the empirical way over a wide range of the flow rate values and is defined equal to 0.21 [56]. Unfortunatelly, it is not the case in limited space of the used duct. The flow around the bluff-body is strongly influenced by the presence of trailing edges, corners and surface roughness. Hence the frequency obtained by (3.22) would be not trustworthy for the used duct and obstacle geometry.

The vortex generation by a bluff-body needs direct contact with the liquid metal flow, which is not appropriate for hot and aggressive fluids. Likewise, Karman street can be created by a non-contact way due to a magnetic obstacle application [55].

3.6.1 Bluff-body

The most effective and widely studied way of the vortex generation is a solid body immersed in a liquid flow. The method cannot be applied within high temperature liquid metals, but can be successfully used for the tests in our model experiment of time-of-flight LFV. The application of a solid bluff-body allows to estimate feasibility of the time-of-flight principle for liquid metal application by well-known vortex generation effect. The goal of a such test is to examine a capability of LFV measurement system to detect fluctuations within the liquid metal flow.

Solid obstacles are generally applied for the generation of Karman vortex street (3.24) in the vortex flowmeter application. The bluff-body can have different shapes and relative sizes;

that depends on goals of an investigation and the measurement conditions. For example, a detailed study of the cylindrical and trapezoidal bluff-bodies for circular pipes is described in [57].

a)

b)

Fig. 3.24: Von Karman vortex street obtained (a) by numerical simulation [58] and (b) experimentally [59]. In both cases the solid bluff-body is considered as a vortex generator; water with artificially created gas bubbles was used for the visualization.

The bluff-body influences the flow in the duct by pressure variations. The level of influence is determined by a blockage ratio β that evaluates a relative perturbation of the flow due to an obstacle:

$$\beta = \frac{A}{A_{\mathrm{bb}}}. \tag{3.23}$$

The resistance coefficient for a bluff-body is defined by follows [57]:

$$K = \frac{0.8C_{\mathrm{d}}(1-\beta)}{\beta^2}. \tag{3.24}$$

The time-of-flight LFV experiments described in the current thesis were occurred with two types of the solid bluff-body: a long cylinder ø 2 mm× 80 mm and a short cylinder ø 5 mm× 5 mm. Their comparative characteristics are presented at table 3.2. The drag coefficient C_{d} depends on the shape of a bluff-body [60].

Tab. 3.2: The parameters of the solid bluff-buddies applied in experiments as the vortex generators for the time-of-flight LFV tests. The results are given for two bluff-bodies: long cylinder ø 2 mm× *80* mm *and short cylinder ø 5* mm× *5* mm

Parameters	ø 2 mm× 80 mm	ø 5 mm× 5 mm
Blockage ratio, β	0.2	0.031
Drag coefficient, C_d	0.82	1.15
Resistance coefficient, K	0.205	0.029

In [28] was investigated the behavior of a long cylinder ø 8 mm× 80 mm as the vortex generator within the applied for the current research duct. It was discovered, that with a such high blockage ratio β equal to 0.8 no Karman street can be generated. It was proved by numerical simulation and physical explanation [57]: the separated shear layers from the bluff-body becomes a jet between the cylinder and the duct wall, and as the result the vortex shedding from bluff-body disappeared.

The preliminary time-of-flight LFV experiments were carried out with a vertical cylindrical bluff-body of ø 2 mm× 80 mm. The plastic cylinder was installed at the distance 330 mm before the LFV flowmeters. Such large distance ensured the fully developed flow conditions within the test section. However, such cylinder undergoing a strong drag effect and oscillates; hence the cylinder cannot hold an expected position in the middle of duct. Furthermore, generation of vortices with vertical axis is not sufficient in narrow duct within the turbulent flow regime. the generated vortices transform or dissipate their energy before reaching the flowmeter due to the duct geometry. Another point against vertical vortex generation is the direction of the permanent magnets field lines. According to MHD [29], the magnetic field suppresses vortices when their axis are orthogonal to the magnetic field lines, hence passing vortex can be destroyed or completely transformed by first pair of the permanent magnets and the generated force signals from two sensors could diverge significantly.

Under further experiments, the Vives-probe was applied as the vortex generator. The part of the Vives-probe is immersed to the liquid metal and has horizontal orientation orthogonally to the main flow. the size of the Vives-probe immersed part is of sizes ø 5 mm× 5 mm. The probe was situated in a such way, that generated by it vortices had generally parallel axes to the magnetic field lines of the LFV magnetic pairs. The small width of the duct also supported this vortex orientation. The measurement results, obtained with the application of Vives-probe as the vortex generator, have satisfactory quality and the bluff-body was used for the main experimental investigation of time-of-flight LFV technique.

The Vives probe was positioned at the two location: at the distance 20mm before both measurement zones and between of the measurement zones. In the first case the generated Karman street reaches magnetic field being unformed. In the second case the Vives-probe is not operating as a vortex generator for time-of-flight LFV, rather disturb the flow and the goal of a such application was to estimate the occurrence of the detectable time-delay signal.

3.6.2 Magnetic obstacle

The vortex generation can be carried out by an electromagnetic influence on the flowing liquid metal. For the purpose permanent magnets as well as an electromagnet were applied within the current research.

Vortices can be produced by a magnetic field interaction with a conductive fluid flow. The strength of interactions between the fluid and the electromagnetic field is described by the interaction parameter N that represents a ratio between the Lorentz and the inertial forces (2.7) [55]. Therefore, starting from a stable flow without vortices, vortex pattern appear by decreasing the flow rate. This is a paradoxical behavior being in contrast to the ordinary hydrodynamics where attached vortices always appear at increasing flow rate. Vortices can be generated by the local action of the Lorentz force on liquid metal. The locally imposed non-uniform magnetic field generates similar effects as observed for flows over solid obstacles. Streamline velocity inside the magnetic obstacle zone is positive according to main flow direction for small N and might be negative when N is higher than a critical value N_{cr}, hence Karman street can be generated. The N_{cr} strongly depends on magnetic blockage ratio β_{mag}:

$$\beta_{\mathrm{mag}} = \frac{d_{\mathrm{mag}}}{d}. \tag{3.25}$$

The β_{mag} is the ratio between the lateral size of the magnet d_{mag} and the width of the duct d.

When $N > N_{\mathrm{cr}}$, the flow structure after the obstacle is analogous to that of a solid cylinder and the vortex shedding frequency depends on β_{mag} (Fig. 3.25).

The experimental and numerical investigation done by different authors showed a possibility to create a stable Karman street by the magnetic obstacles application. However, the most part of researches performed their tests in laminar flow regime[71], [72]. Within the current research, the liquid metal experiments have been performed to examine the magnetic obstacles application for the vortex generation in turbulent flow. The permanent magnets with sizes 20 mm× 20 mm and 20 mm× 40 mm and an electromagnet with the coil diameter 25 mm were used for the tests. The main parameters of the applied magnetic obstacles are collected in table 3.3.

Tab. 3.3: Parameters of the magnetic obstacles examined in experiment as the vortex generators for time-of-flight LFV.

Parameters	20 mm × 20 mm	20 mm × 40 mm	Coil ø 25 mm
Magnetic blockage ratio, β_{mag}	0.25	0.5	0.31
Magnetic field in duct middle, B [T]	0.05	0.13	0.026
Interaction parameter range, N	0.023...0.23	0.218...2.18	0.0064...0.064

the experiments with magnetic obstacles as the vortex generation sources were performed in both static and dynamic ways. In static case a pair of magnets or electromagnets (in the

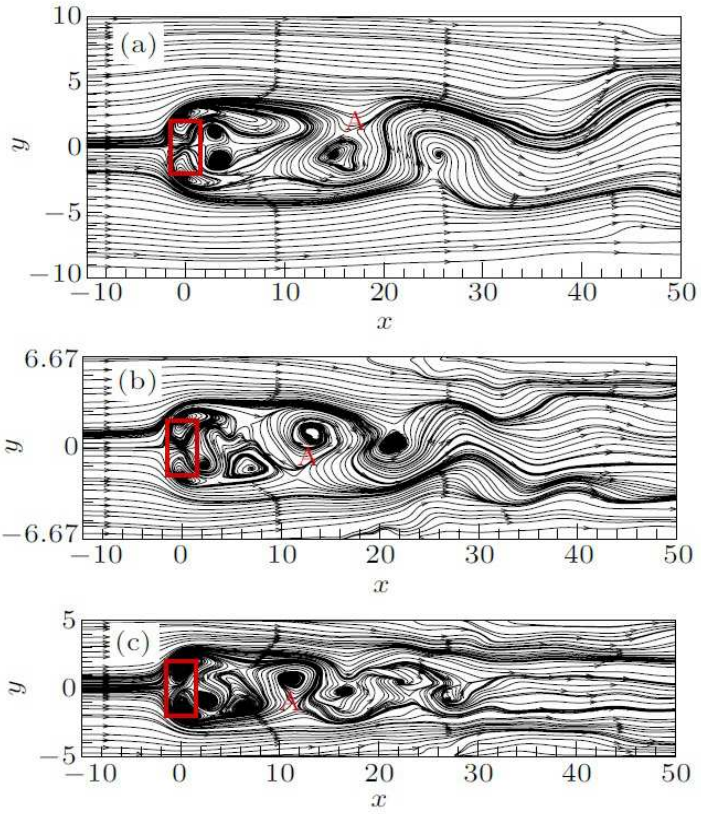

Fig. 3.25: Von Karman vortex street generated by the magnetic obstacle (obtained by a numerical simulation [71]). Three different values of the magnetic blockage ratio were tested under the simulation. All dimensions are given in cm. *the different blockage ratios creates the unique patterns of Karman street. The bigger is the ratio the smaller distance is needed to generate a fully developed vortical structure A.*

form of a copper coil) were positioned from both sides of the duct in the middle of walls height in a such way that their magnetic field penetrates a middle part of the duct flow (Fig. 3.26). The UDV-transducer was used to detect the change of velocity profile under influence of the static magnetic field at the different distances to the transducer: 50 mm, 75 mm and 100 mm. The measurements results showed subtle influence of the applied magnetic field on the flow profile. The influence of electromagnetic forces to inertia forces within a liquid is defined by the dimensionless parameter – Stuart number or interaction parameter N. As was investigated by numerical simulations [**?**], when the value of the interaction parameter N is lower than some critical value, the flow disturbance will have temporary character and will decay without generation of the Karman street. The parameter N for the performed tests had relatively low magnitude (less than one), hence the effect of the electromagnetic forces on the flow was negligible. The investigated static magnetic obstacles were not able to create the Karman street in the duct.

As the addition to the static permanent magnets tests, the dynamic experiments were performed. During the dynamic experiments, permanent magnets were periodically mounted

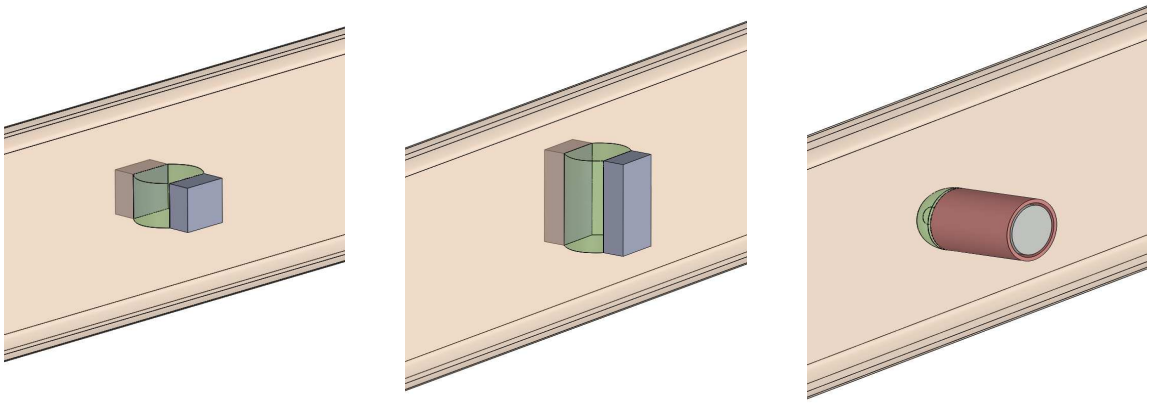

a) b) c)

Fig. 3.26: The magnetic obstacles applied in the experiment. The permanent magnets pairs (a) 20 mm × *20* mm*, (b) 20* mm × *40* mm *and coil ø 25* mm*. All magnets were positioned directly on the duct walls.*

to the walls from both sides of the duct. Each iteration of the magnetic field influence lasted ten seconds and the goal of the tests was to create flow disturbances (not necessary of the vortical structure) and detect them by time-of-flight LFV flowmeters. The UDV method was not applied for the experiment due to its inability to detect fast flow variations. Another way of the dynamic test was a rotation of the permanent magnets pairs with a frequency 0.5 Hz.

Both dynamic experimental techniques were not successful: the time-of-flight LFV flowmeters detected a strong signal immediately after the change of the permanent magnets positions. However the detected signal occurs as the result of the magnetic field influence and its magnitude is significantly stronger than the desired Lorentz force signal generated by a passing vortex. The magnetic field acted on eddy currents created by the electromagnetic pump and crossing through the whole loop. The disturbances of the passing current strongly effect the magnetic system of both time-of-flight LFV flowmeters. Hence no hydraulic disturbances can be detected by the dynamic ways (the signal-to-noise ratio is too low).

A copper coil was also applied for the vortex generation in the dynamic experiments. The tests with the coil had a goal to generate the detectable flow disturbances at predefined time by switching on and off the supply power of the coil. The flow rate of the liquid metal was registered by the time-of-flight LFV system. In this case one LFV flowmeter is sufficient, because the time delay τ can be obtained as a difference between excitation of the flow disturbances (here the moment of time when the power supply of coil is on) and their detection by the LFV flowmeter. However, the practical coil tests showed the same effect as in the context of the dynamic experiment with permanent magnets – the magnetic field influenced the flowmeters directly.

According to obtained experimental data, the available magnetic obstacles were unable to provide stable vortex generation in turbulent flow. For the successful time-of-flight LFV application, the parameter N of a vortex generator should be increased significantly. It can be done by the increase of magnetic flux density or by decrease of the mean flow velocity.

The suggested additional technique for the flow rate measurements by the time-of-flight LFV are based on a coil as the vortex generator. The LFV flowmeters have to be used as

the vortex detectors that is promising for further investigation and can be developed in the achievement-oriented method.

4. EXPERIMENTAL INVESTIGATION OF THE PROBLEM

4.1 Experiment

The numerical simulations of [28] have shown that time-of-flight Lorentz force velocimetry is able to measure the flow rate of a liquid metal. As a further step to prove the information the two types of tests were provided: solid metal and liquid metal tests. Within the solid tests a copper plate was moving through the static magnetic field and force sensors were detecting the movement to estimate the plate velocity. For liquid metal test the duct with GaInSn was positioned in magnetic field and volume structures (here vortices) were moving within the duct. The vortices movement was detected by force sensors. The possibilities to use both methods for velocity estimations have been investigated.

4.1.1 The solid metal tests description

The aim of the solid metal experiment was to demonstrate the behavior of time-of-flight LFV by using solid metal (here copper plate) as a visible obstacle (Fig. 4.1). The measurement system with two force sensors described in the chapter 3 was set up separately from the liquid metal duct. The copper plate was moving manually in the x-direction through both measurement zones in a such way that it penetrated the magnetic field in the middle of the gap between permanent magnets. The manual method of displacement was chosen due to the fact that it creates no additional noise and allows to investigate unperturbed time-of-flight experiment. In fact, the motion has no strictly homogeneous velocity value, but the degree of its uniformity for each test is sufficiently high to assume as non-varying. Such motion generates a braking force of electromagnetic nature (Lorentz force) acting at the plate. The third Newton's law states that when one body (here permanent magnets) exerts a force on a second body (here a copper plate), the second body simultaneously exerts a force equal in magnitude and opposite in direction on the first body [63]. According to the assumption the permanent magnets pair is undergoing the same magnitude of force as the one acting on the plate. The force arises at the moments of time when the plate is entering and leaving the magnetic field zones hence such force influence can be seen as force signal disturbances. The two applied strain gauge force sensors detected the disturbances as peaks on both signal patterns. The time delay τ between two signals can be estimated as time between related peaks from real time experimental data set. Hence velocity u of the copper plate motion can be determined as distance D per time τ:

$$u = \frac{D}{\tau} \tag{4.1}$$

The test was provided as preliminary experimental investigation because it has several significant advantages over the liquid metal case:

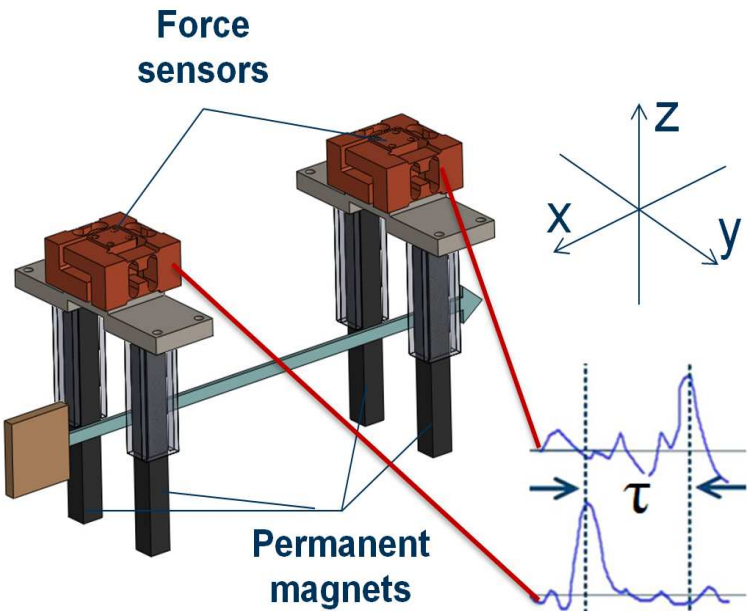

Fig. 4.1: Scheme of the solid tests of time-of-flight LFV. Force signal perturbations are induced by the passing copper plate and shown at the presented signals diagram as peaks. Velocity of the copper plate can be obtained as a relation of the distance between sensors per time between the peaks. (τ - time delay between perturbations, x, y and z specify force measurement directions)

- A solid obstacle is clearly visible and its speed can be estimated by standard methods. For example, a simple electric circle can be constructed in a such way, that a moving conductor will close a loop by passing it and will disturb flowing current.
- The Lorentz force created by a solid obstacle passing the magnetic field will be significantly higher than in the liquid metal experiment due to the higher electrical conductivity of copper ($5.96 \cdot 10^7$ [$\mathrm{Ohm}^{-1} \cdot \mathrm{m}^{-1}$] [62], being ten times higher than for GaInSn).

The test was performed under room temperature conditions. As an obstacle a copper plate was used to create Lorentz force perturbations. The plate has a rectangular shape with dimensions of 50 mm $\times$ 35 mm and thickness of 1 mm which is sufficiently large enough to generate the detectable Lorentz force but small enough to avoid the overlapping of the both measurement systems. The systems were separated by the fixed distance $D = 150$ mm.

The solid metal test is an effective instrument to visualize the time-of-flight Lorentz force measurement technique and to confirm its sustainability for velocity evaluation. The measurement results obtained by the method are presented after the signal processing description.

4.1.2 Liquid metal tests description

Due to opaque liquid and unresolved turbulence within the flow, the liquid metal test is a more challenging task than the solid metal one. Another difficulty of liquid metal test is a low signal-to-noise ratio because of hydraulic and electromagnetic noise generated by the pump, hence the peaks are not visible at the signals before appropriate signal processing.

According to the time-of-flight LFV technique two identical measurement systems we mounted on a duct one by one (Fig. 4.2). Within the liquid metal test, artificially created

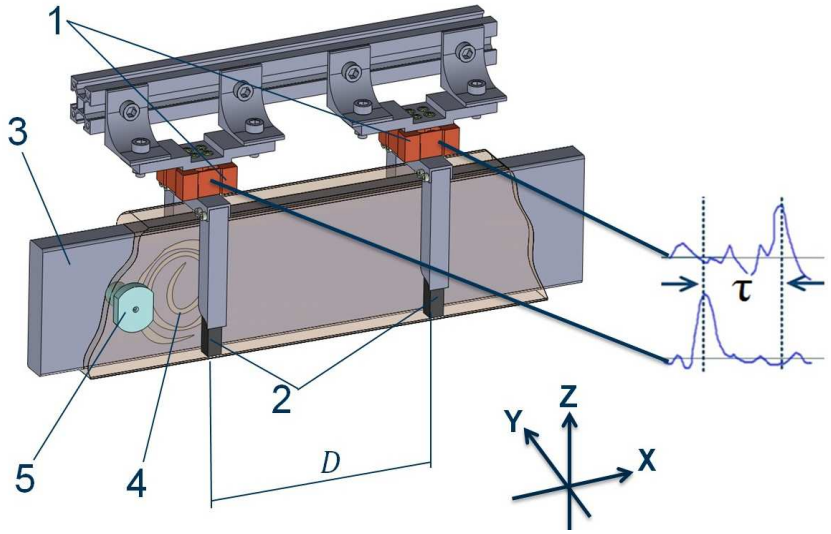

Fig. 4.2: Operating scheme of time-of-flight LFV. Force signal perturbations are induced by the passing vortices and shown as the peaks at the presented signals diagram. Velocity of the liquid metal can be obtained as a relation of the distance between the force sensors per time between the perturbations. (D - distance between flowmeters, τ - time delay between perturbations, 1 - force sensors, 2 - permanent magnets, 3 - liquid metal, 4 - a vortex, 5 - Vives-probe)

vortices are used as perturbing obstacles. The vortices are created by Vives-probe immersed in Galinstan before both measurement zones. Vives-probe in the experiment plays a role of a vortex-generator and a reference velocity measurement setup at the same time. Each vortex is moving with the flow and passing through the measurement volume which results in a force signal perturbation: when a vortex is moving within the liquid metal flow through the measurement zone, it modulates force disturbances and can be detected by the force sensors.

As was proposed in the solid metal tests, the flow rate measurement is based on getting the temporal cross-correlation function of the two force signals. The only difference between the liquid and the solid metal tests is an additional experimental coefficient k that takes into account hydraulic effects affected on moving vortices. The distance between measurement systems D is known. The time shift τ between peaks can be obtained from the cross-correlation function of the force signals. With this data, the flow rate of liquid metal can be calculated by a velocity definition: distance per time (mean velocity u_m) multiplied with the duct cross-section area A:

$$Q \quad = \quad k\frac{AD}{\tau} \quad = \quad kAu_\mathrm{m}. \tag{4.2}$$

The experimental coefficient k should be estimated during a preliminary calibration of the measurement system with identical duct geometry which will be used in further application. The experimental coefficient can be different for varied duct geometries, as well as for a type

of the detection system. To estimate the experimental coefficient k, a reference flow rate or velocity measurement setup has to be used within the duct. Depending on the type of obtained reference data, the experimental coefficient k can be calculated by:

$$k = \frac{Q\tau}{D} = \frac{Au_{\mathrm{m}}\tau}{D}. \tag{4.3}$$

In fact, in the liquid metal experiment the signal-to-noise ratio is significantly lower than in the solid metal case. Strong mechanical vibration and hydraulic perturbations generated by the pump, electromagnetic noise, random outer noises with different frequency ranges create highly chaotic background signal. To analyze the signal frequency components, a power spectra analysis and digital signal processing were applied.

4.2 Signal processing

The signal analysis has the task to estimate various signal parameters – power spectra, signal-to noise ratio, correlation, filtering function design. In measurement technologies, the signal quality is a very important aspect. It can be defined with the help of signal-to-noise ratio which implies to be rather low if the signal quality is poor or the existing noise level is high. In order to study the flow rate of liquid metal with the help of time-of-flight Lorentz force velocimetry, the signal quality of the measurement apparatus has to be investigated and improved, if necessary.

To achieve this goal, power spectra analysis and digital signal processing were performed. The power spectra analysis allowed to distinguish different frequency components of the force signal and evaluate their investment in the original data set. The signal processing applied in the current research included three main steps: segmentation of experimental data, filtering of force signals and their cross-correlation. The segmentation included dividing force signals to equal intervals of the sufficient length to prevent influence of the stochastic noise. Further signal processing included band-pass filtering and calculation of the normalized cross-correlation of force signals. The normalized cross-correlation was applied to evaluate the time delay τ between cognominal force signal components (x and x, y and y, z and z).

Measurement signals undergoing the segmentation process and the segments length had to be sufficient to resolve vortex perturbations in the flow. For this a temporal resolution of the system was calculated. The temporal resolution is the number of detected objects per unit time and depends directly on the object's velocity. Therefore the time delay for each velocity was used to estimate the optimal temporal resolution in the goal experiment.

Depending on the mean flow velocity u_{m} the transit time τ can vary from 0.1 s to 1.5 s, hence continuance of each test should be long enough to contain over ten values of τ within the test duration. This amount is sufficient for precise evaluation of the signal's cross-correlation value. Based on this assumption, the test duration should not be less than 20 s at the lowest velocity u_{m}. During the experimental investigation each provided test lasted more than one minute and its resulting force signals were divided into 20 s segments to avoid an influence of arbitrary outer noise on the result.

For the analysis of the obtained segments, digital signal processing was applied that included the investigation of power spectra density, filtering and cross-correlation. Most of

these operations were done by the instrumentality of the use of the commercial software MatLab.

4.2.1 Power spectra analysis

Spectral analysis [64] considers the problem of determining the spectral content (i.e., the distribution of power over frequency) of a signal. The presence of noise in a signal can have significant effects on the measurement quantities and on a measurements resolution in general [1]. Thus, the power spectra analysis is essential to compare energy of different signal components and to investigate response of the whole measurement system on different sources of noise. The apparent division between signal and noise is artificial and depends on the criteria of the user. In the present case we designate the force signal fluctuation that take place due to a vortex movement as the desired signal and other random disturbances or periodical influences as the undesired noise.

Any machine is a source of oscillation by itself, vibrations especially occur where parts are moving. The algorithm of fast Fourier transform [65] was applied to obtain the power spectra of signals of the goal experiment and to investigate its noise components. The fast Fourier transform reveals periodicities in input data as well as relative strengths of any periodic components. In other words, the algorithm gives the frequency distribution of a signal power and is useful to find the frequency components of the desired signal as well as of the noise. For this purpose a standard Matlab function was used to investigate the experimentally obtained signals in the frequency domain [66].

Despite the mentioned noise sources, the excitations from the environment have to be considered, i. e. building oscillations, vibrations from surrounding laboratories, etc.

The zone of interest of the presented research was limited by frequency of 50 Hz due to the fact that electromagnetic noise and residual echoes of hydraulic noise are dominated at the higher frequencies. According to the observations of different force signal components we obtained the next results: the main sources of noise detected in main flow direction (Fig. 4.3) and collateral directions (Fig. 4.4) are the electromagnetic pump operation and natural frequencies of the construction parts of the measurement system.

The lines of intensive colors represent original frequencies and less intensive ones of the lines represent harmonics of original values. Up to three harmonics of each origin were emphasized by the lines even though more of them are presented at the original power spectra.

The highest power spectrum energy of the selection occurs at the frequencies proportional to the pump rotation frequency w_{p}. These signal component represent electromagnetic and mechanical noise from the moving element of the system. Electromagnetic noise occurs due to the cycles of magnetic field change caused by the permanent magnets rotation. Analyzing the x and y-components of the force signal one can see that the highest power belongs to the frequencies equal to ten and five times of w_{p}. The first one is caused by the interaction of each magnetic pair and the liquid metal. The second one appears mostly within collateral flow directions (y and z) and caused by the simultaneous influence of two pairs of the permanent magnets on the liquid metal from both sides of symmetry axis of the pump discs. Under each pump revolution, the liquid metal in the duct undergoes ten half cycles of magnetic field variations that disturbs the flow and can be detected by the force sensors as force fluctuations

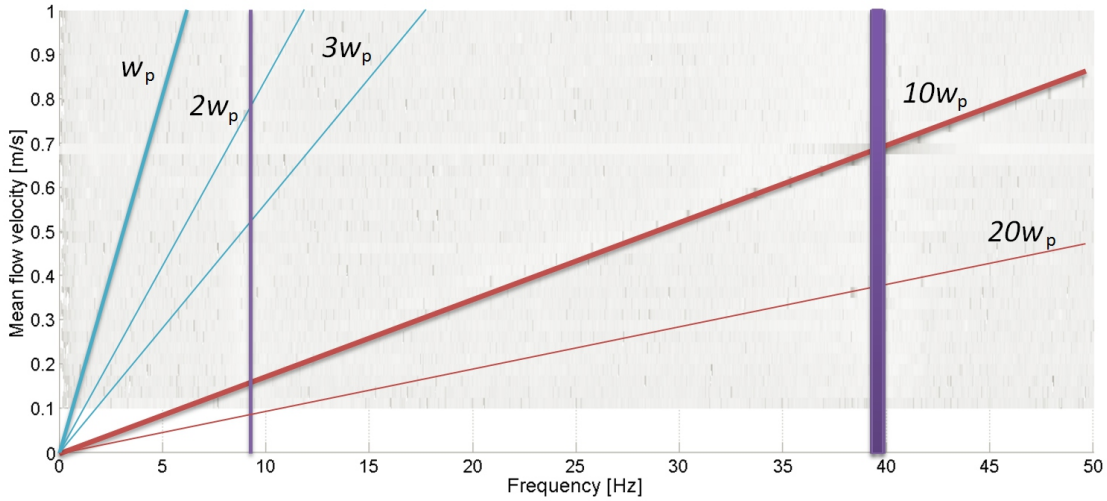

Fig. 4.3: The power spectra density of the typical force signal in the main flow direction (x). The dominant frequencies arising under different mean flow velocities are highlighted as lines. The red and blue lines are related to the pump caused perturbations (of electromagnetic and mechanical nature correspondingly). The purple lines represent natural frequencies of the measurement system.

with the frequency $5w_p$. Another significant component of power spectra has a frequency equal to the pump rotation itself and appears due to the mechanical asymmetry of the pump discs and arrangement of the individual permanent magnets. The power spectra has similar elements for all three components of the force signal, however intensity may vary significantly.

The natural frequencies of the measurement system components are observed at 9 Hz and around 40 Hz. The first value corresponds to the eigen frequency of the support construction of the measurement system. This component has a comparably low energy due to the high weight of the construction and hence high inertia. The second value represent the natural frequency of the applied force sensors. Though the declared value of their natural frequency is 180 Hz, the actual value decreased to the frequency of 40 Hz at the loaded state due to the influence of the weight of relatively heavy magnetic system. The frequency band here is noticeably wider than the other frequency components due to the Lorentz force influence. The bulk flow passing magnetic field is caused the generation of Lorentz force in x-direction which can reach values up to 0.5 N and bias the resulting natural frequency of the force sensors.

The most important finding of the power spectra analysis was the fact that no specific frequency of the vortex generation was observed. Two different reasons can cause such effect:

- The power of the artificial vortex generators is very weak and their frequency cannot be observed in the power spectra against the background noise.
- The detected signal does not depend on the artificial vortex generation and the revealed flow perturbations are created by natural reasons within the liquid metal flow (in specific on the conditions of the goal experiment).

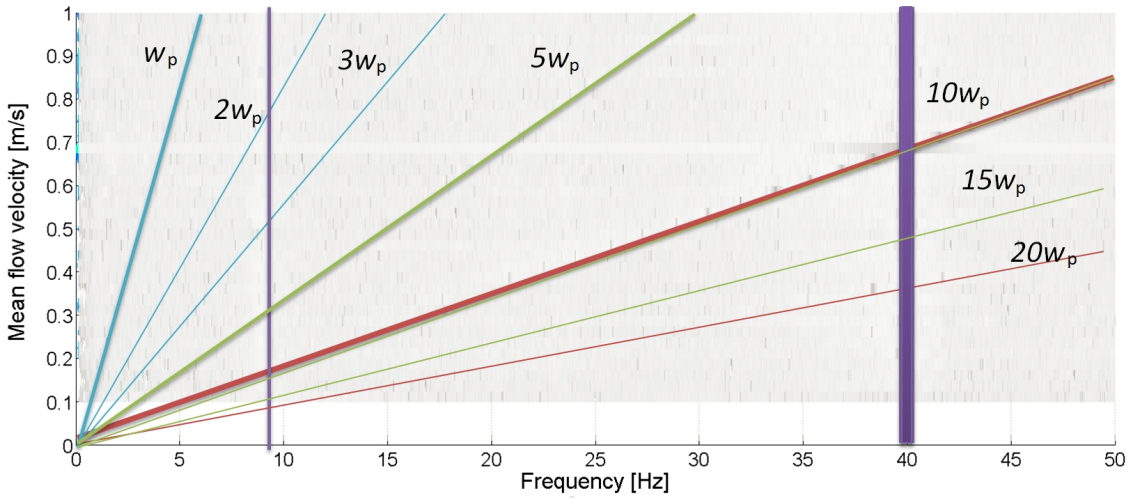

a)

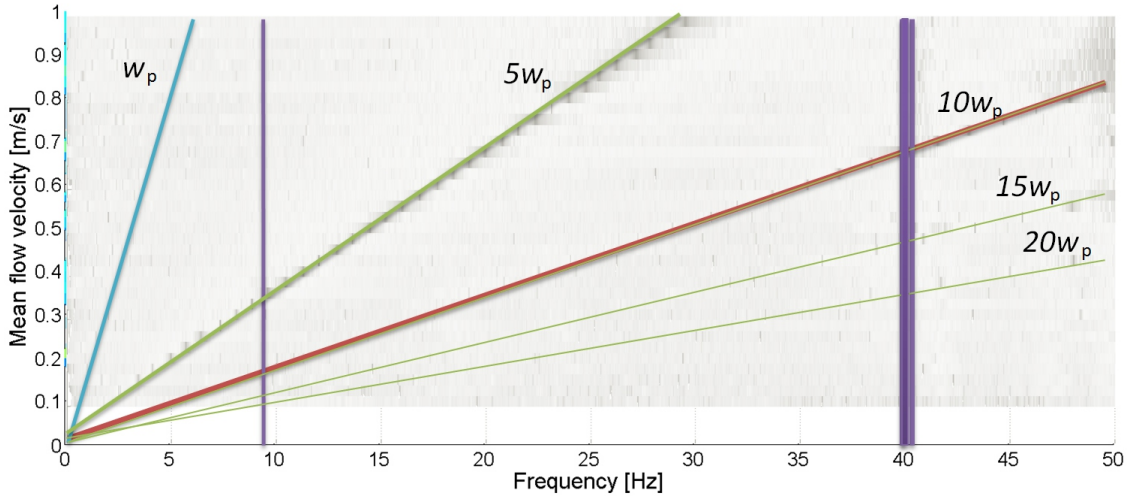

b)

Fig. 4.4: The power spectra density of the typical force signals measured in the collateral to the main flow directions. The dominant frequencies arising under different mean flow velocities are highlighted as lines. The red, green and blue lines are related to the pump caused perturbations of electromagnetic (red and green) and mechanical (blue) nature correspondingly. The purple lines represent natural frequencies of measurement system. The power spectra of force signals in y (a) and z-directions (b) are presented.

4.2.2 Filtering and correlation analysis

A measured signal can be influenced by unknown disturbances and effects. A high level of noise can generate the adulterate correlation peaks and suppress the useful ones. Within the provided experiments it was observed that the raw measurement signals have low signal-to-noise ratio. This leads to a low magnitude of the normalized cross-correlation function between force signals, furthermore the noise present in the signals causes a high value of the adverse correlation function, which can disguise the desired one. This implies searching for a proper filtering technique to improve signals quality in our specific case.

The measurements within the goal experiment can be classified as static ones – experimental data are collected at the system's steady state with constant mean flow velocity. Slow change of signals values in time due to temperature rise or natural signal drifting has no significant effect on the measured values. Hence averaging and other classical filter techniques can be applied in the presented case. According to the fact that the time-of-flight LFV measurements have a goal to detect small fluctuations of the flow, the mean component of signals was extracted from the further processing. This operation has the name detrending [67] and provides removing means, offsets, or linear trends from the regularly sampled time-domain data signals. The detrended data describe the changes in force signals without concerning an offset and enable to obtain a more precise correlation value between the processed signals.

After the detrending procedure each measurement segment (of 20 s duration) is undergoing a digital filtering to distinguish the desired signal from the noise and improve the signal-to-noise ratio. The noise contribution to the signal can be decreased and the signal-to-noise ratio can be increased by a targeted bandpass filtering of the force signals. However, to do this the cut-off frequencies of the filter must be carefully chosen so as not to suppress the useful signals. The advantage of the application of bandpass filters is that the noise influence can be decreased both in the low and high frequency range, keeping the desired signal in operation. The applied filter has the band-pass in the low frequency region (3...9 Hz) which corresponds to the hydraulic signals frequencies. The values of band were chosen empirically after analyzing the signals power spectrum for three force components. The higher frequency noise corresponds to the electromagnetic influence of the pump rotation and electrical net. The lower frequencies represents the stochastic and mechanical oscillations. For the filtering purpose Butterworth filter with zero shift was designed with Matlab code application.

The comparison of the raw force signals and the filtered ones is presented at Fig. 4.5. The

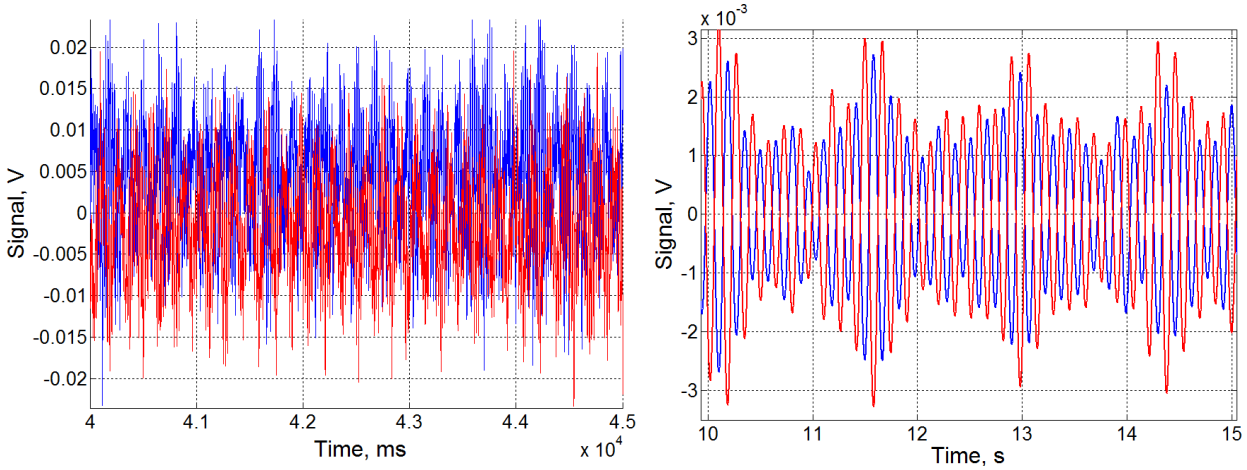

Fig. 4.5: The comparison between the raw force signals and the filtered ones. The force signals were obtained during the time-of-flight LFV experiments, they did undergo the detrending procedure (a) and were filtered by the band-pass zero shift filter (b).

presented force signals were measured at the mean flow velocity 0.4 m/s. As one can see, the raw signals contain a high frequency noise that was excluded after the filtering. Nevertheless, the low frequency fluctuations are still present.

As opposed to power spectra analysis and filtering, whose task is to estimate cut-off frequencies and to distinguish the desired signal, the cross-correlation uses these estimated parameters from two force signals to derive a certain time-of-flight value between them. The normalized cross-correlation [68] is a standard method to estimate the degree to which two data series are correlated. The maximal value of a correlation coefficient δ shows the value when both investigated curves match the most. Under the normalized cross-correlation the range of the correlation coefficient can vary from -1 to 1 (Fig. 4.6).

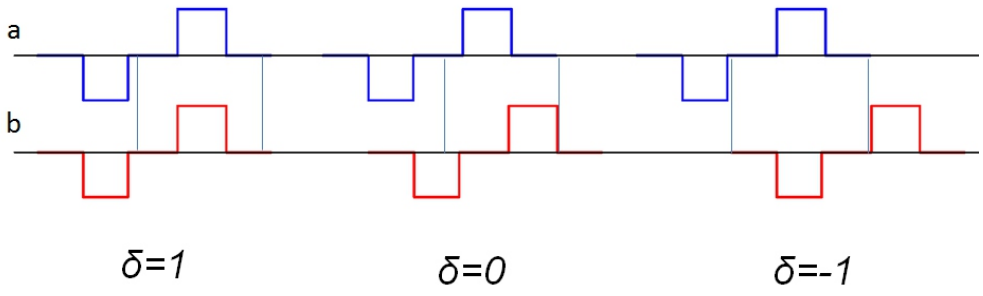

Fig. 4.6: Correlation coefficient implication. Two diagrams are presented at three different positions to each other. Every position is characterized by the correlation coefficient δ of a current localization: δ=1 means full agreement between the functions (positive correlation), δ=0 means the independent behavior of the functions, δ=-1 means that the functions are opposite to each other (negative correlation).

Different algorithms can be applied to estimate δ. Two types of techniques were examined before the optimal algorithm for the current research was discovered.

The first one is a non-normalized cross-correlation function calculated by fast Fourier transform. The sample non-normalized cross-correlation of two input signals requires that $Corr$ be computed by a sample-shift (time-shifting) along one of the input signals $x1$ and $x2$. For the numerator, this is called a sliding dot product or sliding inner product. The dot product is given by fast Fourier transform. We can compute correlations using the fast Fourier transform as follows [69]:

$$Corr(x1, x2)_\tau \quad = \quad X1_\tau X2^*_\tau. \tag{4.4}$$

Where X1 and X2 are the fast Fourier transforms of x1 and x2, and the asterisk denotes complex conjugation. The discrete Fourier transform algorithm was applied to find the correlation between the force signals taken simultaneously from both sensors. But the magnitude of δ in this case has no physical meaning. In other words, it was impossible to estimate how the signals match. As an alternative method the normalized cross-correlation was applied.

An one-dimensional normalized cross-correlation between two input signals $x1$ and $x2$ can be defined as [70]:

$$\delta \quad = \quad \frac{\sum([x1(t) - \overline{x1}][x2(t-\tau) - \overline{x2}])}{\sqrt{\sum[x1(t) - \overline{x1}]^2 \sum[x2(t-\tau) - \overline{x2}]^2}}. \tag{4.5}$$

The coefficient δ is a measurement of the size and direction of a linear relationship between the signals $x1$ and $x2$. The normalized cross-correlation of two force signals was calculated

by the described algorithm with Matlab function *xcorr*2 and the results allow to estimate the time-delay τ and evaluate the liquid metal flow rate Q by (4.2).

The results obtained by the represented signal processing are described in the sections 4.3.

4.3 Measurement results and discussion

4.3.1 The results of the solid metal tests

This section presents the results obtained with the solid metal tests. The results not only give a first impression on the magnitude of the Lorentz forces generated in the laboratory time-of-flight LFV experiment, but are also used to estimate the mechanical noise level generated by the motor and the electromagnetic pump. It allows to distinguish the different noise components and examine their influence on the measured force signals. The mechanical noise is generated as an unavoidable result of the motor's work and rotation of the electromagnetic pump and it arises even though there is no mechanical contact between the pump and the duct. To investigate an effect of the mechanical noise, the solid metal experiment with the several rotation frequencies of the pump was performed (Fig. 4.7).

The raw experimental observations allow to assume that Lorentz force generated by the copper plate motion creates relatively strong force perturbations. The perturbations are detected by the force sensors. the resulting peaks are visible by the unaided eye even against the background of the different mechanical noise levels. A relatively high level of the observed noise at 2 Hz is conditioned by the resonance overlapping of the pump frequency and the natural frequency of the measurement system construction. The observed peaks have different height due to a non-uniformity of manual motion of the copper plate. The generated Lorentz force depends on the copper plate path through the magnetic field.

Another important sequence of the solid metal experiments is the possibility to test the signal processing scheme. Both filtering and cross-correlation techniques were applied to examine the obtained measurement results. The comparison of the obtained time-delay values for the raw measurement data and after the applied filtering is presented in table 4.1. Two cutting-off frequencies were tested for the signals filtering: 10 Hz and 25 Hz. As a type of

Tab. 4.1: Transition time values that were expended by the copper plate to cover 0.15 m *distance (the plate was moving with a different velocity in each case). All values are estimated with the Matlab correlation function*

Signal type	Time delay τ [s]			
	w_p=0 Hz	w_p=2 Hz	w_p=3.33 Hz	w_p=6.67 Hz
Raw signal	0.378	0.392	0.316	0.249
Low-pass 25 Hz	0.373	0.391	0.311	0.329
Low-pass 10 Hz	0.376	0.39	0.317	0.319

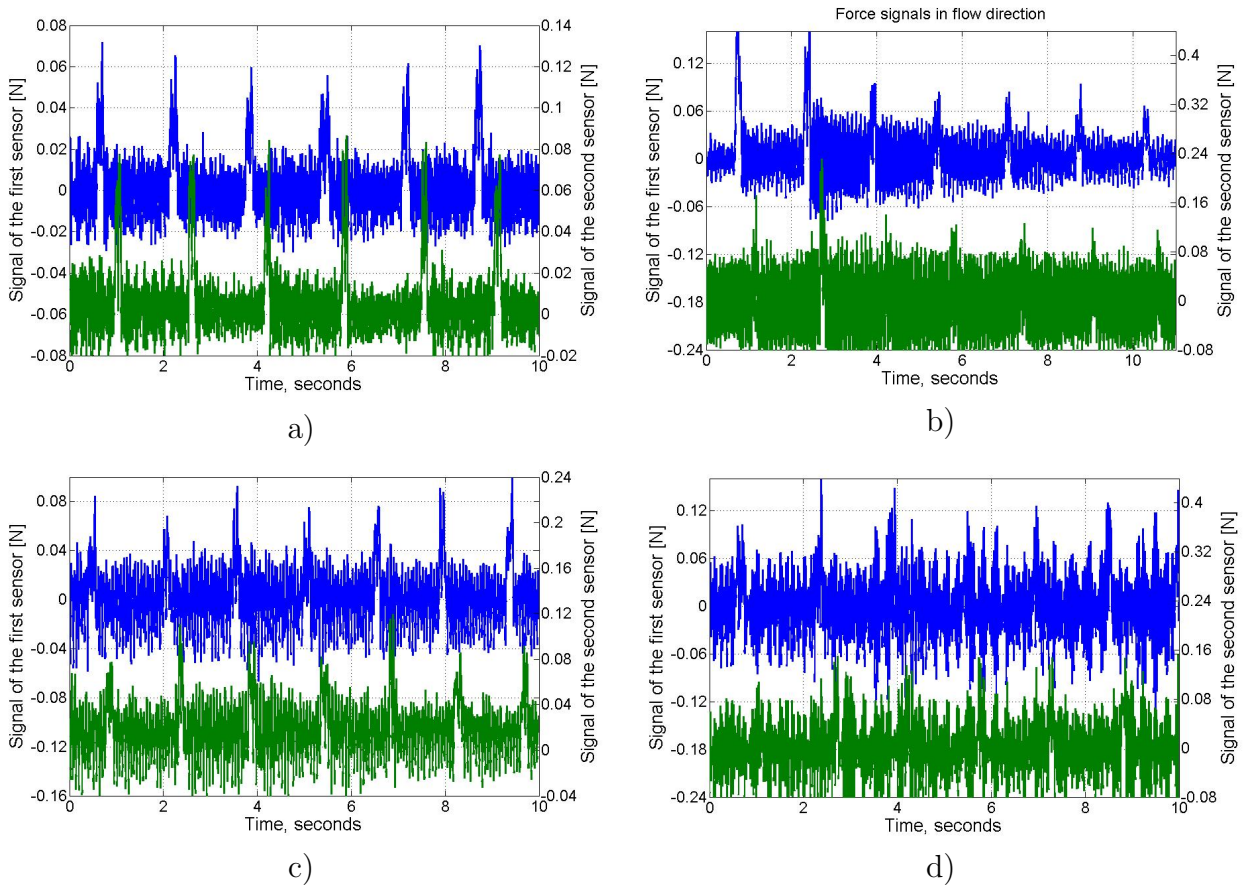

Fig. 4.7: Solid metal tests results The raw measured force signal with different levels of the motor and the pump noise: (a) the pump is off; (b) pump rotation frequency is equal to 2 Hz*; (c) pump rotation frequency is equal to 3.33* Hz*; (d) pump rotation frequency is equal to 6.67* Hz

filter, the low-pass one was used which was assumed to be sufficient for the solid metal tests. According to the obtained results, the time delay values showed only small discrepancies when the system was undergoing the effect of low rotation frequencies of the pump. After reaching the frequency of 6 Hz, the amplitude of the mechanical noise is strong enough to conceal the desired signal and after the reaching of the noise level, the filtering is becoming crucial.

The high signal-to-noise ratio of the performed tests with solid metal occurred due to the low level of the internal, outer and supplementary disturbances. The measured Lorentz force has a magnitude around 60...70 mN, which well corresponds to the expected force value 120 mN, evaluated by (2.4). The characteristic length L for the Lorentz force calculations was estimated by the area of the copper plate part under the magnetic field influence.

4.3.2 The results of the liquid metal tests

The liquid metal tests provided under the current research can be divided into two big parts: the measurement of the liquid metal bulk flow and investigation of the fluctuation behavior

to determine the time delay τ. The bulk velocity plays a crucial role in the classical Lorentz force velocimetry technique [17] and the value is used to estimate the mean flow velocity as well as the flow rate of conductive liquids. Both experiments were performed for the two position of the permanent magnets according to the duct: with complete (symmetric) and half (asymmetric) overlap of the duct height by the magnetic field. The second type of tests was intended to examine the behavior and distribution of the Lorentz force components in case of asymmetric magnetic field applied to the flow. Another reason for asymmetric position is to investigate the effect of passing vortices detection and system resolution for the different areas of the magnetic field influence.

4.3.2.1 Bulk flow investigation

As the first experimental series, the tests with the symmetric magnetic field were performed. The permanent magnets were situated in a such way, that their magnetic field penetrated the whole height of the duct. The forces acted on the magnet system in the vicinity of the metal flow can be predicted by equation(2.4), where the characteristic length L is calculated as hydraulic diameter D_{H} (2.8) of the whole cross-section area of the duct ($10{\times}80$ mm^2). For the Lorentz force estimation it was assumed that the liquid metal moves at uniform velocity, and the velocity field is not significantly affected by the magnetic field (kinematic approximation and relatively low interaction parameter N).

The magnitude of velocity u_{m} was taken from 0.1 m/s to 1 m/s with a step 0.1 m/s. The Lorentz force calculation results are summarized in table 4.2 and compared with the experimentally obtained values. We took the mean values for each obtained force component under the steady part of the Lorentz force signal. All three measured force components are presented in the table as well as their vector product. The ratio of analytically obtained values of Lorentz force and the vector product of the measured Lorentz force are given for the plain comparison.

According to the obtained experimental data, the next observations have been made:

- As it was expected, the x-component of the measured force (in main flow direction) has the highest influence on the resulting Lorentz force (the vector-product); the y-component of the measured force is equal to approximately equal to 10% of the x-component. The z-component of the force is rather random (the measured data includes as positive so negative the force values).

- Both x and y components of the force show linear behavior of their change with the velocity rise. This behavior is apprehensible [29] according to low value of magnetic Reynolds number $Re_{\mathrm{m}} \ll 1$ in the experiment. The essence of the low-R_{m} approximation is that the magnetic field associated with the induced currents j is negligible by a comparison with the imposed magnetic field. Hence influence of the flow velocity on the magnetic flux density can be neglected. The z-component of the force does not show dependence on the flow velocity value and caused by local flow perturbations in the measurement zone. Moreover, the z-component of the force is not reproducible from one experiment to another. The perturbations are assumed to have an asymmetric distribution within the flow volume. this caused the asymmetric force distribution throughout the height of the duct.

Tab. 4.2: Analytical and experimental estimation of Lorentz force for the bulk flow of the liquid metal. The theoretical values are calculated for the different velocities u_m. The experimental values are given for all three force components (x, y, and z). The vector-product of the three force components is represented. The measurements are provided under the symmetrical magnetic field influence.

Velocity [m/s]	0.1	0.2	0.3	0.4	0.5	0.6	0.7	0.8	0.9	1.0
Theoretical LF [mN]	21	41	62	82	103	124	144	165	185	206
Exper. LF (x) [mN]	19.6	37.2	51.2	66	76.1	85.1	96.6	103.5	108.7	120
Exper. LF (y) [mN]	3.6	4.6	5.2	5.9	6.6	7.2	7.7	8.1	8.4	8.8
Exper. LF (z) [mN]	-2.0	-2.6	1.6	1.7	0.6	3.2	2.5	4.1	4.2	4.5
Resulting LF [mN]	20	37.6	51.5	66.3	76.4	85.5	96.9	103.9	109.1	120.4
Ratio Exp./Theory	0.95	0.92	0.83	0.81	0.74	0.69	0.78	0.63	0.59	0.58

- The ratio between experimentally and theoretically obtained Lorentz force values is decreasing with growth of the flow velocity due to intensifying of the turbulence fluctuations within the liquid metal under the relatively high Reynolds number Re [75] (over $Re = 15000$). Turbulence in the flow is not something that can be calculated precisely, but the concept of the Reynolds number is a helpful one for a general understanding of the process and flow examination. At low velocities the experimental/analytical Lorentz force ratio is close to one, which means that the calculated results correspond well to the experimental values. With the increase of velocity, the ratio is reducing due to occurred hydraulic effects inside the duct.

As the second experimental series, the tests with the asymmetric magnetic field influence were performed. The permanent magnets were situated in a such way that their magnetic field penetrated the upper half-height of the duct. The analytical value of Lorentz force for the bulk flow can be estimated by (2.4). The characteristic length L is calculated as hydraulic diameter D_H (2.8) of the half cross-section area of the duct (10×40 mm^2). The vector product of the measured Lorentz force components for both cases (symmetric and asymmetric magnetic field) are presented in Fig. 4.8. A dependence between the measured Lorentz forces and the velocity showed linear behavior.

The calculated Lorentz force components are summarized in table 4.3 and compared with the experimentally obtained Lorentz force data. The mean values of each component of the measured Lorentz force were obtained from the steady part of the force signals.

As one can see from the table, the bulk Lorentz force of the asymmetric magnetic field influence is significantly less than in the symmetric case. This observation can be explained by the hydrodynamic principles: the liquid metal flow tended to avoid the magnetic obstacle created by the permanent magnets pair. Due to this fact, the flow velocity increases in lower part of the duct (where no magnetic field was acting) and decelerate at the upper part of

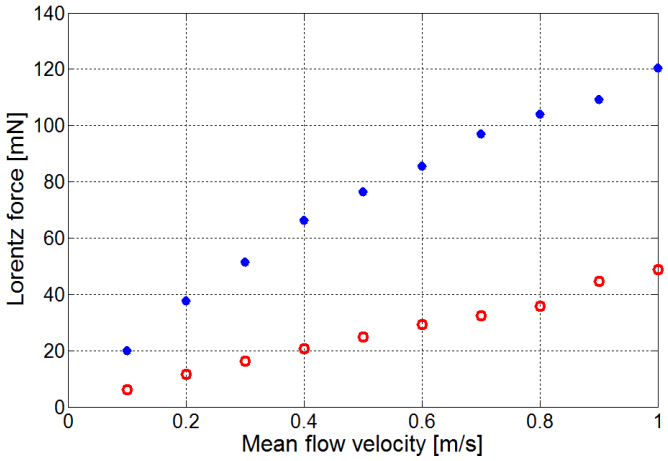

Fig. 4.8: The vector-product of Lorentz force values measured under symmetric (blue spots) and asymmetric (red rings) magnetic field influence.

the duct (measurement zone). Hence the velocity distribution has an asymmetric character and the actual measured Lorentz force is substantially less than the analytical one. However, this asymmetry of the velocity field does not contradict the kinematic approximation. Even though the magnetic field does not change the flow profile itself, it still decelerates the liquid metal flow as was proved by the Vives-probe measurements (section 3.4).

In the case of asymmetric magnetic field the x-component of the force shows the behavior dependent on the flow velocity. Unlike the symmetric case, here both y and z-components of the force are distributed randomly around zero force level and do not show reproducible behavior in the experiments.

The investigation of the bulk velocity components is of interest for researchers in hydrodynamics and fluid-dynamics. However it was not the main aim of the current project. The dynamical data analysis (for example, wavelet algorithm [73]) as well as the higher sampling rate are still needed for the estimation of the local instantaneous velocity components. Nevertheless, the Lorentz force velocimetry allows to estimate the velocity components at different flow regimes and various Reynolds numbers Re.

4.3.2.2 Time-of-flight LFV investigation

The time-of-flight LFV measurements included two identical flowmeters and a vortex generator, in the role of which the Vives-probe was used. The generated vortical structures are moving with the flow through both measurement zones consequently and caused fluctuations of the measured forces. The distance between the LFV flowmeters is defined. The mean flow velocity can be defined as the distance per the time between the force fluctuations equation (4.2).

The time-of-flight Lorentz force measurements were performed in four different configurations of the measurement system (Fig. 4.9):

- The Vives-probe is situated before both measurement zones and the magnetic field penetrates the whole height of the duct (Fig. 4.9a).

Tab. 4.3: The analytical and experimental estimation of Lorentz force for the bulk flow of the liquid metal. The theoretical values are calculated for different velocities u_m. The experimental values are given for all three force components (x, y, and z) as well as their vector-product. The measurements were performed under the asymmetric magnetic field influence.

Velocity [m/s]	0.1	0.2	0.3	0.4	0.5	0.6	0.7	0.8	0.9	1.0
Theoretical LF [mN]	15	30	45.1	60.1	75.2	90.2	105.2	120.2	135.3	150
Exper. LF (x) [mN]	4.98	11.1	16.1	20.3	24.5	28.6	31.9	35.7	44.4	48.8
Exper. LF (y) [mN]	2.13	2.78	2.22	3.31	3.65	3.15	5.25	3.2	3.9	3.6
Exper. LF (z) [mN]	-2.9	1.7	1.25	-0.5	2.5	3.2	2.5	1.35	1.8	-0.5
Resulting LF [mN]	6.14	11.6	16.3	20.6	24.9	29.2	32.4	35.9	44.6	48.9
Ratio Exp./Theory	0.41	0.39	0.36	0.34	0.33	0.32	0.31	0.30	0.33	0.33

- The Vives-probe is situated between of the measurement zones and the magnetic field penetrates the whole height of the duct (Fig. 4.9b).
- The Vives-probe is situated before both measurement zones and the magnetic field penetrates the half height of the duct (Fig. 4.9c).
- The Vives-probe is situated between of the measurement zones and the magnetic field penetrates the half height of the duct (Fig. 4.9d).

The flow rate estimation results for the all four cases are presented (Fig. 4.10 – 4.13). In the figures one can see the dependence between the measured flow rate (obtained by the Vives-probe and time-of-flight LFV) and the pump rotation frequency. The experimental results of the time-of-flight tests are given without taking into account the experimental coefficient k. Basically here we gave the raw measurement data, the coefficient k will be estimated further. The obtained measured data showed a wide scatter of the flow rate values, hence evaluation of the resulting flow rate relative to the pump rotation frequency can be provided by the trendlines estimated with a script written in Matlab software. The flow rate estimation was based on the measured time delay τ between perturbations of the two measured force signals. The passing vortex generated flow disturbances and hence the force perturbations in all three dimensions. To detect these perturbations, the three pairs of the force components were measured and analyzed – streamline direction (x), gravity force direction (z) and magnetic lines direction (y).

The forces measured in x-direction contained the main hydraulic and electromagnetic noise components due to the pump influence. The signal-to-noise ratio of the signals in streamline direction (x) is considerably low to distinguish the desired signal from it. The behavior of the flow rate curves at (a) parts of (Fig. 4.10 – 4.13) shows different behavior in comparison with the reference curve. The first part of the time-of-flight LFV data has a higher

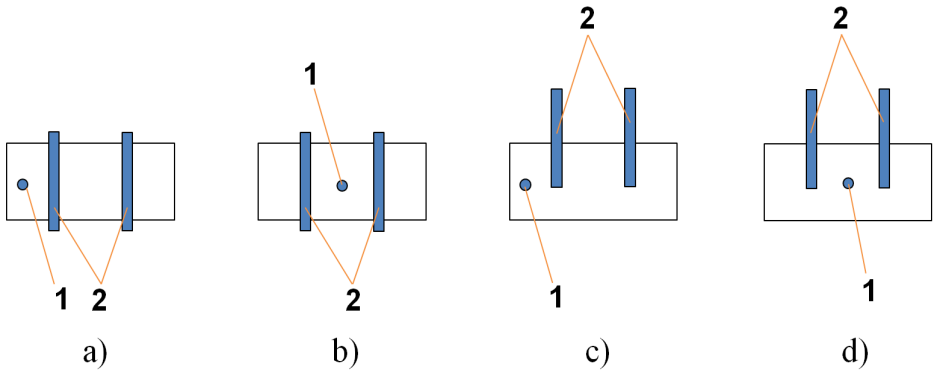

Fig. 4.9: Positioning of the measurement system and the vortex generator. 1 – vortex generator, 2 – permanent magnets.

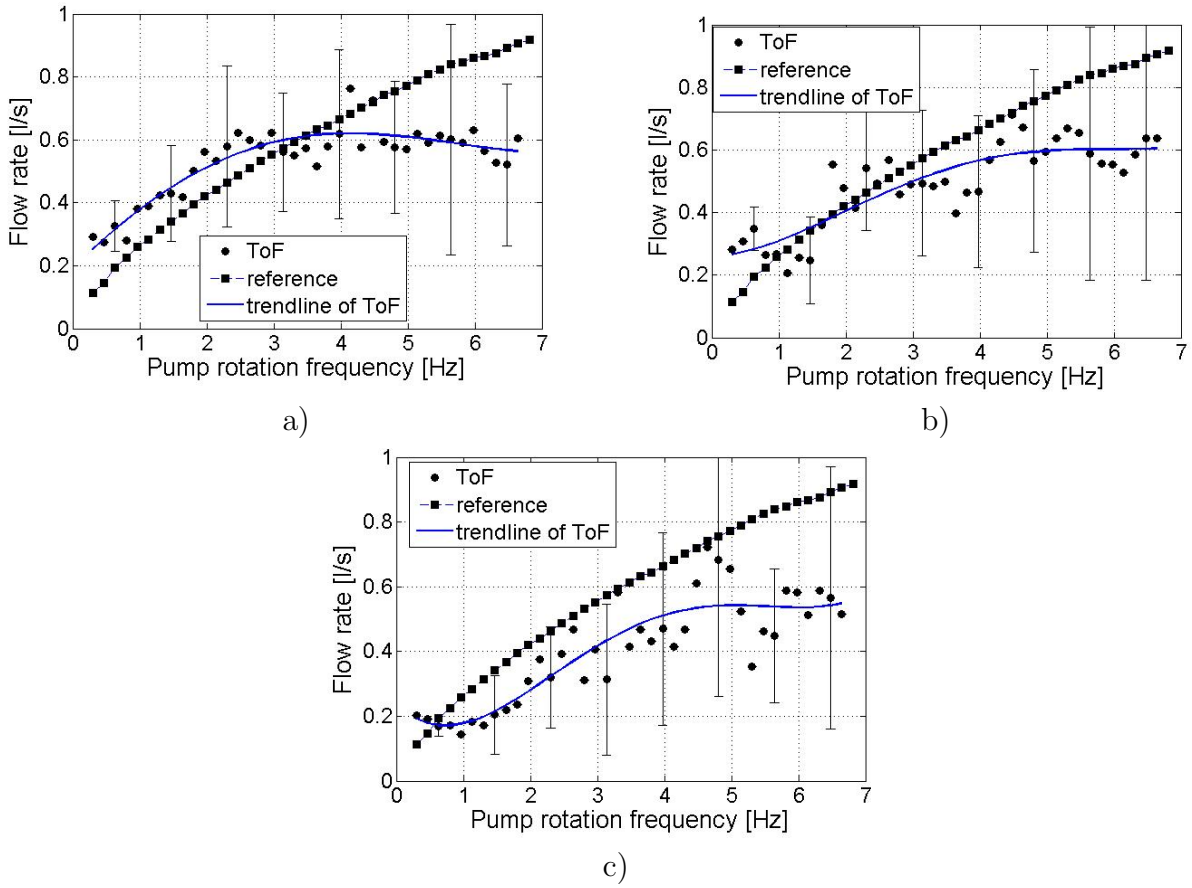

Fig. 4.10: The flow rate values obtained by the time-of-flight (ToF) and Vives-probe for three force directions. The Vives-probe is positioned between of the measurements zones, the magnetic field penetrates the whole duct height. The x (a), y (b) and z (c) force components are presented. Squares represent the measurement data obtained by the Vives-probe; diamonds are results of the time-of-flight measurements.

value than the reference ones (the zone of a low pump rotation frequency), which is scarcely probable from the physical point of view (a vortex structure in flow cannot move faster than the flow itself within a narrow duct). The second half of the time-of-flight curve shows a weak dependence on the pump rotation frequency. The signal-to-noise ratio is decreasing with rise of the flow velocity because of the rise of a noise energy. Hence the second part of the curve becomes contaminated by the noise and the whole applied signal processing is not sufficient to distinguish the desired signal form the measured data. According to the observation, the x-direction forces cannot be sufficient enough for flow rate estimation. Hence the flow rate results obtained by the time-of-flight LFV in streamline direction are rather questionable.

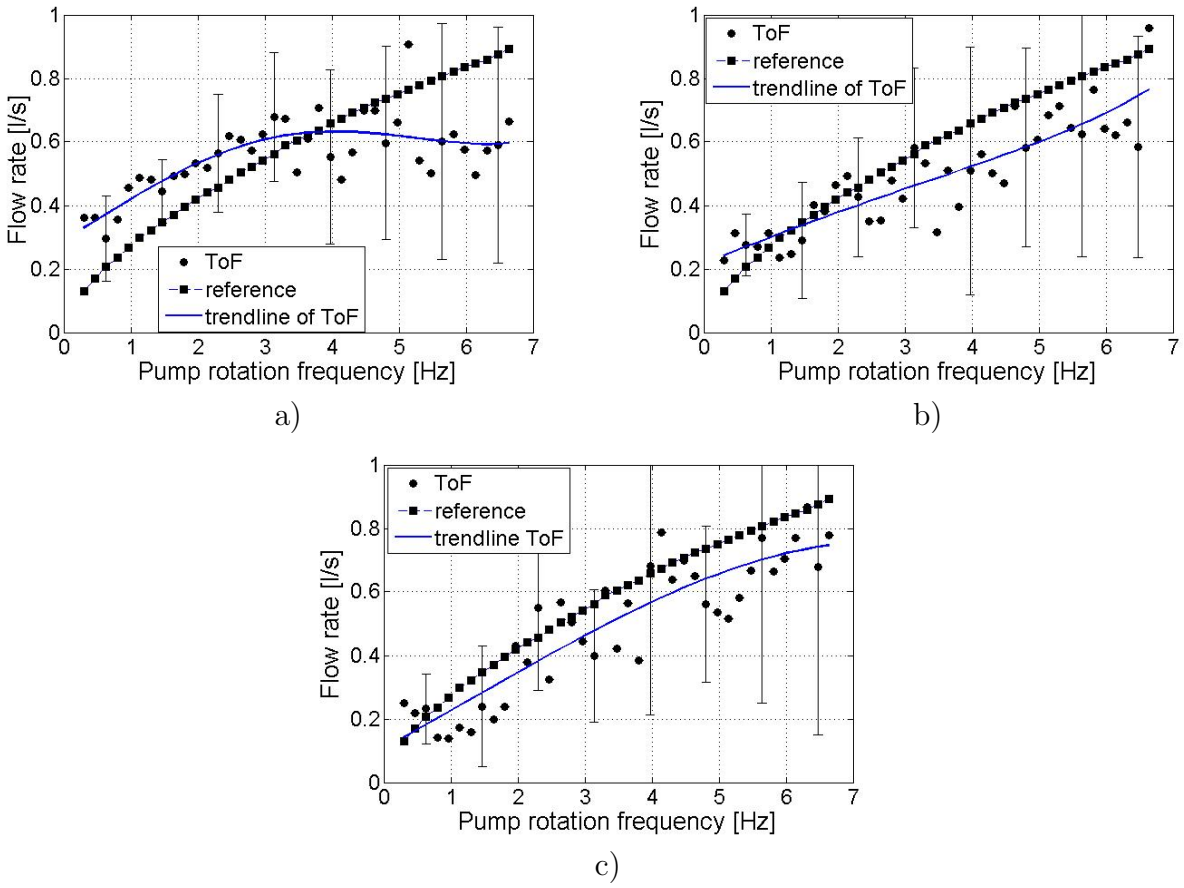

Fig. 4.11: The flow rate values obtained by the time-of-flight (ToF) and Vives-probe for three force directions. The Vives-probe is positioned between of the measurements zones, the magnetic field penetrates half of the duct height. The x (a), y (b) and z (c) force components are presented. Squares represent the measurement data obtained by the Vives-probe; diamonds are results of the time-of-flight measurements.

In the y-direction ((b) at the all four figures) no Lorentz force was expected because the y velocity vector is parallel to the magnetic field lines. According to the equation (2.1), this combination of the velocity and the magnetic flux density $\mathbf{u} \times \mathbf{B}$ does not generate eddy currents. This fact, according to (2.3), leads to nonoccurence of the Lorentz force in the liquid metal athwart to the flow direction. In fact, a certain dependence between the flow rate obtained by the time-of-flight LFV and reference flow rate values was observed in

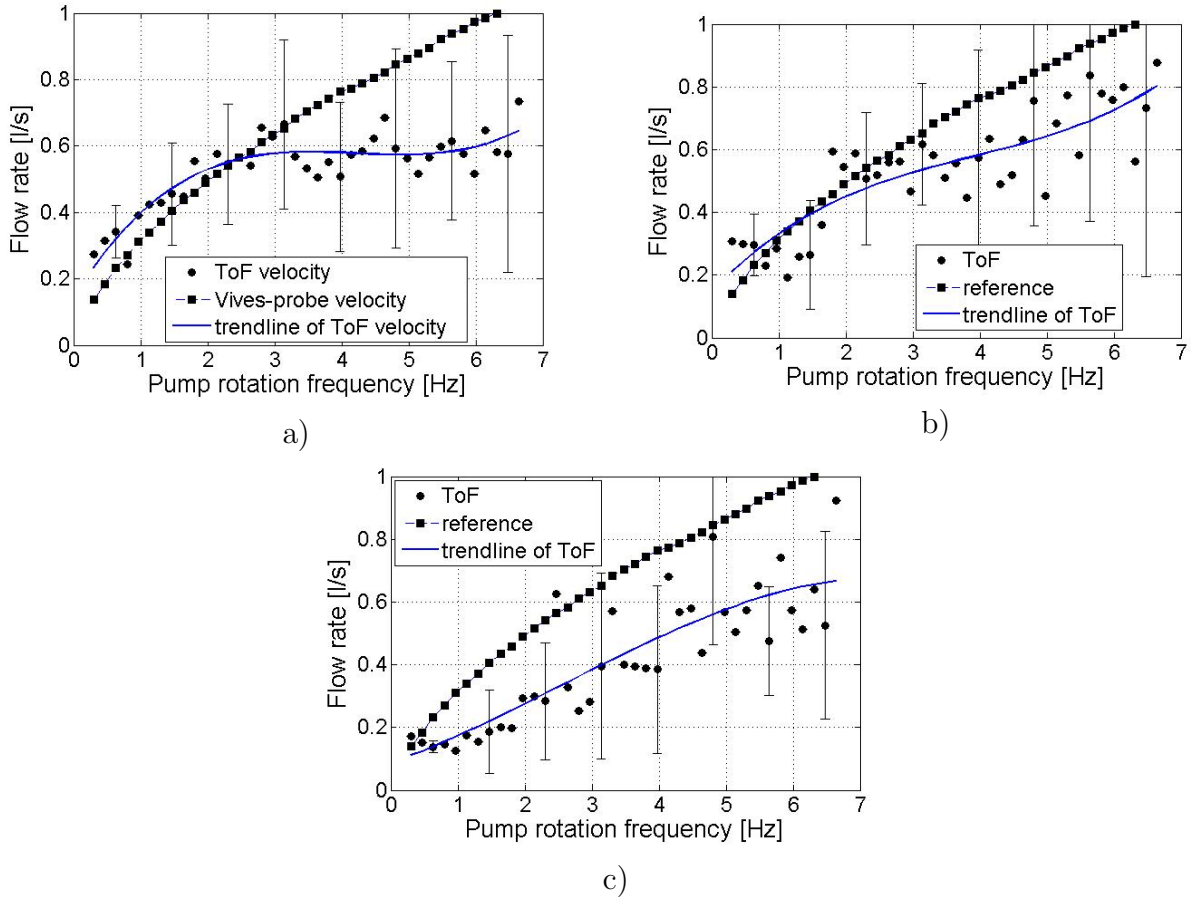

Fig. 4.12: The flow rate values obtained by the time-of-flight (ToF) and Vives-probe for three force directions. The Vives-probe is positioned before both measurements zones, the magnetic field penetrates the whole duct height. The x (a), y (b) and z (c) force components are presented. Squares represent the measurement data obtained by the Vives-probe; diamonds are results of the time-of-flight measurements.

the all four cases of the measurement system positioning. However, the relation between the estimated flow rate and the pump rotation frequency is not certain enough to use it for flow rate evaluation in the whole range. At the figures, one can see that the first half (the zone of low pump rotation frequency) of the flow rate obtained by the time-of-flight LFV in y-direction shows better agreement with the reference data than the values obtained in x-direction (the trendlines). This observation allows to assume that at the region of low pump rotation frequency the signal-to-noise ratio is high enough to measure the desired signal adequately after the applied signal processing. The second half of the curve at figure 4.11 locates in the region of the reference flow rate data. At the other three cases the second part of the flow rate curve obtained by the time-of-flight LFV has significant disarrangement between the time-of-flight LFV and the reference flow rate values.

At the z-direction ((c) at the all four figures) the force component is mostly influenced by the lifting force occurred due to the passing vortical structures. The assumptions underlying our observation are based on the low level of the bulk flow effect on the z-component of

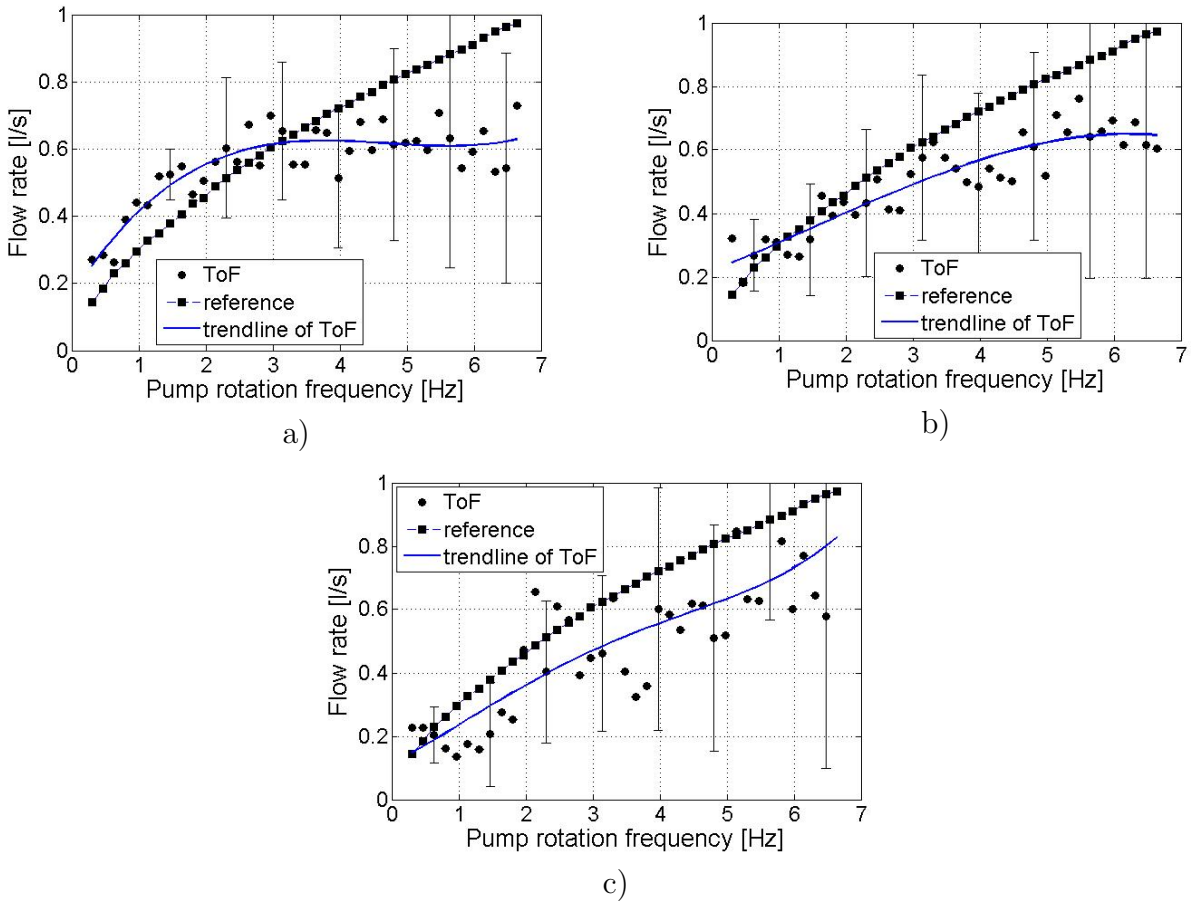

Fig. 4.13: The flow rate values obtained by the time-of-flight (ToF) and Vives-probe for three force directions. The Vives-probe is positioned before both measurements zones, the magnetic field penetrates half of the duct height. The x (a), y (b) and z (c) force components are presented. Squares represent the measurement data obtained by the Vives-probe; diamonds are results of the time-of-flight measurements.

force as was proved previously. The force disturbances occurred due to vortex movement can have the same order of magnitude at each direction. The flow rate values estimated by the time-of-flight LFV in z-direction allowed us to observe a certain correspondence between the reference and the time-of-flight flow rates. Nevertheless, the calibration of the method should be applied to improve the quality and compatibility of the experimental data. The vortices behavior and their velocity in the flow depends on the duct geometry and the vortex generator aside from the liquid metal flow rate. The moving vortices are attracted to the static walls according to [61]; the attraction decrease the vortex velocity. Hence observed time-of-flight LFV flow rate has lower value than the reference one and the difference increase with the mean flow velocity rise.

The errors, shown at all four figures, occurred mostly due to the hydraulic noise effects and inferiority of the signal processing. The errors reflect an influence of the Lorentz force fluctuations caused by the electromagnetic pump rotation. The permanent magnets in the pump discs are discrete, hence the pumping force impulses are also discontinuous. The

hydraulic distortions by the pump operation occur due to the flow disturbances and cannot be completely eliminated from the desired signal.

It should be noted here that all measurements presented in this subsection have a high error value of up to 50%, which is depicted explicitly in the graphs as error bars. The error values were estimated by a standard deviation [74] as $2SD$. It was assumed that the measured signal is a random variable x appearing periodically during the experiment for n times. The variance or dispersion ϵ of the random variable x with statistical average of expectation G is defined as:

$$\epsilon \quad = \quad G[(x - x_m)^2]. \tag{4.6}$$

The variance ϵ of a stationary random process is the intensity of the varying components and the positive square root of the variance is known as standard deviation SD.

If we compare the experimental results of each measurement system position we can see that the most promising flow rate values were obtained at the asymmetric magnetic field position (4.11). The Vives-probe was situated between the two measurement zones. Here the trendline of the measured data has the closest location to the reference values. Nevertheless the error bar is still significant to assume it as a complete success of the time-of-flight LFV measurement method. The experimental errors are rather substantial and to overcome the method drawback one should improve the measurement and signal processing schemes further to reduce the noise level. To reach this goal, one can modify the existing liquid metal duct. The duct has sharp edges between the sections; this generates additionally the internal flow perturbations. Such undesired perturbations influence the measured force signal and complexify the further data processing. Another important source of the flow disturbances is the applied electromagnetic pump. The pump causes the periodical flow oscillations in the streamline direction (x-component) due to the repetitive and discrete influence of permanent magnets during the pump rotation. Eddy currents generated by the interaction between the liquid metal and the magnetic field of the permanent magnets are mainly concentrated in a zone of the pump direct influence. However, a part of the current is expanded and circulate around the whole loop, as was proved by numerical analysis [76]. This causes an appearance of the supplementary Lorentz force. The force arises periodically and has variable behavior due to oppositely directed magnetic pairs within the pump.

Another interesting conclusion from the data analysis can be made: the best results were obtained in the case, when the Vives-probe was positioned between of the two measurement zones, hence it could not be used as an artificial vortex generator. The vortices generated by the Vives-probe will not be able to pass through both magnetic pairs. Following this line of reasoning one can assume that original turbulence within the investigated flow is sufficient to realize the time-of-flight principle. The existing turbulent flow structures are enough to induce the detectable force perturbations and calculate the flow rate of the liquid metal.

To decrease the level of noise within the registered signal, the several developments of the measurement system design have to be made:

- To damp hydraulic oscillations we can install the specific construction elements to the loop, for example pulsation dampening devices [77], [78], [79].
- The edges of the duct have to be round to prevent the occurred disturbances.

- To reach the laminar flow regimes one can provide the duct with an additional valve element. In this case the flow rate will be controlled not only by the electromagnetic pump, but by the additional valve and hence precision of velocity settlement will be increased.
- The problem with supplementary Lorentz force due to circulated eddy currents can be solved by shortening the circuit from both sides of the pump. For this aim, a highly conductive material (for example a copper wire) should be immersed into liquid metal.

For the improvement of the method accuracy one needs to perform the calibration of the measurement system to find the experimental coefficient k:

$$k = \frac{Q\tau}{D}. \tag{4.7}$$

Within the current research the coefficient k was estimated for the experimental data. The analyze of the flow rate data obtained by the time-of-flight LFV can be carried out using the trendlines of Fig. 4.10 – Fig. 4.13. The empirical equations of the observed trendlines were used to calculate the flow rate Q_{exp} under each rotation frequency of the pump. The obtained result served for the estimation of the experimental coefficient k as follows:

$$k = \frac{Q}{Q_{\text{exp}}}. \tag{4.8}$$

For the every separate force component (x, y and z) and for each experiment (presented in Fig. 4.10 – Fig. 4.13), the mean experimental coefficient k was estimated (table 4.4). The presented items of the experiments (from 1 to 4) corresponds to the numerical order of Fig. 4.10 – Fig. 4.13. The relative value of measurement error was calculated for the obtained flow rate by [80]:

$$Error = \frac{Q - Q_{\text{exp}}}{Q_{\text{exp}}} 100\%. \tag{4.9}$$

Tab. 4.4: The experimental coefficient k and the relative error of the measured flow rate by time-of-flight LFV with k application.

Exp.	1(x)	1(y)	1(z)	2(x)	2(y)	2(z)	3(x)	3(y)	3(z)	4(x)	4(y)	4(z)
Coef. k	0.98	1.08	1.24	0.95	1.03	1.03	0.98	0.94	1.21	0.94	1.02	1.02
Error [%]	23.5	10.4	3.02	26.8	5.87	1.25	23.4	8.05	4.14	24.6	10.2	0.97

According to the observations one can clearly see that the flow rate value estimated by the z-direction fluctuations has the lowest measurement error. Such generalization yields the z-direction fluctuations as the reliable source of time delay τ data.

The obtained experimental results proved the time-of-flight LFV feasibility as the flow rate measurement technique for conductive fluids, in particular for the liquid metals application. Nevertheless, there are ways to improve the technique. Except the mentioned developments of construction, the signal processing can be adapted to the specific demands of measurement scheme. In particular, the digital filtering can be improved by the modifying band-pass width and a steepness of the filter function.

4.4 Uncertainties analysis

In this section we aim to describe a particular aspect of the validation process: the uncertainty of measurement. All of the known or suspected components of error have been evaluated in the section. The uncertainty does not represent the difference between the measured and the true value (which will be always unknown), but it is an estimated interval that includes all the possible results of the measurement – including the true value – at the chosen confidence level [81].

A detailed report of the uncertainty should consist of a complete list of the components, specifying for each method used to obtain its numerical value [82]. The mathematical model of the measurement that transforms the set of repeated observations into the measurement result is of critical importance because, in addition to the observations, it generally includes various influence quantities that are inexactly known. This lack of knowledge contributes to the uncertainty of the measurement result, as do the variations of the repeated observations and any uncertainty associated with the mathematical model itself.

As in the most cases, in the current research a measurand Q_{exp} is not measured directly, but is determined from other quantities: distance D, time delay τ, duct cross-section area A (duct width m and height d), experimental coefficient k through a functional relationship g_1:

$$Q \quad = \quad \frac{kmdD}{\tau} \quad = \quad g_1(D, \tau, m, d, k). \tag{4.10}$$

The values in brackets are called input quantities and one of them – the experimental coefficient k – is a composite input quantity and is dependent itself on the other parameters:

$$\begin{aligned} k \quad &= \quad \frac{0.85md\tau(4.3 \cdot 10^{-4}\sqrt{V_{\mathrm{NS}}^2 + V_{\mathrm{EW}}^2} + 0.3)}{Dmd} = \\ = \quad \frac{\tau(3.7 \cdot 10^{-4}\sqrt{V_{\mathrm{NS}}^2 + V_{\mathrm{EW}}^2} + 0.26)}{D} \quad &= \quad g_2(D, \tau, V_{\mathrm{NS}}, V_{\mathrm{EW}}). \end{aligned} \tag{4.11}$$

Here V_{NS} and V_{EW} are representing the reference velocity u_{m} measured by the Vives-probe, g_2 is a functional relationship between k and the input quantities. The velocity is evaluated by the potential difference magnitudes measured by the two pairs of copper electrodes (3.16). The functions g_1 and g_2 are to be interpreted as the functions which contain every quantity, including all the corrections and correction factors, that can contribute a significant component of uncertainty of the measurement result. The standard uncertainty of the flow rate value Q_{exp} depend on the standard uncertainties of values in brackets.

For measurement instruments with the discrete scale, the uncertainty can be evaluated depending on scale interval q. In this case a priory distribution of the measured value has

a rectangular shape (inside the interval q all values are equally possible), which give us the absolute value of uncertainty:

$$v(value) = \frac{q}{\sqrt{3}}. \tag{4.12}$$

This method can be applied for length measurements within the current research because all of them were done by the digital caliper with 0.01 mm resolution and 0.02 mm accuracy, hence $v(D) = v(m) = v(d) = 0.0116$ mm. The same technique can be applied to time delay value τ: the measured forces themselves do not influence the time value directly and the only their effect on τ can be estimated by the sampling rate of the measurement system. The sampling rate applied within the experiments is equal to 1000 Hz, hence one gets $v(\tau) = 0.00058$ s.

The uncertainty value for voltage (potential difference) depends on standard deviation SD, because the measured value a priori distribution has Gaussian distribution law. We can estimate SD for case of discrete random variables of n segments as follows [83]:

$$SD = \sqrt{\frac{1}{n}\sum_{i=1}^{n}(x_i - \overline{x})^2}. \tag{4.13}$$

Where $\overline{x}$ is a mean value of the investigated variable:

$$\overline{x} = \frac{1}{n}\sum_{i=1}^{n} x_i. \tag{4.14}$$

To calculate the uncertainty of voltage V_{NS} and V_{EW} values the measured results were divided into ten intervals with the interval length 5 μV each. The estimation was performed for one particular experimental segment (20 s) in the middle of measurement range of the flow rate according to assumption that the resulting uncertainty will be sufficient for the flow rate uncertainty evaluation. The standard deviation SD was estimated for both components of the measured voltage (along streamline and orthogonal to the main flow directions). The sampling rate of multimeter, that was applied for registering of potential differences between electrodes of Vives-probe, was 10 Hz, hence we obtained 200 measured voltage values (Fig. 4.14).

The standard deviation value of the measured voltage for orthogonal to the main flow direction component was estimated by (4.13) and the obtained distribution of samples. The mean potential difference V_{NS} magnitude was calculated as $\overline{x} = 300$ μV. In this conditions the standard deviation is equal to 14.8 μV or 4.9% in relative value. Similar estimations were provided for different flow rate values, but relative error was kept at 5% range. The SD for streamline flow component was estimated by the similar way. For a mean magnitude of potential difference V_{EW} $\overline{x} = 3000$ μV the SD was estimated as 43.1 μV or 1.4% in relative value. According to these obtained results, one can observe that the absolute values of velocity fluctuations are higher at the streamline direction. Nevertheless, due to the fact that a mean magnitude of potential difference in the streamline direction is approximately ten times greater than in orthogonal one, the relative values show an opposite picture: relative velocity fluctuations are stronger for the orthogonal flow component.

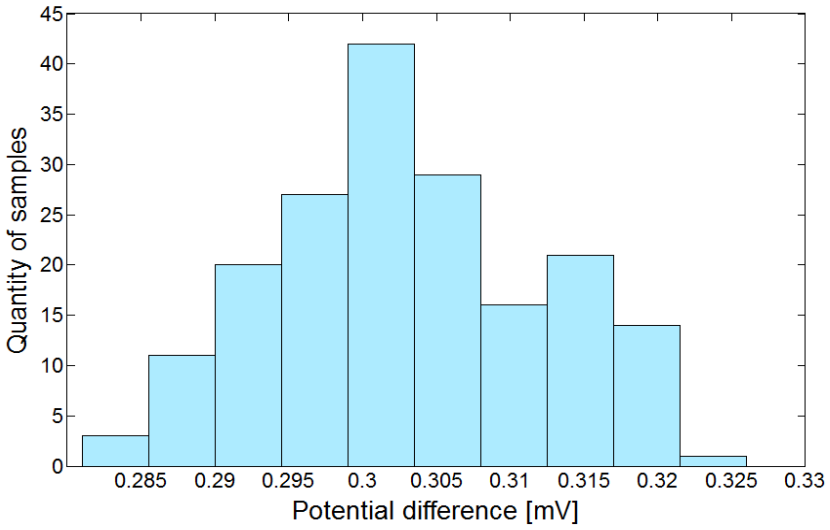

Fig. 4.14: Distribution histogram of the potential difference measured by Vives-probe electrodes for the main flow direction component. The horizontal axis represents potential difference between the copper electrodes, the vertical axis represents the amount of matching magnitudes per data fetch.

The standard uncertainty of the measurand Q_{exp} and is obtained by appropriately combining the standard uncertainties of the input estimates D, τ, m, d, k (see 4.10). This combined standard uncertainty of the estimate Q is denoted by $v(Q)$. The combined standard uncertainty $v(Q)$ is the positive square root of the combined variance of the uncertainties elements, which is given by:

$$v(Q_{\text{exp}})^2 = (\frac{\partial g_1}{\partial D}v(D))^2 + (\frac{\partial g_1}{\partial \tau}v(\tau))^2 + (\frac{\partial g_1}{\partial m}v(m))^2 + (\frac{\partial g_1}{\partial d}v(d))^2 + (\frac{\partial g_1}{\partial k}v(k))^2. \quad (4.15)$$

Where $v(k)$ can be defined as:

$$v(k)^2 = (\frac{\partial g_2}{\partial D}v(D))^2 + (\frac{\partial g_2}{\partial \tau}v(\tau))^2 + (\frac{\partial g_2}{\partial V_{\text{NS}}}v(V_{\text{NS}}))^2 + (\frac{\partial g_2}{\partial V_{\text{EW}}}v(V_{\text{EW}}))^2. \quad (4.16)$$

The partial derivatives $\partial g_1/\partial x_i$ and $\partial g_2/\partial x_i$ are called sensitivity coefficients and describe how the output estimate $g_1(x_i)$ and $g_2(x_i)$ varies with the changes in the values of the input estimates x_i. A combined uncertainty values for the experimental coefficient k and flow rate Q_{exp} were investigated and the results are presented in a form of tables 4.5 and 4.6, correspondingly.

The highest uncertainty magnitude of the retrieving data is generated by the time component τ for the both investigated parameters. The combined uncertainty $v(Q_{\text{exp}})$ reached a significant value of 0.5 dm^3/s or the measured flow rate can be written as: 0.5 $\text{dm}^3/\text{s}\pm$0.5 dm^3/s. The high uncertainty magnitude we can observe as error bars of Fig. 4.10 – Fig. 4.13.

As the conclusion we can point that currently applied sampling rate frequency of the time-of-flight Lorentz force velocimetry is not sufficient for a precise estimation of the liquid metal flow rate. However, increase of the sampling rate is meaningless until the applied force

Tab. 4.5: A combined uncertainty of the experimental coefficient k and its components.

Input estimates x_i	τ	D	V_{EW}	V_{NS}	Resulting value
$v(x_{\mathrm{i}})$	0.00058 s	$5.8{\cdot}10^{-6}$ m	$43.1{\cdot}10^{-6}$ V	$14.8{\cdot}10^{-6}$ V	–
$v(k_{\mathrm{i}})$ (components)	0.0012	$3.9{\cdot}10^{-5}$	$4.3{\cdot}10^{-5}$	$1.5{\cdot}10^{-5}$	0.0012

Tab. 4.6: A combined of the flow rate value Q_{exp} and its components.

Input x_i	τ	D	m	d	k	Resulting value
$v(x_{\mathrm{i}})$	0.00058 s	$5.8{\cdot}10^{-6}$ m	$5.8{\cdot}10^{-6}$ m	$5.8{\cdot}10^{-6}$ m	0.0012	–
$v(Q_{\mathrm{i}})$	$4.9{\cdot}10^{-4}$	$9.6{\cdot}10^{-9}$	$1.4{\cdot}10^{-7}$	$1.8{\cdot}10^{-8}$	$2.9{\cdot}10^{-7}$	$4.9{\cdot}10^{-4}$ m^3/s

sensors are in use. As was discovered in the section 3.3, the force sensors bring a limitation to the resolution value due to the relatively high reaction time, hence further increase of the sampling rate will increase the approximation accuracy, but will not increase the actual measurement accuracy.

5. CONCLUSIONS

In continuous metal casting of steel a reliable, accurate and fast flow measurement method is required for efficient control of flow rate and hence quality of final product. The proposed method of flow rate measurement – time-of-flight Lorentz force velocimetry – is a prospective technique that can be applied in case of high temperature liquid metal examination. The method is based on a detection of flowing vortical structures by non-contact electromagnetic sensors. Feasibility of the flow measurements without contact probes and signal particles is significant under condition of industrial manufacture. Our investigation shows that time-of-flight LFV can measure flow rate of the liquid metal in cases of unstable temperature conditions and does not depend on the change of electrical conductivity of the liquid during measurements. In addition, the application of the three-dimensional force sensors allows to investigate velocity components of turbulent duct flow. During the the present study, two remarkable experimental investigation were carried out. The main one included examination of time-of-flight LFV and includes solid and liquid metal tests. The solid metal tests included experiments with a copper plate moved through magnetic field of LFV flowmeters and generated by it fluctuations. The time between fluctuations and the distance between flowmeters are enough to estimate the copper plate velocity (the distance per time). This was done to confirm the feasibility of the method by the application of the visible disturbances with the defined velocity. The liquid metal tests were performed to examine the capability of the measurement system for flow rate estimation and to define the optimal design for the LFV flowmeter itself.

For this dissertation, we successfully developed and implemented the prototype of the time-of-flight LFV flowmeter. The next findings were discovered under work done on this research:

- The performed time-of-flight LFV experiments showed faithworthy flow measurement results in the flow rate range from 0.1 dm^3/s to 1.0 dm^3/s and the dimensionless hydraulic parameter Reynolds number Re from 4000 to 60000.

- The applied magnetic system was examined in detail. The system of permanent magnets directly influences the magnitude of Lorentz force arising within a flow. Moreover, the force depends on square value of the magnetic flux density penetrated the flow, hence the change of the magnetic field is a significant factor for this flow measurement technique. However, at the same time the magnetic system effects an existing flow pattern by magnetic field and the first magnetic system can ruin or dramatically change vortical structures before they will reach the second measurement zone. This fact imposes restrictions to a strength of the magnets. The weight of the permanent magnets is an another important factor that affect the force measurement. As part of a research effort aimed at establishing a sustainable measurement system the both

mentioned factors should be considered. The optimal ratio between the magnetic flux density and the weight of permanent magnets was established for our particular case.

- The applied force measurement element has several essential parameters. Foremost, resolution of the force sensor plays crucial role – the sensor should be able to detect relatively weak flow fluctuations against the bulk velocity background. Besides the resolution, the time of sensor's reaction is important due to the fact that the passing vortical structures intervene the measurement zone just for a fraction of a second. And thirdly, the Lorentz force should be measured in the whole three directions simultaneously, because the vortices can generate the flow fluctuations in each direction. Moreover, the fluctuation can be detected more simply in the orthogonal directions to the main flow due to nonoccurence of bulk effects.

- The developed signal processing technique is capable of the useful force perturbations resolving. The perturbations created by passing vortical structure have relatively low signal-to-noise ratio and cannot be distinguished by the raw force signals examination, hence the filtering algorithm was designed for our specific case.

- The electromagnetic pump operation significantly influences the flow in the duct not only by the pumping process itself. Additional hydraulic effects are generated by permanent magnets rotation due to discrete character of their positioning, hence the flow itself is pulsating. This makes the task to detect the fluctuations even more challenging. Another complication is caused by electromagnetic effects: the pump induces eddy currents around the whole loop which affects the magnets by the appeared adverse Lorentz force. As can be seen on the performed power spectrum analysis, the noise related to the pump rotation has the highest energy among others. The electromagnetic pump applied in experiments was precisely investigated in the context of its influence on the flow and hence on the measurement conditions for time-of-flight LFV to design the proper filtering scheme and distinguish the desired signal.

- The investigation of the three flow components clarified the picture of the velocity distribution in turbulent duct flow. Such analysis can be provided by LFV method by application of a three dimensional force sensor. In the combination with permanent magnets the force sensors works as a flow measurement device and one can investigate velocity components, which was done for the used duct. According to the obtained result, the distribution of velocity components is $u_\mathrm{y} \sim 10\% u_\mathrm{x}$; u_z is rather random and does not depend on the main velocity component.

- Several vortex generation methods were investigated. For vortical structures creation, electromagnetic and bluff-body techniques were applied for different sizes and geometries of vortex generators. Important parameters of invasive and non-invasive vortex generators were defined and tested experimentally.

The feasibility of the time-of-flight Lorentz force velocimetry was confirmed in the course of the flow rate estimation with the existing measurement system. However, the actual uncertainty value of estimated flow rate has the same range as the measured flow rate itself, hence further improvement of the measurement system should be provided. The special emphasis

should be placed on the force sensing element and the signal processing to obtain higher-precision measurement results. The research presented in this thesis shows as achievements so arisen challenges and also suggests directions in which further work could be done.

APPENDIX

A. PROPERTIES OF GALINSTAN

Tab. A.1: Properties of GaInSn provided by its supplier: Geratherm

Thermal conductivity	40 $\mathrm{W/(m^2 \cdot K)}$
Electrical conductivity	$3.29{\cdot}10^6 1/(\mathrm{Ohm \cdot m})$
Specific electrical resistance	$0.453\ \mathrm{Ohm \cdot mm^2/m}$
Density (under 20°C)	$6.44\ \mathrm{g/cm^3}$
Dynamic viscosity (from 20°C to 110°C)	$6\ \mathrm{Pa \cdot s}$
Volume expansion (from 25°C to 210°C)	$12.73{\cdot}10^{-5}\mathrm{K^{-1}}$
Surface tension (under 20°C in vacuum)	0.38 N/m
Melting temperature	−19.3°C

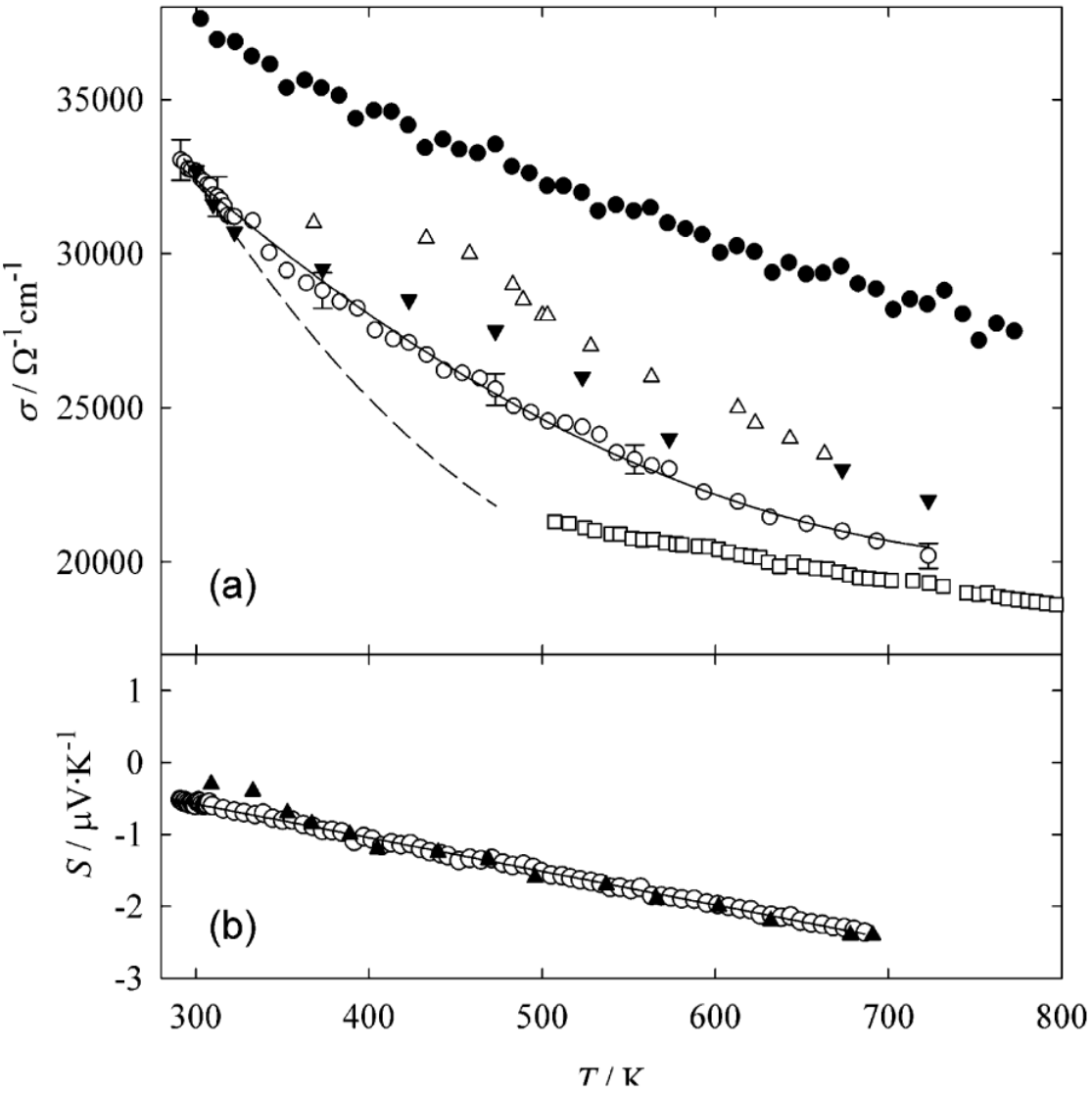

Fig. A.1: Temperature dependence of (a) electrical conductivity from different sources and (b) thermoelectric power for the liquid GaInSn eutectic alloy [35].

B. TIME-OF-FLIGHT LFV MEASUREMENT SYSTEM (CONSTRUCTION ELEMENTS)

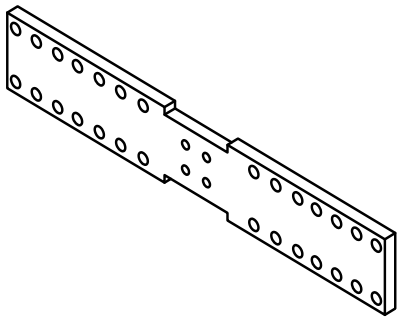

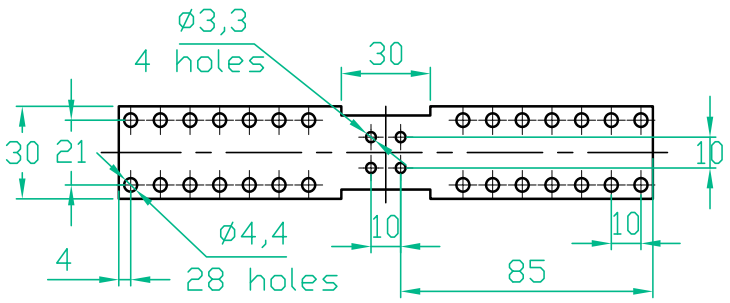

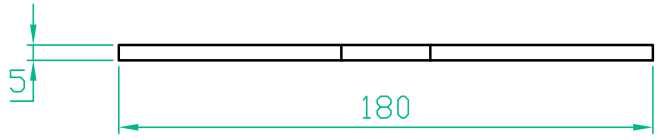

WENN NICHT ANDERS DEFINIERT: BEMASSUNGEN SIND IN MILLIMETER OBERFLÄCHENBESCHAFFENHEIT: TOLERANZEN: LINEAR: WINKEL:	OBERFLÄCHENGÜTE:		ENTGRATEN UND SCHARFE KANTEN BRECHEN		ZEICHNUNG NICHT SKALIEREN	ÄNDERUNG
	NAME	SIGNATUR	DATUM		BENENNUNG: Plate. A shielding element.	
GEZEICHNET						
GEPRÜFT						
GENEHMIGT						
PRODUKTION						
QUALITÄT				WERKSTOFF:	ZEICHNUNGSNR.	A4
				GEWICHT:	MASSSTAB:1:2	BLATT 1 VON 1

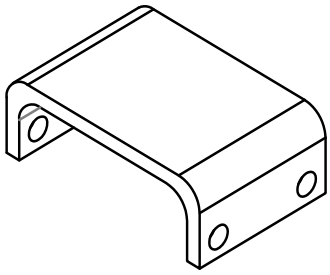

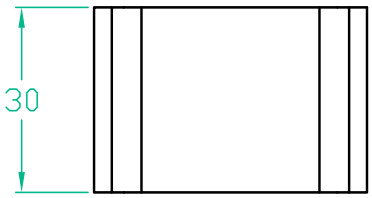

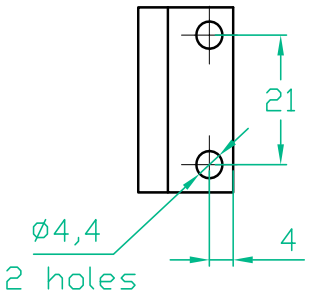

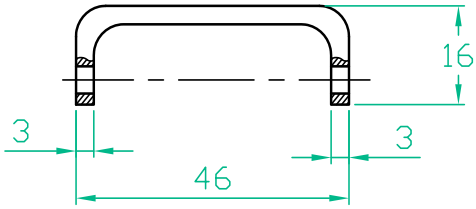

WENN NICHT ANDERS DEFINIERT: BEMASSUNGEN SIND IN MILLIMETER OBERFLÄCHENBESCHAFFENHEIT: TOLERANZEN: LINEAR: WINKEL:	OBERFLÄCHENGÜTE:			ENTGRATEN UND SCHARFE KANTEN BRECHEN	ZEICHNUNG NICHT SKALIEREN	ÄNDERUNG
	NAME	SIGNATUR	DATUM		BENENNUNG: Clip. An element of shielding.	
GEZEICHNET						
GEPRÜFT						
GENEHMIGT						
PRODUKTION						
QUALITÄT				WERKSTOFF:	ZEICHNUNGSNR.	A4
				GEWICHT:	MASSSTAB:1:1	BLATT 1 VON 1

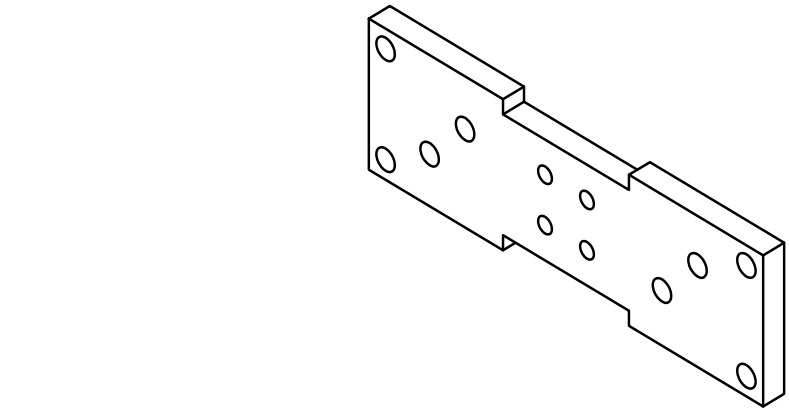

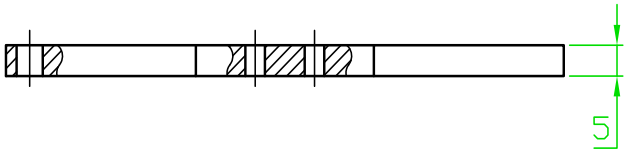

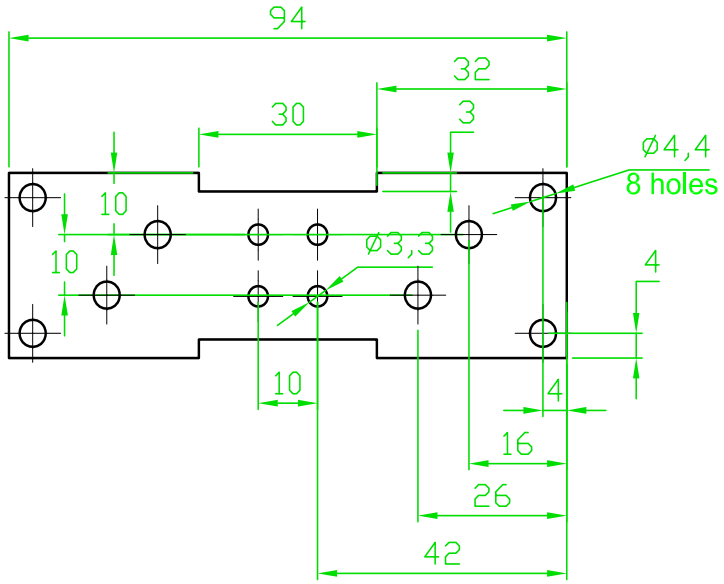

WENN NICHT ANDERS DEFINIERT: BEMASSUNGEN SIND IN MILLIMETER OBERFLÄCHENBESCHAFFENHEIT: TOLERANZEN: LINEAR: WINKEL:	OBERFLÄCHENGÜTE:		ENTGRATEN UND SCHARFE KANTEN BRECHEN		ZEICHNUNG NICHT SKALIEREN	ÄNDERUNG
	NAME	SIGNATUR	DATUM		BENENNUNG:	Plate (The second connection system)
GEZEICHNET						
GEPRÜFT						
GENEHMIGT						
PRODUKTION						
QUALITÄT				WERKSTOFF:	ZEICHNUNGSNR.	A4
				GEWICHT:	MASSSTAB:1:1	BLATT 1 VON 1

Product outlook and dimensions

Front view

Rear view

Top view

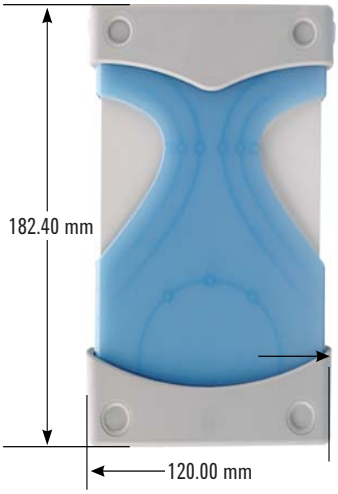

Standard shipped accessories

- AC/DC Power adapter
- Power cord
- USB extension cable
- L-Mount kit (used with modular product chassis)
- Keysight USB Modular Products Quick Start Guide
- Keysight USB Modular Products Reference CD-ROM
- Keysight Automation-Ready CD-ROM (contains the Keysight IO Libraries Suite)
- Certificate of Calibration

Optional accessories

- U2901A Terminal block and SCSI-II 68-pin connector with 1-meter cable
- U2902A Terminal block and SCSI-II 68-pin connector with 2-meter cable

Product characteristics and general specifications

Remote interface
- Hi-Speed USB 2.0
- USBTMC-USB488[1]

Power requirement
- +12 VDC (TYPICAL)
- 2 A (MAX) input rated current

Power consumption
+12 VDC, 550 mA maximum

Operating environment
- Operating temperature from 0 °C to +55 °C
- Relative humidity at 15% to 85% RH (non-condensing)
- Altitude up to 2000 meters
- Pollution Degree 2
- For indoor use only

Storage compliance
–20 °C to 70 °C

Safety compliance

Certified with:
- IEC 61010-1:2001/EN 61010-1:2001 (2nd Edition)
- USA: UL61010-1: 2004
- Canada: CSA C22.2 No.61010-1:2004

EMC compliance
- IEC/EN 61326-1 1998
- CISPR 11: 1990/EN55011:1991, Class A, Group 1
- Canada: ICES-001: 1998
- Australia/New Zealand: AS/NZS 2064.1

Shock and vibration
Tested to IEC/EN 60068-2

IO connector
68-pin female VHDCI Type

Dimension (W × D × H)

Module dimension:
- 120.00 mm × 182.40 mm × 44.00 mm (with plastic casing)
- 105.00 mm × 174.54 mm × 25.00 mm (without plastic casing)

Terminal block dimension:
- 103.00 mm × 85.20 mm × 42.96 mm

Weight
- 565 g (with plastic casing)
- 400 g (without plastic casing)

Warranty
Three years for U2300A series DAQ devices
Three months for standard shipped accessories

[1] Compatible with Microsoft Windows operating systems only. Requires a direct USB connection to the PC so the appropriate driver can be installed in the USB DAQ module.

Electrical specifications

Basic multifunction USB DAQ

Model number	U2351A	U2352A	U2353A	U2354A
Analog input				
Resolution	16 bits, no missing codes			
Number of channels	16 SE/8 DI (software selectable/channel)			
Maximum sampling rate[1]	250 kSa/s		500 kSa/s	
Scan list memory	Up to 100 selectable channel entries			
Programmable bipolar input range	±10 V, ±5 V, ±2.5 V, ±1.25 V			
Programmable unipolar input range	0 to 10 V, 0 to 5 V, 0 to 2.5 V, 0 to 1.25 V			
Input coupling	DC			
Input impedance	1 GΩ / 100 pF			
Operational common mode voltage range	±7.5 $V_{maximum}$			
Overvoltage protection	Power-on: Continuous ±30 V, Power-off: Continuous ±15 V			
Trigger sources	External analog/digital trigger, SSI/Star trigger[2]			
Trigger modes	Pre- trigger, delay-trigger, post-trigger, and middle-trigger			
FIFO buffer size	Up to 8 MSa			
Analog output				
Resolution	16 bits	-	16 bits	-
Number of channels	2	-	2	-
Maximum update rate	1 MSa/s	-	1 MSa/s	-
Output ranges	0 to 10 V, ±10 V, 0 to AO_EXT_REF, ±AO_EXT_REF[3]	-	0 to 10 V, ±10 V, 0 to AO_EXT_REF, ±AO_EXT_REF[3]	-
Output coupling	DC	-	DC	-
Output impedance	0.1 Ω typical	-	0.1 Ω typical	-
Stability	Any passive load up to 1500 pF	-	Any passive load up to 1500 pF	-
Power-on state	0 V steady state	-	0 V steady state	-
Trigger sources	External analog/digital trigger, SSI/Star trigger[2]	-	External analog/digital trigger, SSI/Star trigger[2]	-
Trigger modes	Post-trigger and delay-trigger	-	Post-trigger and delay-trigger	-
FIFO buffer size	One channel: Maximum 8 MSa Two channels: Maximum 4 MSa/ch	-	One channel: Maximum 8 MSa Two channels: Maximum 4 MSa/ch	-
Function generation mode	Sine, square, triangle, sawtooth, and noise waveforms	-	Sine, square, triangle, sawtooth, and noise waveforms	-

LIST OF FIGURES

LIST OF TABLES

BIBLIOGRAPHY

[1] Tropea C, Yarin A L and Foss J F 2007 *Handbook of experimental fluid mechanics* (Berlin: Springer-Verlag Berlin Heidelberg).

[2] Baker R C 2000 *Flow measurement handbook* (New York: Cambridge University Press).

[3] Sydenham P and Thorn R 2005 *Handbook of measuring system design* (New York: John Wiley and Sons, Inc.).

[4] Tezuka K, Michitsugu M, Suzuki T and Kanamine T 2008 *Flow Meas. Inst.*, **19**, issues 3-4, 155 – 162 pp.

[5] Jayanthy A K, Sujatha N and Reddy M R 2011 *Int. J. Res. Rev. Appl. Sci.*, **6**, 2, 203 – 216 pp.

[6] Schroeder A and Willert C E 2008 *Particle Image Velocimetry* (Berlin: Springer).

[7] Stern M D 1985 *Appl. Optics*, **24**, 13, 1968– 1986 pp.

[8] Gendrich C P, Koochesfahani M M and Nocera D G 1997 *Exp. Fluids*, **23**, 361– 372 pp.

[9] Yasushi T 2012 Ultrasonic Doppler Velocity Profiler for Fluid Flow (Tokyo: Springer Japan).

[10] Liptak B G 1993 *Flow measurement* (Radnor, Pensyilvania: Chilton book company).

[11] Venugopal A, Agrawal a and Prabhu S V 2011 *Sensors and actuators A* **170** 8–23 pp.

[12] Peng J, Fu X and Chen Y 2004 *Sensors and actuators A*, **115** 53–59 pp.

[13] Liu R, Sengupta J, Crosbie D et.al. 2011 *Annual TMS meeting*, TMS Proceedings, 51–58 pp.

[14] Wiedermann C 2012 *Design and laboratory test of a Lorentz force flowmeter for pipe flows* (Dissertation, Technischen Universität Ilmenau).

[15] Shercliff J A 1962 *The theory of electromagnetic flow-measurement* (Cambridge: Cambridge University Press).

[16] Ricou R and Vives Ch 1982 *Int J Heat Mass Transfer* **25**, 1579–1588 pp.

[17] Thess A, Votyakov E, and Zikanov O 2007 *N. J. Phys.* **9** p. 299.

[18] Vasilyan S and Froehlich T 2014 *Apl. Phys. Lett.* **105** 223510.

[19] Kolesnikov Yu, Karcher Ch, Thess A 2011 *Met. Mat. Trans. B* **42** 441–450 pp.

[20] Weidermann C, Thess A, Lieftucht D and Reifferscheid M 2012 *5th Int. Congress Sci. Tech. Steelmaking.*

[21] Jain D and Karcher Ch 2012 *Meas. Sci. Tech.*, **23**, 074021.

[22] Axel L, Yu, Shimakawa A and MacFall J 1986 *Magn. Resonance Im.* **4**, 3, 199–205 pp.

[23] Granwehr J, Harel E, Han S-I et.al. 2005 *Lawrence Berkeley National Laboratory*, http://escholarship.org/uc/item/67k9q5tr.

[24] Rodrigues J B and Furlan R 2009 *J. Int. Circuits Sys.* **4**, 2, 84–88 pp.

[25] Miller T E and Small H 1982 *Anal. Chem.* **54** 907–910 pp.

[26] Yu H, Li D, Roberts R C et.al. 2012 *J. Micromech. Microeng.* **22**, 055009.

[27] Lippmann J M and Pisano A P 2012 *Sensors and Actuators A* **177**, 60–66 pp.

[28] Jian D 2013 Flow measurement in liquid metals using Lorentz force velocimetry: laboratory experiments and numerical simulations (Dissertation, Technischen Universität Ilmenau).

[29] Davidson P A 2001 *An Introduction to Magnetohydrodynamics* (Cambridge: Cambridge University Press).

[30] Tillack M S and Morley N B 1998 *Magnetohydrodynamics* (McGraw-Hill).

[31] Thess A, Krasnov D J, Boeck T at.al. 2007 *GAMM-Mitt.* **30**, 1, 125–132 pp.

[32] Idelchik I E 1966 *Handbook of hydraulic resistance* (Israel: Israel program for scientific translation).

[33] Bates C J and Franklin B 2004 *Measurement* **35** 399–408 pp.

[34] Morley N B, Burris J, Cadwallader L C and Nornberg M D 2008 *Review Sci. Instr.* **79** 056107.

[35] Plevachuk Yu, Sklyarchuk V, Eckert S et al. 2014 *J Chem. Eng. Data* **59** 757763 pp.

[36] Dubovikova N, Kolesnikov Yu and Karcher Ch 2015 *Meas Sci Tech*, **26**, No. 11, 115304.

[37] Desai P D, James H M and Ho C Y 1984 *J Chem. Ref. Data* **13**, 4, 11311172 pp.

[38] Dubovikova N, Karcher Ch, Kolesnikov Yu 2014 *EPJ Web of Conferences* **67** 02022.

[39] Goldsteins L, Bucenieks I, Buligins L 2014 *Magnetohydrodynamics* **50** No. 2.

[40] Dixon J 2007 *The Shock Absorber Handbook* (Wiley: Professional Engineering Publishing).

[41] Bucenieks I, Kravalis K 2011 *Magnetohydrodynamics* **47** No. 1.

[42] Bucenieks I 2014 *Magnetohydrodynamics* **50** No. 2, 157–164 pp.

[43] Stefanescu D M 2011 *Handbook of force transducers: Principles and components* (Berlin: Springer-Verlag Berlin Heidelberg).

[44] Razzaq Z and Aridi N F 2003 *Proceedings 2nd Intern. Conf. Structural stability and dynamics*, 813–819 pp.

[45] ME-Messsysteme *Skalierung des Ausgangssignals* (http://www.me-systeme.de/).

[46] Leeungculsatien T and Lucas G P 2013 *Flow Meas Inst* **31**, 86–95 pp.

[47] Pedcenko A, Bojarevics A and Priede J, et. al. 2013 *Exp Fluids* **54**, 1558.

[48] Cramer A, Zhang C and Eckert S, et. al. 2004 *Flow Meas Inst* **15**, 145–153 pp.

[49] Eckert S and Gerbeth G 2002 *Exp. Fluids* **32**, 542–546 pp.

[50] Stefani F, Gundrum T, Gerbeth G et. al 2006 *Phys. Rev. Lett.* **97**, 184502.

[51] User's manual DOP2000 Signal Processing S.A.

[52] Heinicke C 2013 Local Lorentz Force Velocimetry for liquid metal duct flows (Dissertation, Technischen Universität Ilmenau).

[53] Hamid A H A, Hussam W K, Pothrat A and Sheard G J 2015 *Physics of Fluids* **27**, 053602.

[54] Pankanin G L, Berliski J, Chmielewski R 2005 *Metr and Meas Syst* **12**, 413-425 pp.

[55] Votyakov E V, Kolesnikov Yu, etc. 2007 *Phys. Rew. Letters* **98**, 144504.

[56] Sumer B M and Fredsoe J 2006 *Hydrodynamics Around Cylindrical Structures. Revised edition* (Singapore: World Scientific Publishing).

[57] Igarashi T 1999 *JSME Int. J. series B* **42**, 586—595 pp.

[58] Hamid A H A, Hussam W K, Pothrat A and Sheard G J 2015 *Physics of Fluids* **27**, 053602.

[59] Pankanin G L, Berliski J, Chmielewski R 2005 *Metr and Meas Syst* **12**, 413-425 pp.

[60] McCormick and Barnes W 1979 *Aerodynamics, Aeronautics, and Flight Mechanics* (New York: John Wiley and Sons, Inc.).

[61] Saffman P G 1992 *Vortex Dynamics* (Cambridge: Cambridge University Press).

[62] National Bureau of Standards handbook 1966 *Copper wire tables* (Washington: U.S. Govt. Print. Off.).

[63] Marshall L B 2012 *Modern physics for science and engineering* (Tuskegee: Physics Curriculum and Instruction, Inc).

[64] Stoica P, Moses R 2005 *Spectral analysis of signal* (New Jersey: Prentice hall).

[65] Welch P D 1967 *IEEE Trans. on Audio and El. acoustic* **AU-15**, 2, 70-73 pp.

[66] Quinquis A 2008 *Digital Signal Processing Using MATLAB* (Chippenham: John Wiley and Sons, Inc.).

[67] Pouzols F M 2010 *IEEE World Congress on Comput. Int.*, 1730-1736 pp.

[68] Lewis J P 1995 *Vision Interface* **95**, 120-123 pp.

[69] Press W H, Teukolsky S A, Vetterling W T and Flannery B P 2007 *Numerical Recipes 3rd Edition The Art of Scientific Computing* (Cambridge: Cambridge University Press).

[70] Lyon D A 2010 *Journal of Object Technology* **9**, 2, 17-22 pp.

[71] Zhang X D and Huang H L 2013 *Chin. Phys. B* **22**, No. 7 075202.

[72] Samsami F, Thess A and Kolesnikov Yu 2011 *EUROMECH Colloquium 525* **1**, hal-00600512.

[73] Goswami J C and Chan A K 2011 *Fundamentals of wavelets* (New Jersey: John Wiley and Sons, Inc.).

[74] Davenport W B and Root W L 1987 *An introduction to the theory of random signals and noise* (New York: John Wiley and Sons, Inc.).

[75] Davidson P A 2004 *Turbulence. An Introduction for Scientists and Engineers* (Oxford: Oxford University Press).

[76] Bandaru V 2015 *Private conversation.*

[77] Stein J 1987 *Liquid pulsation dampening device* US Patent, 4,679,597.

[78] Glover R C 1973 *Liquid pulsation dampener* US Patent, 3,731,709.

[79] Kaech R 2006 *Pulsation damper* US Patent, 7,029,250 B2.

[80] Cacuci D 2003 *Sensitivity and uncertainty analysis. Volume 1* (Boca Raton: Chapman and Hall/CRC).

[81] Zilli M 2013 *The Open Toxicology Journal* **6**, (Suppl 1, M3), 20-26 pp.

[82] JCGM 100: 2008 *Evaluation of measurement data Guide to the expression of uncertainty in measurement* (JCGM 2008).

[83] Mueller M E 2009 Computational Aspects of Measurement Uncertainty Calculation (Dissertation, Swiss Federal Institute of Technology, Zuerich).

ERKLÄRUNG

Ich versichere, dass ich die vorliegende Arbeit ohne unzulässige Hilfe Dritter und ohne Benutzung anderer als der angegebenen Hilfsmittel angefertigt habe. Die aus anderen Quellen direkt oder indirekt übernommenen Daten und Konzepte sind unter Angabe der Quelle gekennzeichnet.

Bei der Auswahl und Auswertung folgenden Materials haben mir die nachstehend aufgeführten Personen in der jeweils beschriebenen Weise unentgeltlich geholfen:

- Jonas Ketterer hat als wissenschaftliche Hilfskraft Messungen zur Kalibrierung der elektromagnetischen Pumpe durchgeführt.
- M.Sc. Anna Kholodova hat als wissenschaftliche Hilfskraft bei Geschwindigkeitsmessungen von Flüssigmettal sowie bei der Automatisierung der Auswertung assistiert.

Weitere Personen waren an der inhaltlich-materiellen Erstellung der vorliegenden Arbeit nicht beteiligt. Insbesondere habe ich hierfr nicht die entgeltliche Hilfe von Vermittlungsbzw. Beratungsdiensten (Promotionsberater oder anderer Personen) in Anspruch genommen. Niemand hat von mir unmittelbar oder mittelbar geldwerte Leistungen für Arbeiten erhalten, die im Zusammenhang mit dem Inhalt der vorgelegten Dissertation stehen.

Die Arbeit wurde bisher weder im In- noch im Ausland in gleicher oder ähnlicher Form einer Prüfungsbehörde vorgelegt.

Ich bin darauf hingewiesen worden, dass die Unrichtigkeit der vorstehenden Erklärung als Täuschungsversuch bewertet wird und gemäß §7 Abs.10 der Promotionsordnung den Abbruch des Promotionsverfahrens zur Folge hat.

_____ _____

Ort, Datum Nataliia Dubovikova